Electrophysiological Characterization of Cation Coupled Symporters and Investigation of Physicochemical Surface Processes with a Solid-Supported Membrane

Dissertation

Zur Erlangung des Doktorgrades

Der Naturwissenschaften

Vorgelegt beim Fachbereich Biochemie, Chemie, Pharmazie

der Johann Wolfgang Goethe – Universität

in Frankfurt am Main

von

Juan José García Celma

Aus Tortosa – Tarragona (Spanien)

Frankfurt 2009

(D30)

Vom Fachbereich Biochemie, Chemie, Pharmazie der

Johann Wolfgang Goethe – Universität als Dissertation angenommen

Dekan : Prof. Dr. D. Steinhilber

1. Gutachter: Prof. Dr. J. Wachtveitl

2. Gutachter: Prof. Dr. K. Fendler

Datum der Disputation:

Table of Contents

Table of Figures

Abbreviations

α-NPG	*p*-nitrophenyl α-D-galactopyranoside
ABC	ATP-binding cassette
ATP	Adenosine-5'-triphosphate
BLM	Black lipid membrane
bR	Bacteriorhodopsin
DDM	n-Dodecyl-β-D-maltoside
DTT	1,4-Dithiothreitol
DOPG	Dioleoyl-phosphatidylglycerol
DOTAP	Dioleoyl-trimethylammonium-propane
Eq.	Equation
Fig.	Figure
GTP	Guanosine-5'-triphosphate
Hepes	4-(2-hydroxyethyl)-1-piperazineethanesulfonic acid
ISO	Inside-out
Lactose	4-*O*-*β*-D-galactopyranosyl-D-glucose
Lactulose	4-*O*-*β*-D-galactopyranosyl-D-fructofuranose
LacY	Lactose permease from *Escherichia coli*
LPR	Lipid to protein ration (weight/weight)
MelB	Melibiose permease from *Escherichia coli*
MFS	Major facilitator superfamily
Melibiose	6-*O*-*α*-D-galactopyranosyl-D-glucose
MIANS	2-(4'-maleimidylanilino)naphthalene-6-sulfonic acid
Mono	Monoolein (1-monooleoyl-rac-glycerol)
Mono-squal	Monoolein in squalene
Na^+/K^+ATPase	Sodium/Potassium ATPase
NhaA	Sodium/proton antiporter from *Escherichia coli*

NEM	*N*-ethylmaleimide
$N(CH_3)_3^+$	Ammonium lipid headgroup
OG	Octylglucoside
PC	diphytanoyl-phosphatidylcholine
PO_4^-	Phosphate lipid headgroup
PTS	Phosphotransferase system
PupP	Sodium/proline transporter from *Escherichia coli*
RSO	Right-side-out
SAM	Self-assembled monolayer
SE	Standard error
SSM	Solid-supported membrane
Sucrose	O-*β*-D-fructofuranosyl-(2→1)-*α*-D-glucopyranoside
trFTIR	Time-resolved Fourier-transform infrared
Tris	Tris(hydroxymethyl)aminomethane

Amino acids

A	Ala	alanine	M	Met	methionine
C	Cys	cysteine	N	Asn	asparagine
D	Asp	aspartic acid	P	Pro	proline
E	Glu	glutamic acid	Q	Gln	glutamine
F	Phe	phenylalanine	R	Arg	arginine
G	Gly	glycine	S	Ser	serine
H	His	histidine	T	Thr	threonine
I	Ile	isoleucine	V	Val	valine
K	Lys	lysine	W	Trp	tryptophan
L	Leu	leucine	Y	Tyr	tyrosin

1. Introduction

1.1. Translocation through Membranes

A cell or an organelle can be neither wholly open nor wholly closed to its surroundings. Its interior must be protected from certain toxic compounds, and yet metabolites must be taken in and waste products removed. Because the cell must contend with thousands of substances, it is not surprising that much of the complex structure of the membranes is devoted to the regulation of transport. Here, three main categories of transport across the membrane will be described: passive, facilitated and active.

1.1.1. Passive Transport: Diffusion

For ions and other hydrophilic substances, the energy barrier of a pure membrane results in an extremely slow diffusion rate. Only tiny non-polar molecules, like O_2 or CO_2, can move rapidly through the membrane by passive diffusion.

1.1.2. Facilitated Transport: Accelerated Diffusion

Two types of facilitated transport are utilized by the cells to increase the transport rate of solutes: pore-facilitated transport and carrier-facilitated transport. In pore-facilitated transport, the interior of the pore represents a hydrophilic environment that is utilized to increase the transport rate of hydrophilic substances. Instead, in carrier-facilitated transport the carrier effectively increases the solubility of the substrate in the membrane: a carrier can diffuse to one surface of the membrane, pick up an ion, and then diffuse to the other surface and release it.

1.1.3. Active Transport: Transport against a Concentration Gradient

In active transport, a substance can be transported against its concentration gradient. To achieve that, the transport must be coupled with an energy source. Transporters are fascinating molecular machines that couple the transport of a substance with an energy source. Three main categories of systems, each with a distinct energy source, are involved in active transport: primary active transporters, secondary active transporters, and group translocators.

Primary active transporters utilize a primary energy source, such as ATP hydrolysis, photon absorption, or redox energy to translocate molecules across the membrane. Secondary active transporters couple the translocation of molecules with a secondary source of energy, e.g., an ion electrochemical gradient; these transporters utilize the free energy released from the energetically downhill movement of a cation (mainly H^+ or Na^+) in response to an electrochemical ion gradient to catalyze the transport of a substrate against its concentration gradient. Group translocation systems transport and concomitantly phosphorylate their substrates during transport, e.g., the glucose phosphotransferase system (PTS) of *Escherichia coli*.

1.2. The Relevant Role of the Transporters

Statistical analysis of all known genome sequences predicts that 20 to 30% of all open reading frames encode integral membrane proteins (Wallin & von Heijne, 1998). Transporters are one group of integral membrane proteins allowing the uptake of essential nutrients and ions and the excretion of deleterious substances and end products of the metabolism. In the last years, transporters have gained enormous interest, as many human diseases turned out to be associated to defects in transport. For example, transporters play key roles in cystic fibrosis, resistance to antibiotics and chemotherapeutic drugs, gastric ulcer, and glucose/galactose malabsorption. Furthermore, they are also key players in neurobiology and they represent targets for psycho-pharmaceutical drugs, like fluoxetine (Prozac).

1.3. Ion-Gradient-Driven Permeases

The ion-gradient-driven permeases belong to the secondary active transporters. They are able to catalyze solute/ion symport in both directions across the membrane (influx and efflux) in response to a chemiosmotic ion gradient. In this thesis, two important paradigms for ion-gradient coupled membrane transport proteins are electrophysiologically investigated: The lactose permease (LacY) and the melibiose permease (MelB), both from *Escherichia coli*.

In the transport classification system (Saier, 1999; Saier, 1998), transporters are classified according on the mode of transport and energy coupling mechanism, molecular phylogeny, and substrate specificity. According to this classification system, LacY belongs to the major facilitator superfamily (MFS), which is one of the two largest families of membrane transporters found on Earth. More precisely, LacY

belongs to the oligosaccharide:H1 symporter (OHS) family, which is included in the MFS (Saier, 2000). MelB, however, is not a member of the MFS but belongs to the galactoside-pentose-hexuronide transport family (GPH). Mechanistically, while LacY couples the transport of galactosides to H^+ (Guan & Kaback, 2006), MelB can use either Na^+, Li^+ or H^+ as coupling ions (Tsuchiya & Wilson, 1978; Wilson & Wilson, 1987). Indeed, it has been proposed that MelB may serve as an evolutionary link between the proton-coupled transport that commonly occurs in primitive microorganisms and sodium-coupled transport prevalent in animal cells (Yazyu *et al.*, 1984).

1.4. Why SSM-based Electrophysiology?

The study of the charge transport of bacterial secondary active transporters is one of the most direct methods to get insight into the mechanism of these enzymes. Standard electrophysiological studies (like two electrode voltage clamp or patch clamp) require targeting of the plasma membrane of eukaryote cells. However, except for a few rare exceptions, bacterial transporters do not target the plasma membrane of eukaryote cells, and conversely, it is highly problematic to functionally express eukaryotic membrane transport proteins in bacteria. The lactose permease (LacY) from *Escherichia coli* is not an exception to this rule. Although the *lacY* gene is expressed well in frog oocytes and other eukaryotic cells, LacY remains in the *cis*-Golgi and the peri-nuclear membrane and does not target to the plasma membrane to any extent whatsoever (J. Liu &, H. Ronald Kaback, personal communication). As a result, LacY (as well as many other bacterial transporters) has been impervious to all attempts at standard electrophysiological analysis.

Alternatively, black lipid membranes (BLM) could be used to perform electrophysiological studies of bacterial transporters. Due to the low turnover numbers of the transporters, the electrical responses of 10^4 – 10^7 transporters need to be added to achieve a measurable electrical current. This can be achieved by absorption of proteoliposomes or membrane vesicles containing the transporter of interest to a BLM, which acts as capacitive electrode. The principle of the capacitive electrode was described for the first time in 1974 (Drachev *et al.*, 1974). Afterwards, the kinetics of light-driven proton transport by bacteriorhodopsin (bR) were studied on a BLM to which purple membrane fragments from *Halobacterium halobium* had been attached (Bamberg *et al.*, 1979; Fahr *et al.*, 1981; Herrmann & Rayfield, 1978;

Keszthelyi & Ormos, 1980). There, it was shown that a BLM is an appropriate model system to characterize photobiological systems, like bR.

In addition, membrane fragments containing the Na^+/K^+ ATPase from pig kidney were electrophysiologically characterized in a BLM by utilizing photolabile ATP derivative ("caged ATP") (Fendler *et al.*, 1985). In this case, synchronization was achieved by a light-induced concentration jump of ATP from caged ATP. However, only a few substrates are available as caged substances, like caged phosphate, caged GTP, caged ATP, and caged Calcium (Adams & Tsien, 1993). In particular, there is no caged Na^+, melibiose, lactose, or lactulose. Furthermore, a caged substrate can act as a competitive inhibitor (Fendler *et al.*, 1993; Forbush, 1984; Nagel *et al.*, 1987) or the cage itself may present a problem (McCray *et al.*, 1980; Seifert *et al.*, 1993).

Despite those achievements with photobiological systems and caged substrates, several difficulties exclude the electrophysiological characterization of the melibiose permease (MelB) or the lactose permease (LacY) from *Escherichia coli* utilizing a BLM as a capacitive electrode: (i) the turnover numbers of MelB and LacY are approximately one order of magnitude smaller than the turnover of bR or Na^+/K^+ ATPase (MelB presents a turnover of ~ 4 s^{-1} (Pourcher *et al.*, 1990) while the turnover of LacY during downhill lactose/H^+ symport is ~ 10 s^{-1} (Viitanen *et al.*, 1984)); therefore, ~ 10^6 transporters have to be activated simultaneously to produce a stationary current of 1 pA; (ii) there are no available caged forms for melibiose, lactose, lactulose, or Na^+; (iii) the mechanical stability of a BLM does not allow rapid concentration jumps. These three points represent major difficulties in the characterization of the electrogenic activity of MelB or LacY utilizing a BLM as capacitive electrode.

To circumvent all these difficulties for the electrophysiological investigation of bacterial secondary active transporters, like MelB or LacY, we make use of the solid-supported membrane (SSM) based electrophysiology (Ganea & Fendler, 2009; Schulz *et al.*, 2008). The SSM used in this technique is a hybrid bilayer composed of a painted lipid monolayer on a hydrophobic support, which consists on a gold surface functionalized by an alkanethiol (Florin & Gaub, 1993; Seifert *et al.*, 1993). Reconstituted transporters can be readily absorbed to the SSM, forming a capacitively coupled system. Importantly, mechanical perturbations, which usually destroy a BLM, do not influence the life-time of a SSM. Indeed, the capacitive electrode, composed by the SSM and proteoliposomes, is mechanically so stable that solutions may be rapidly exchanged at its surface (Pintschovius & Fendler, 1999). Therefore, there is no need for caged substrates in order to perform a

concentration jump. This property allows the electrophysiological characterization of MelB or LacY on an SSM-electrode.

2. Materials and Methods

2.1. Film-forming solutions of the SSM

For the electrophysiological characterization of MelB and LacY, the lipid film-forming solution contains diphytanoyl-phosphatidylcholine 1.5% (w/v) in n-decane and 1:60 (w/w) octadecylamine. The specific interactions between ions and solid-supported membranes (SSM) were investigated on a number of lipids in the absence of octadecylamine. The different lipid film-forming solutions were: diphytanoyl-phosphatidylcholine 1.5% (w/v) in n-decane, dioleoyl-phosphatidylglycerol 1.5% in n-decane, dioleoyl-trimethylammonium-propane 1.5% in n-decane, and monoolein (1-monooleoyl-rac-glycerol) 1.5% in n-decane or squalene.

2.2. Preparation of the Sensor Chips

The electrodes are prepared by a lithographic process on a 1-mm-thick 9 × 22 mm^2 borofloat glass chip (Fraunhofer Institut Schicht und Oberflächentechnik, Braunschweig, Germany). The 100 nm thick gold structure consists of a 1mm diameter circular active area which is connected to a contact pad via a thin contact strip. A convenient method for the preparation of self-assembled monolayers (SAMs) consists on immersing the gold surface into a saturated solution of alkanethiol (Xu & Li, 1995). Typically, the gold electrodes are incubated for a 6 hour period in a 1 mM ethanolic octadecyl mercaptan solution. A second monolayer of lipid is attached to the first hydrophobic one by a painting technique (Florin & Gaub, 1993; Seifert *et al.*, 1993). A small amount of the film-forming solution (see above) is spread over the SAM of octadecanethiol (hydrophobic surface). The resulting hybrid bilayer constitutes the SSM used for the SSM-based electrophysiology, and it will be also referred as the sensor.

2.3. SSM Set-up

The sensor chip is mounted in a flow-through cuvette with an inner volume of 17 µL (Figs. 1A &B). The cuvette is plugged to a flow system (Figs. 2A &B) composed by pressurized solution containers and a system of valves. The whole flow system is enclosed in a faraday cage. The valves are switched using home made valve drivers

which are controlled via computer. The sensor chip is connected to a current amplifier (Keithly Instruments Inc., model 427, amplification 10^8 – 10^9 V/A) and rinsed with buffer to remove the excess of lipid. The reference electrode is an Ag/AgCl electrode separated from the solution by a salt bridge (Figs. 1A & B and Figs. 2A & B). The capacitance and conductance of the SSM are determined until they became constant. Typical values are 300 – 500 nF/cm^2 for the specific capacitance and 50 – 100 nS/cm^2 for the specific conductance of the SSM. These values are in good agreement with literature data obtained from symmetric BLM's (Florin & Gaub, 1993; Seifert *et al.*, 1993).

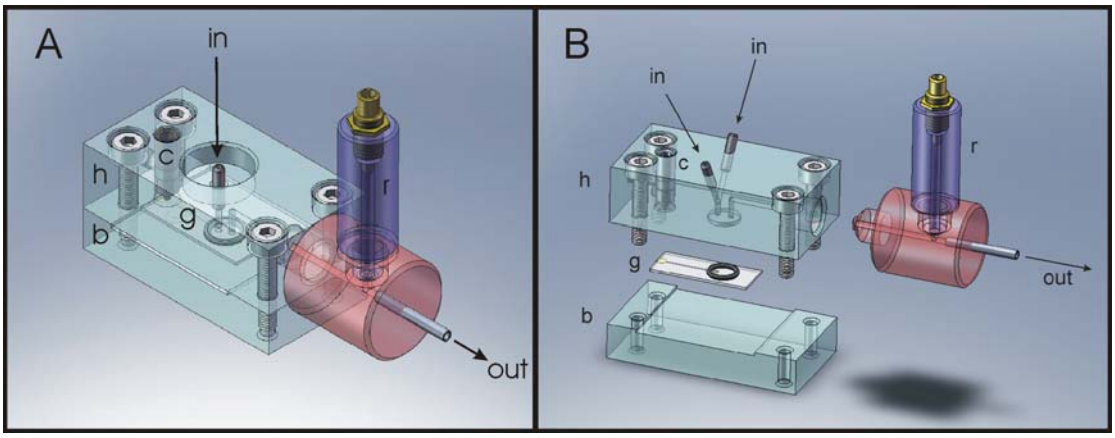

Fig. 1. Flow-through cuvettes.

(***A***) Classical cuvette employed in the valve-controlled diverter geometry (Fig. 2A). (***B***) Fast solution exchange cuvette utilized in the valve-less diverter flow geometry (Fig. 2B). Cuvette heads (h) and bases (b) are made out of Plexiglas. Inlet (in) and outlet (out) bores have a diameter of 1 mm. In the outlet pathway the reference electrode assembly (r) is placed. The cuvette volume is cylindrical and 0.75 mm deep with an internal volume of 17µl in both cases (net volume with O-ring mounted). The SSM is formed on a gold coated glass slide (g) and has a diameter of 1 mm. Contact with the amplifier are made through spring contact pins (c). When mounted the SSM is centered under the inlet bore.

2.4. Addition of the Protein Sample

MelB or LacY were reconstituted into proteoliposomes to a final protein concentration of ~1 mg/ml (see section 2.6 for the reconstitution protocols). The samples were stored in liquid nitrogen or in a freezer at -80 °C. Before use, the proteoliposomes were thawed and briefly sonicated in a bath (three sonication cycles of 10 s with 20 s cooling intervals on ice in between). Then, 30–40 µl of the proteoliposome suspension were applied to the SSM using a standard pipette via the exit bore of the cuvette with the reference electrode assembly removed. The proteoliposomes containing either MelB or LacY were allowed to adsorb to the SSM for 1 h.

2.5. Flow Protocol

Two types of solutions are needed for the electrophysiological characterization of the transporter under investigation: activating solutions containing one of the substrates of the transporter, and non-activating solutions containing none of the substrates (in ion concentration jump experiments, the terms activating and non-activating solutions are replaced by test and reference solutions, respectively). Activating and nonactivating solutions are placed into solution containers of polyethylene (100 mM bottles) and pressurized with compressed air at pressures between 0.1 – 1.0 bar. Using the system of valves, solutions are exchanged at the surface of the SSM. A typical solution exchange protocol consists of three phases (Figs. 2A & B) with adjustable duration: 1) nonactivating solution, 2) activating solution and 3) nonactivating solution. The valves are switched using home made valve drivers, which are controlled via computer. Two different flow geometries have been studied in this thesis: a valve-controlled (Fig. 2A) and valve-less (Fig. 2B) diverter geometry. The diverter–SSM distance, i.e. the common pathway for activating and nonactivating solutions between terminal valve V2 and SSM (Fig. 2A) or between confluence point and the SSM (Fig. 2B) is critical for the concentration rise time (see section 5). Unless otherwise specified, this pathway is a cylindrical tube of 1 mm diameter made from Polyethylene (valve-controlled diverted geometry) or Plexiglas (valve-less diverted geometry).

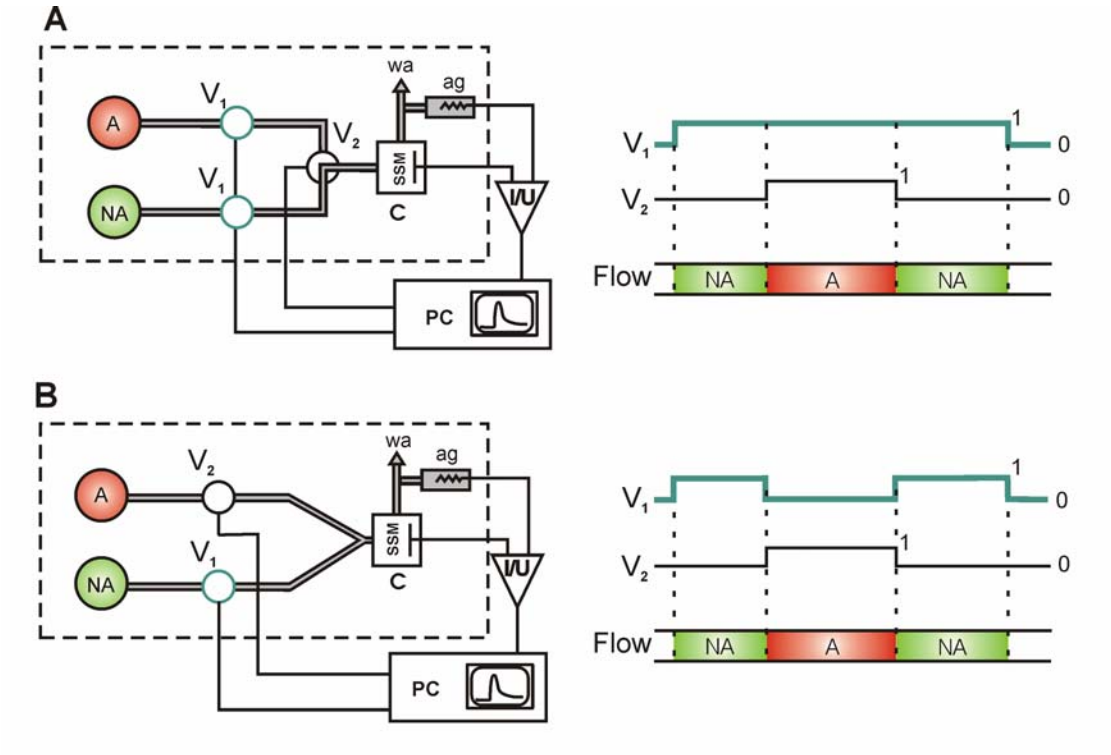

Fig. 2. Flow configuration, valve timing, and flow protocol for the two employed diverter geometries.

The current is measured with reference to an Ag/AgCl electrode (ag) and amplified by a current/voltage converter (I/U). Valves are controlled and current is recorded by computer (PC). After passing through the cuvette the solutions are directed to a waste container (wa). (***A***) Valve-controlled diverter geometry. The two pressurized containers with nonactivating (NA) and activating (A) solutions are connected to the cuvette (C) via 2-way isolation valves V_1 and a 3-way isolation valve V_2 or a 3x3-way isolation valve V_2. Opening of valves V_1 initiates flow of the nonactivating solution. Subsequently, when V_2 is switched on, the activating solution is directed to the cuvette. (***B***) Valve-less diverter geometry. The cuvette is equipped with a Y-shaped double inlet bore (see Fig. 1B). The two pressurized containers are now connected to the cuvette via 2-way isolation valves $V_1 = V_2$. Opening of valve V_1 initiates flow of the nonactivating solution. Subsequently, simultaneous opening of V_2 and closing of V_1 directs the activating solution into the cuvette.

2.6. Reconstitution of Transporters into Liposomes

Solubilization of transporters from the bacterial membrane requires the utilization of detergents in a harsh process: the transporter is removed from the bacterial membrane and incorporated into detergent micelles. Non-ionic detergents are preferred for the solubilization process as they are considered mild and non-denaturing. Other types of detergents (ionic, zwitterionic detergents or bile acid salts) tend to denaturalize the proteins (Seddon *et al.*, 2004) and are, therefore, generally avoided.

To explore the basic mechanisms of transport, it is desirable to achieve reconstitution of the transporters into proteoliposomes, which provide and excellent membrane model. One of the most widely utilized reconstitution approaches consists in adding the transporter protein in detergent micelles to a mixture of lipids and detergents, forming mixed micelles. Subsequent removal of the detergent triggers the micelle to vesicle transition (review in (Ollivon *et al.*, 2000; Seddon *et al.*, 2004)). Two of the most widely utilized techniques to achieve the micelle to vesicle transition are detergent removal by adsorption onto polymeric materials (such as bio-beads) or rapid dilution. In particular, bio-beads have been utilized to reconstitute MelB (Ganea *et al.*, 2001) into proteoliposomes, and rapid dilution to reconstitute LacY (Newman *et al.*, 1981; Viitanen *et al.*, 1984). Both methods will be briefly described.

Detergent removal by bio-beads is based on the physical adsorption of detergents onto the surface of the hydrophobic polymer beads (Holloway, 1973; Ueno *et al.*, 1984). To date, three bacterial secondary active transporters from *Escherichia coli*, reconstituted by the bio-bead procedure, have been electrophysiologically characterized by means of the SSM-based electrophysiology (review in (Ganea & Fendler, 2009)): the melibiose permease MelB (Ganea *et al.*, 2001); the Na^+/ H^+ antiporter (NhaA) (Zuber *et al.*, 2005); and, the Na^+/Proline transporter (PupP) (Zhou *et al.*, 2004). However, this approach was problematic in the reconstitution and characterization of LacY: even the best reconstitutions contained only small amounts of protein incorporated into the proteoliposomes (Fig. 3A), and no measurable transient currents were observed. In addition, big protein aggregates appeared in some of the freeze-fracture images (data-not-shown).

The transition between micelles to vesicles can also be achieved by rapid dilution of the mixed micelles in detergent-free buffer (Jiskoot *et al.*, 1986; Ollivon *et al.*, 1988; Schurtenberger *et al.*, 1984). Due to its high critical micelle concentration, octylglucoside (OG) is usually the detergent of choose (Garcia-Celma *et al.*, 2009; Jiskoot *et al.*, 1986). However, LacY presents a higher stability in detergent micelles of n-Dodecyl-β-D-maltoside (DDM) than in detergent micelles of OG. To circumvent this difficulty, LacY was purified in DDM and incubated during 5 minutes with a mixture of lipids and OG. Afterwards, rapid dilution was applied ensuring the incorporation of functional active LacY into proteoliposomes. LacY proteoliposomes were finally concentrated by ultracentrifugation and freeze-fracture images were taken from the proteoliposomes reconstituted at lipid to protein rations (LPR;weight/weight) of 10 (Fig. 3B) and 5 (Fig. 3C).

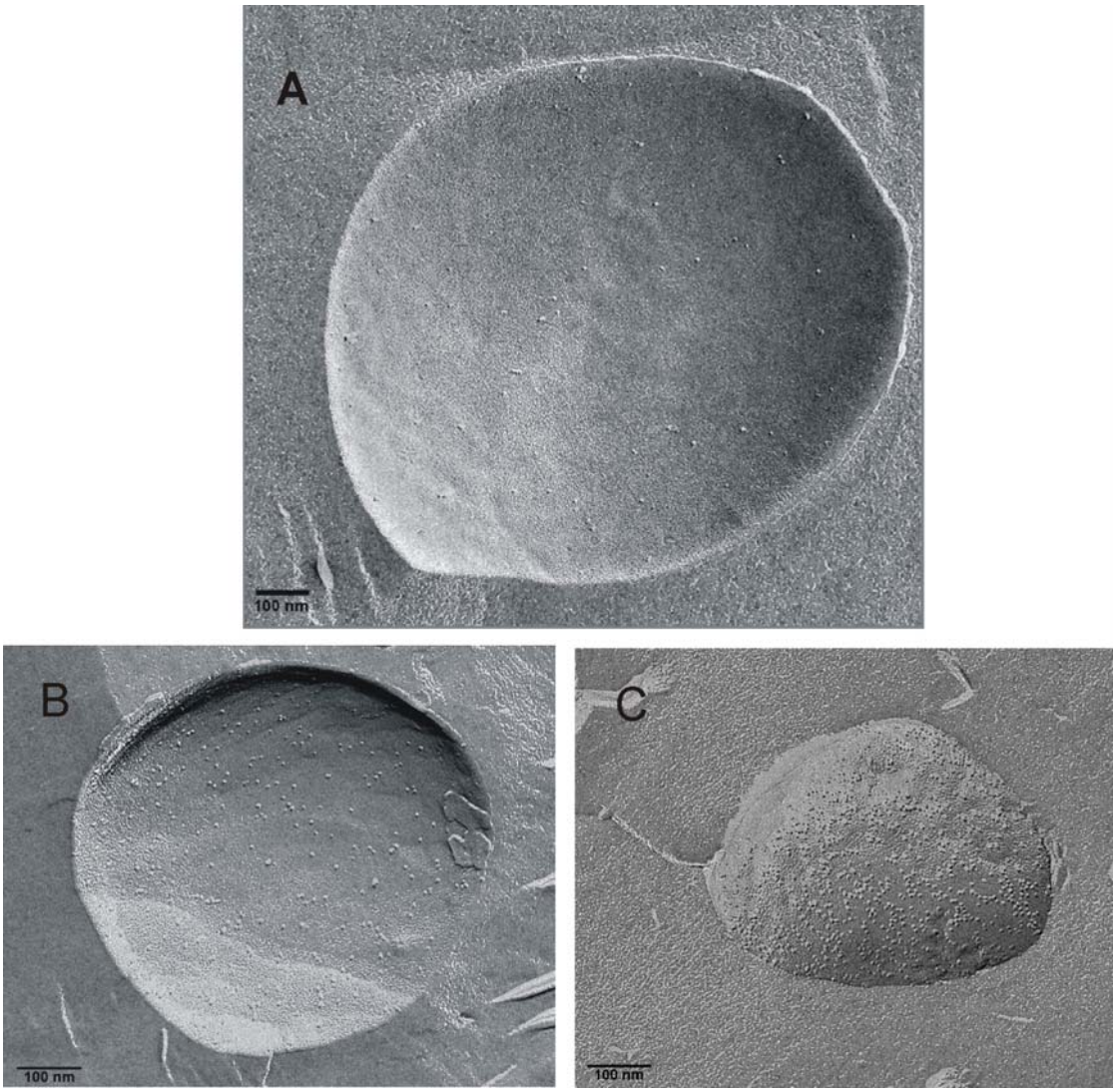

Fig. 3. Freeze-fracture images of LacY proteoliposomes.

LacY was reconstituted at a lipid to protein ratio (LPR) of 10 (weight/weight) by means of the bio-beads (***A***) and rapid dilution (***B***) procedures. In addition, LacY was reconstituted at LPR of 5 by means of the rapid dilution procedure (***C***). The freeze-fracture micrographs of the reconstituted LacY proteoliposomes are courtesy of Dr. Winfried Hasse. The purified LacY was provided by the laboratory of Prof. Dr. H. Ronald Kaback.

Surprisingly, although random orientation of the reconstituted transporters into proteoliposomes is expected *a priori*, the four reconstituted bacterial secondary active transporters investigated with the SSM-based electrophysiology insert into the liposomes in nearly perfect unidirectional orientation: MelB (Meyer-Lipp *et al.*, 2006) and PupP (Jung *et al.*, 1998) are inside-out oriented (ISO) while NhaA (Zuber *et al.*, 2005) and LacY (Herzlinger *et al.*, 1984) are right-side-out (RSO) oriented. This

unidirectional orientation is critical for the analysis of the structure-function relationships of the reconstituted transporters.

3. Analysis of the Transient Currents

3.1. The Measured Output Current does not directly correspond to the Current generated by the Transporter.

Application of a substrate concentration jump to LacY or MelB proteoliposomes immobilized on a SSM-electrode results in transient currents (see sections 5 and 6), which are recorded through the measuring device (Fig. 4A). The measured output current I(t) differs from the current generated by the immobilized transporters $I_T(t)$ due to two effects: (i) the measuring device distorts $I_T(t)$; (ii) $I_T(t)$ depends on the time course of the surface substrate concentration. To discuss these two effects independently, a model current will be introduced $I_{Model}(t)$, which represents the current generated by the transporters after a step substrate concentration jump.

First, the effect of the measuring device will be discussed considering that the current generated by the transporters is triggered by a step substrate concentration jump $I_{Model}(t)$. The effect of the measuring device will be described as a system of differential equations that converts the model current $I_{Model}(t)$ into the output current of the circuit $I_{Circuit}(t)$. Please note that $I_{Circuit}(t)$ is defined as the response of the measuring device to $I_{Model}(t)$, not the response to $I_T(t)$. Additionally, two limiting cases will be considered for $I_{Model}(t)$. Second, the time course of the surface substrate concentration will be introduced through the transfer function of the system f(t), which relates $I_T(t)$ with $I_{Model}(t)$ by means of a convolution operation.

3.2. The Measuring Device

The electrogenic activity of the transporter (LacY or MelB) gives rise to a current which is directly proportional to the amount of transporters incorporated into proteoliposomes N_T and the number of proteoliposomes immobilized on the SSM-electrode N_P. The current generated by the transporters after a step substrate concentration jump $I_{Model}(t)$ is coupled to the measuring device (Fig. 4A) via the equivalent circuit (Fig. 4B), which distorts $I_{Model}(t)$ and converts it into $I_{Circuit}(t)$.

The equivalent circuit is composed of three membranes, each represented by a certain conductivity *G* and capacitance *C* (Fig. 4B): the uncovered part of the SSM (G_u and C_u); the proteoliposome membrane (G_p and C_p); and the membrane between the gold electrode and the interior of the proteoliposomes (G_m and C_m). An external

voltage could be applied through the voltage source (V_{Ext}). The uncovered parts of the SSM would contribute, if any, to a certain stationary current. As the currents are analyzed with respect of the base line, the equivalent circuit shown in Fig. 4B can be reduced to Fig. 4C (Bamberg *et al.*, 1979; Fendler *et al.*, 1993; Herrmann & Rayfield, 1978).

An external voltage could be applied through the voltage source (V_{Ext}). To test the effect of V_{Ext} on the protein activity, LacY proteoliposomes were allowed to adsorb to the SSM, and the transient currents triggered by 50 mM lactose concentration jumps were investigated in the absence or presence of V_{Ext} (Fig. 5). The only effect of the external voltage was a small stationary current (not shown on the figure, ~30pA), which can be corrected with the "Offset Nulling" of the amplifier or during data analysis. Neither the magnitude nor the time constant of the transient currents relative to the baseline were affected by the application of an external voltage (Fig. 5). Probably, the external voltage drops mainly in the membrane between the gold electrode and the interior of the proteoliposome and not on the proteoliposome membrane, which implies that $G_m << G_p$. Furthermore, this experiment also shows one of the present limitations of the SSM-based electrophysiology: the lack of control over the voltage on the proteoliposome membrane.

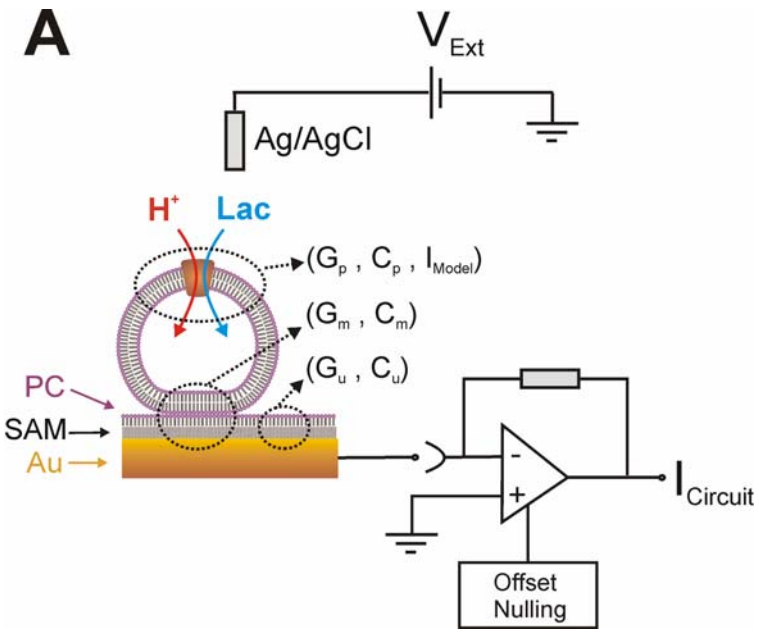

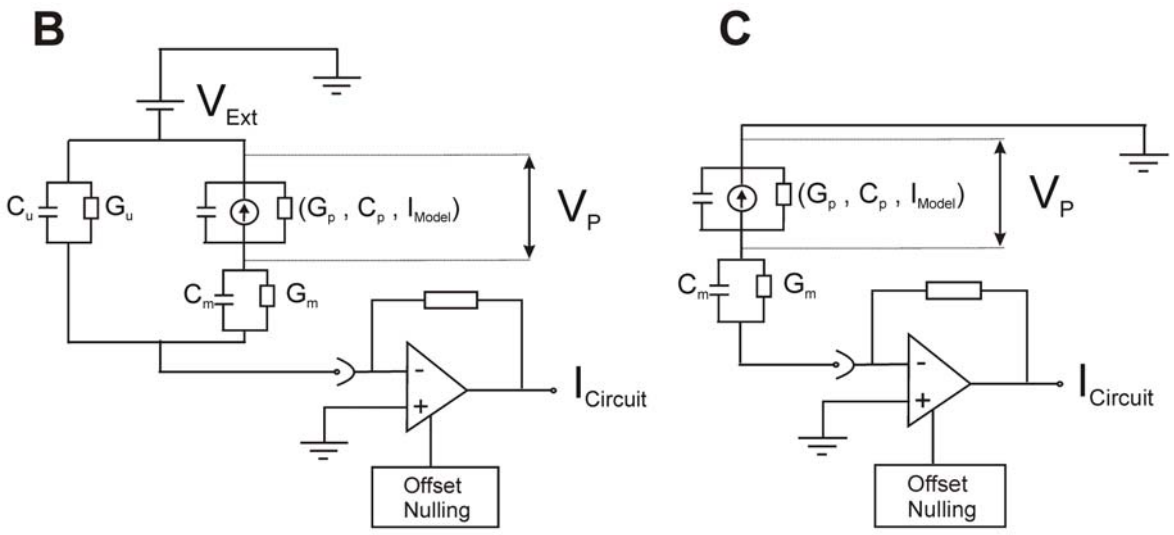

Fig. 4. Measuring device and equivalent circuit.

(***A***) The solid-supported membrane (SSM) is composed of a self-assembled monolayer (SAM) of octadecanethiol and a lipid monolayer of diphytanoyl-phosphatidylcholine (PC). The equivalent circuit consists on three membranes, each represented by a certain conductivity G and capacitance C: the uncovered part of the SSM (G_u and C_u); the proteoliposome membrane (G_p and C_p); and the membrane between the gold electrode and the interior of the proteoliposomes resulting from the adsorption of the proteoliposomes on the surface of the SSM (G_m and C_m). The external voltage source is represented by V_{Ext}. The response of the measuring device to the current generated by the transporter after a step substrate concentration jump is represented by $I_{Circuit}$, and the voltage on the proteoliposome membrane by $V_p(t)$. (**B**) Equivalent circuit of the measuring device described in (***A***). (***C***) As the currents are analyzed with respect to the base line, the equivalent circuit in (***B***) can be simplified to (***C***) (Bamberg *et al.*, 1979; Fendler *et al.*, 1993; Herrmann & Rayfield, 1978).

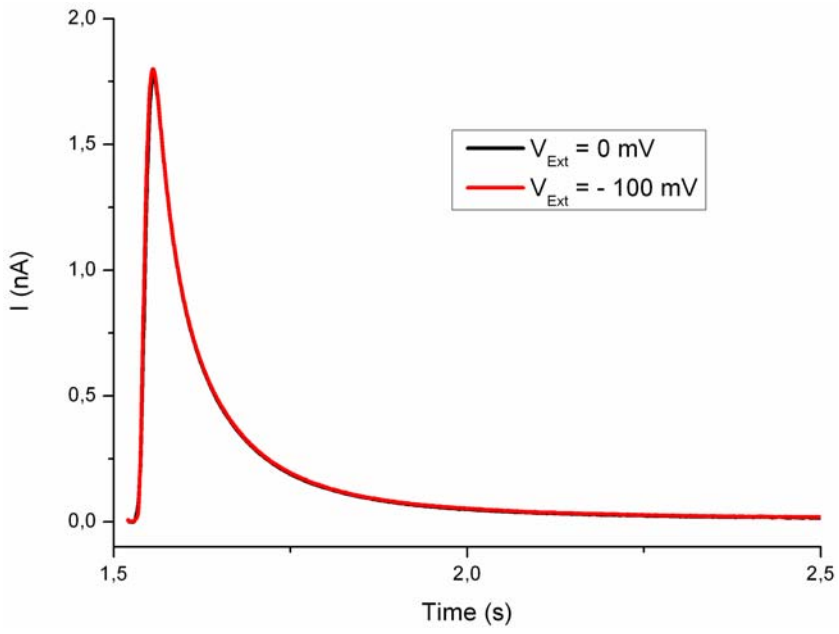

Fig. 5. Effect of the potential between the electrodes on the activity of LacY.

LacY proteoliposomes absorbed to a SSM were investigated at different external constant voltages V_{Ext}. The black trace was recorded in the absence of applied voltage (V_{Ext} = 0 mV), while the red trace was obtained in the presence of voltage V_{Ext} = - 100 mV and was baseline corrected (~30pA). As shown in the figure, the magnitude the kinetics of the transients are independent of the applied voltage, indicating that the voltage V_{Ext} does not drop on the proteoliposome membrane.

The differential equations describing the circuit are (Bamberg *et al.*, 1979; Fendler *et al.*, 1993; Herrmann & Rayfield, 1978):

$$-\frac{dV_p}{dt} = \frac{1}{C_m + C_p} \times I_{Model}(t) + k_0 \times V_p$$
$$-\frac{1}{C_m} \times I_{Circuit}(t) = \frac{dV_p}{dt} + \frac{G_m}{C_m} \times V_p \qquad \text{(Eq. 1)}$$

$$\text{with } k_0 = \frac{G_m + G_p}{C_m + C_p} \qquad \text{(Eq. 2)}$$

The voltage on the proteoliposome membrane is represented by $V_p(t)$ and k_0 is the reciprocal system time constant. As the current $I_{Model}(t)$ starts after activation of the transporters, which takes place at t = 0, the system of differential equations can be solved using the boundary condition $V_p(0) = 0$. To better understand the effect of the equivalent circuit, two limiting cases will be considered for the current generated by the transporter after a step substrate concentration jump $I_{Model}(t)$:

3.2.1. Continuous Electrogenic Transport Activity

Here, we will consider that the current $I_{Model}(t)$ is only due to the continuous electrogenic transport activity of the transporter, and it depends linearly with respect to $V_p(t)$. This limiting case was already considered in the interpretation of the transient currents generated by bR when purple membrane fragments were absorbed to a BLM (Bamberg *et al.*, 1979; Herrmann & Rayfield, 1978). Here, the current generated by the transporter after a step substrate concentration jump $I_{Model}(t)$ is represented by:

$$I_{Model}(t) = N_p \times N_T \times I_{T0} \times (1 - V_p(t)/V^*) \qquad \text{(Eq. 3)}$$

The current generated per transporter I_{T0} is the product of the charge translocated per turnover and the turnover. V* is a constant which couples $I_{Model}(t)$ and the

potential on the proteoliposome membrane $V_p(t)$ in a linear way. As derived in (Bamberg *et al.*, 1979), the response of the measuring device is represented by:

$$I_{Circuit}(t) = N_p \times N_T \times I_{T0} \times \left[\beta + (\alpha - \beta) \times Exp\left(-t \times k_0^{'}\right)\right] \quad \text{(Eq. 4)}$$

$$\alpha = \frac{C_m}{C_m + C_p} \quad \text{(Eq. 5)}$$

$$\beta = \frac{G_m}{G_m + G_p + I_{T0}/V^*} \quad \text{(Eq. 6)}$$

$$k_0^{'} = k_0 + N_T \times \frac{I_{T0}}{V^* \times (C_m + C_p)} \quad \text{(Eq. 7)}$$

The reciprocal system time constant k_0 was defined in Eq. 2. As shown in Eq. 4, $I_{Circuit}(t)$ is a transient current that decays with a reciprocal time constant k'_0, which depends on the current generated per transporter I_{T0} and the amount of transporters incorporated into proteoliposomes N_T (Eq. 7). An increase in N_T results in transient currents of higher magnitude and faster decay (Garcia-Celma *et al.*, 2009; Zuber *et al.*, 2005). Furthermore, in this limiting case the measured peak current can be approximated to I(0) (Zuber *et al.*, 2005), which is directly proportional to the turnover (Eq. 4). Consequently, an increase in the turnover results in transients with higher peak currents and faster decay towards the base line (Bamberg *et al.*, 1979; Garcia-Celma *et al.*, 2009).

3.2.2. Initial Charge Displacements

In this limiting case, $I_{Model}(t)$ is only due to initial charge displacements and no continuous electrogenic transport activity takes place. This initial charge displacement results from one or several electrogenic partial reactions. For simplicity, we will consider that there is only one electrogenic partial reaction although this formalism is easily generalized for an infinite number of electrogenic partial reactions (Fendler *et al.*, 1993). Due to the absence of continuous electrogenic transport, the voltage generated by the electrogenic partial reaction in the proteoliposome membrane can be approximated by zero. Under this assumption, $I_{Model}(t)$ and $I_{Circuit}(t)$ are represented by (Borlinghaus *et al.*, 1988; Fahr *et al.*, 1981; Fendler *et al.*, 1993):

$$I_{Model}(t) = N_p \times N_T \times A \times Exp\left(-t \times k\right) \quad \text{(Eq. 8)}$$

$$I_{Circuit}(t) = N_p \times N_T \times A \times \alpha \times \left[a_1 \times Exp\left(-t \times k\right) - a_0 \times Exp\left(-t \times k_0\right)\right] \quad \text{(Eq. 9)}$$

$$a_1 = \frac{k - G_m/C_m}{k - k_0} \qquad \text{(Eq. 10)}$$

$$a_0 = \frac{k_0 - G_m/C_m}{k - k_0} \qquad \text{(Eq. 11)}$$

k_0 and α are defined in Eq. 2 and Eq. 5, respectively, and A is an amplitude. Here, the time curse of $I_{Circuit}(t)$ is characterized by two exponentials with opposite amplitudes. Importantly, the rate constant of the electrogenic reaction k is, in this case, unaffected by the equivalent circuit (Fendler *et al.*, 1993).

In general, a mixed situation between the two limiting cases is to be expected. However, it will be shown in sections 5 and 6 that the equations derived above represent a useful benchmark for the analysis of the electrogenic activity of the investigated transporters. Furthermore, these equations allow us to identify the properties that a SSM (and also a BLM) should fulfill to be utilized as capacitive electrodes. As in both limiting cases the initial input current is proportional to α (Eq. 4 and Eq. 8), which has a value between zero ($C_m = 0$) and one ($C_m >> C_p$), a situation where $C_m >> C_p$ is desirable. In addition, a low G_m is required to reduce the background noise current, which leads to masking of the signal. As shown by Florin and Gaup (Florin & Gaub, 1993), a SSM presents high specific capacitance and low specific conductance, allowing the use of the SSM as a capacitive electrode.

3.3. Analysis of the Charge Translocated in an Ion Concentration Jump.

Prior to the investigation of a transporter, important information about the time course of the substrate concentration rise time at the surface of the SSM can be obtained by utilizing ion concentration jumps. Application of an ion concentration jump results in a transient current that is integrated to obtain the displaced charge Q(t), which can be fitted with a semi-empirical model function (see sections 4 and 5):

$$Q(t) = Q_0 \frac{(t - t_0)^3}{(t - t_0)^3 + \tau^3} \qquad \text{(Eq. 12)}$$

The delay t_0 and the rise time τ represent the time needed for the solution to flow from the terminal valve to the SSM and the rise time of the translocated charge, respectively. Q_0 represents the total charge displacement generated when ions with different propensities to “bind” to the membrane are exchanged, and this parameter is strongly dependent on the particular ion concentration jump (see section 4). As it

will be discussed later, the time course of Q(t) reflects the time course of the substrate surface concentration (see section 5). Therefore, the rise time τ represents, indeed, the rise time of the substrate surface concentration and the electrogenic activity of the transporter starts at $t = t_0$.

3.4. The Time Resolution.

In section 3.2, the current resulting from the electrogenic activity of the transporter was estimated assuming a step substrate concentration jump. Experimentally, however, the rise time of the substrate surface concentration (the rise time τ) differs from zero, which limits the time resolution of the experiment. For a linear time-invariant system, the limited time resolution of a measurement can be described by a transfer function f(t) (Varju, 1977). In this case, the current generated by the transporter $I_T(t)$ results from the convolution between $I_{Model}(t)$ and the transfer function of the system f(t):

$$I_T(t) = \int_{t_0}^{t} f(t-t')I_{Model}(t')dt' \qquad \text{(Eq. 13)}$$

The time needed for the solution to reach the SSM surface is represented as t_0, and f(t) corresponds in our case to the derivative of Eq. 12 (see also section 5).

As discussed in section 3.2, the electrogenic activity of the transporter may be due to initial charge displacements and/or continuous electrogenic transport. Considering that the electrogenic activity is only due to initial charge displacements (see section 3.2.2), the effect of the measuring device can be represented by a linear time-independent operator. As the convolution also constitutes a linear time-independent operation, these mathematical operators can be interchanged. In this case, therefore, it is possible to calculate the measured output current I(t) from the convolution between $I_{Circuit}(t)$ and the transfer function f(t).

In case that some continuous electrogenic transport activity takes place, a certain voltage will be built up in the proteoliposome membrane. However, as long as the effect of this build-up potential on the rate constants of the electrogenic partial reactions is negligible, it is still possible to recover these rate constants from the measured output current I(t) through the convolution between $I_{Circuit}(t)$ and the transfer function f(t).

4. Specific Anion and Cation Binding to Lipid Membranes

4.1 Introduction

Lipid membranes represent the most important biological interface. They not only contain the whole transport and sensory machinery of the cell but also are important for a large number of mechanical tasks like cell adhesion, fusion, growth and migration. Here, the ionic composition of the aqueous medium plays a significant role essentially modulating the properties of the lipid membrane like the surface potential (Eisenberg *et al.*, 1979), the dipole potential (Clarke & Lupfert, 1999), the structure and dynamics of the lipid molecules (Sachs *et al.*, 2004; Zhao *et al.*, 2007) or intermembrane forces (Petrachet *et al.*, 2006), the transition from micelles to vesicles in surfactants (Renoncourt *et al.*, 2007) and the swelling of vesicles (Claessens *et al.*, 2004). Furthermore, the ionic composition of the aqueous medium also affects the critical micelle concentration of ionic and non-ionic surfactants (Kameyama *et al.*, 1997; Miyagishi *et al.*, 2001), which may influence the process of reconstitution membrane proteins into proteoliposomes.

A convenient model system for a biological membrane is a solid-supported lipid membrane (SSM). SSMs have been extensively used as capacitive electrodes to characterize electrophysiologically several transporters from eukaryotes or prokaryotes either reconstituted into proteoliposomes or in native membranes (reviewed in (Schulz *et al.*, 2008)). Furthermore, the bare SSM, i.e., the alkanethiol/lipid hybrid membrane, exhibit physical properties very similar to free-standing lipid membranes (BLM) such as comparable lipid mobility, conductivity and capacitance (Florin & Gaub, 1993; Seifert *et al.*, 1993). The thickness determined previously by surface plasmon spectroscopy of 4.1 nm (Florin & Gaub, 1993) agrees within the experimental error with the dimensions expected for an octadecyl mercaptan/diphytanoyl-phosphatidylcholine hybrid bilayer suggesting a conventional bilayer-like order of the lipid layer. Taken together all experimental evidence available argues for a lipid surface very similar to that of a free standing lipid membrane (BLM).

Here, the first systematic study about the interaction between ions (cations and anions) and lipid membranes investigated on a SSM is presented. Transient currents were observed via the supporting gold electrode when solutions of different ion composition are exchanged at the surface of the SSM. The displaced charge, obtained from the numerical integration of the transient currents, represent the relaxation of the different ions in their respective equilibrium positions. Ions are

characterized relative to a reference ion, which was Na^+ for cations and Cl^- for anions. A positive charge displacement after a cation exchange or a negative charge displacement after an anion exchange means that the average equilibrium position of the ions is closer to the underlying electrode than that of Na^+ (for cations) or of Cl^- (for anions) and/or that more ions reside in this position. This is frequently called 'binding' and we will use this term in the following, keeping in mind that it can be anything between a diffuse accumulation in or very close to the lipid headgroup up to specific binding at a well defined binding site (Leontidis, 2002). Ions will be classified as kosmotropic (water-structure maker) or chaotropic (water-structure breaker). These expressions derive from the Jones-Dole viscosity B-coefficients (Jones & Dole, 1929) and were first introduced by Frank and Evans in 1945 (Frank & Evans, 1945).

4.2 Results

4.2.1. Transient Currents generated by Ion Concentration Jumps

In the solution exchange process two solutions of different ionic composition were applied to the surface, the test solution and the reference solution. The test solution contained the salt of interest and the reference solution (unless otherwise specified) contained NaCl. To generate pure cation concentration jumps a constant Cl^- concentration was used throughout the experiment, i.e. for a monovalent cation X the test solution contained the same concentration of XCl as the reference solution NaCl. For a divalent or trivalent cation the concentrations were 1/2 and 1/3 of the NaCl concentration. For pure anion concentration jumps the Na^+ concentration was kept constant using an equivalent procedure. This guaranteed that the observed effect was only due to the anion or the cation to be investigated. A slightly different protocol was used for uncompensated salt concentration jumps where the reference solution contained only buffer.

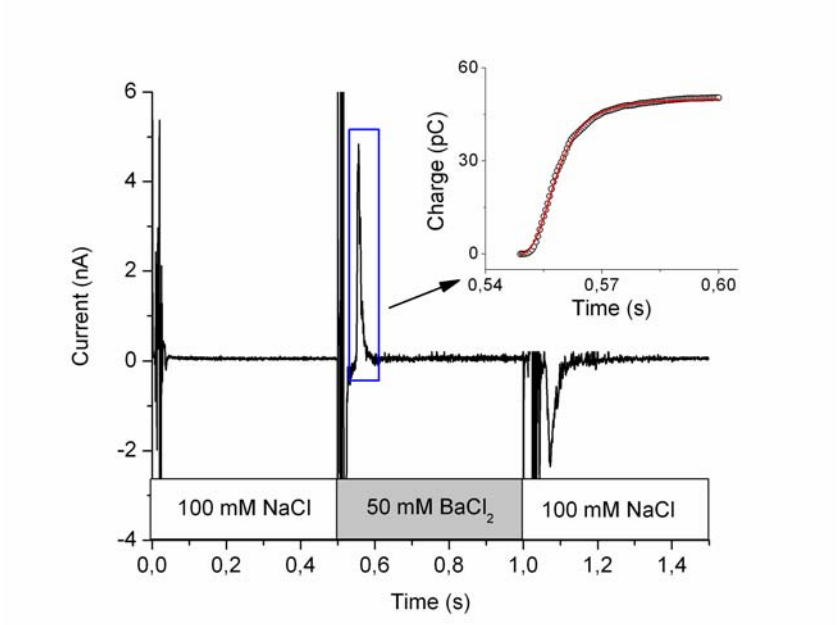

Fig. 6. Flow protocol and analysis of the translocated charge in an ion concentration jump.

As an example for the recorded transient currents the charge translocation after a $BaCl_2$ concentration jump on a PC membrane is shown. The integrated signal (circles) with a fit according to Eq. 12 (red line) is shown in the insert. All solutions were buffered in 10 mM Tris/Hepes at pH 7.0. The reference solution contains 100 mM of NaCl while the test solution 50 mM $BaCl_2$.

Fig. 6 shows a typical transient current after an ion concentration jump. The example in Fig. 6 represents a 50 mM Ba^{2+} concentration jump (or more precisely a solution exchange of 100 mM NaCl vs. 50 mM $BaCl_2$) at an SSM formed from diphytanoyl-phosphatidylcholine (PC). The recorded transient current is integrated and fitted according to Eq. 12. From the fitting, the total charge displacement Q_0 is obtained.

4.2.2. Dependence of the Translocated Charge on the Nature of the Applied Cation or Anion.

100 mM salt concentration jumps of different cations and anions generated transient currents that were strongly dependent on the nature of the applied ion (Fig. 7). In the case of the cations the data show an approximately linear dependence on the hydration energy forming three isolated patches for monovalent, divalent and trivalent cations. The translocated charge yields the following series (for PC): La^{3+} > Ca^{2+} > Mg^{2+} > Ba^{2+} > Sr^{2+} > Li^{+} > Na^{+} > K^{+}, Rb^{+}, Cs^{+}. The anions show the reverse behavior with respect to the free energy of hydration. Here the following series for the translocated charge is obtained (for PC): ClO_4^- > SCN^- > I^- > NO_3^- > Br^- > F^- > Cl^- = SO_4^{2-}. For monooleoyl-glycerol (Mono) the same general trend is obtained although not all positions of the individual ions are conserved.

4.2.3. Interaction of the Different Cations and Anions with Different Lipid Headgroups.

To test the influence of the chemical nature of the lipid headgroup we determined the charge translocation using different lipids in the hybrid lipid bilayer on the solid-support. Dioleoyl-trimethylammonium-propane (DOTAP) is a lipid with a positively charged headgroup, diphytanoyl-phosphatidylcholine (PC) is zwitterionic, monooleoyl-glycerol (Mono) is uncharged and dioleoyl-phosphatidylglycerol (DOPG) carries a negative charge. All lipids were prepared in n-decane; Mono was also used in squalene (Mono-squal) to assess the influence of the solvent. For a broader scan of different surfaces two cations and two anions were chosen and were applied at a concentration of 100 mM: the chaotropic ions K^+, Br^- and ClO_4^-, and the kosmotropic cation La^{3+}. As expected, cations generate a larger charge displacement at a negative surface while anions do that at a positive one. The zwitterionic PC represents an intermediate case and the uncharged Mono shows the least effect. It is, however, interesting to note that cations as well as anions interact with significant

efficiency with the lipid Mono although it does not have neither $N(CH_3)_3^+$ nor PO_4^- groups. This observation rules out the possibility of specific binding to those groups as a major cause of the interaction.

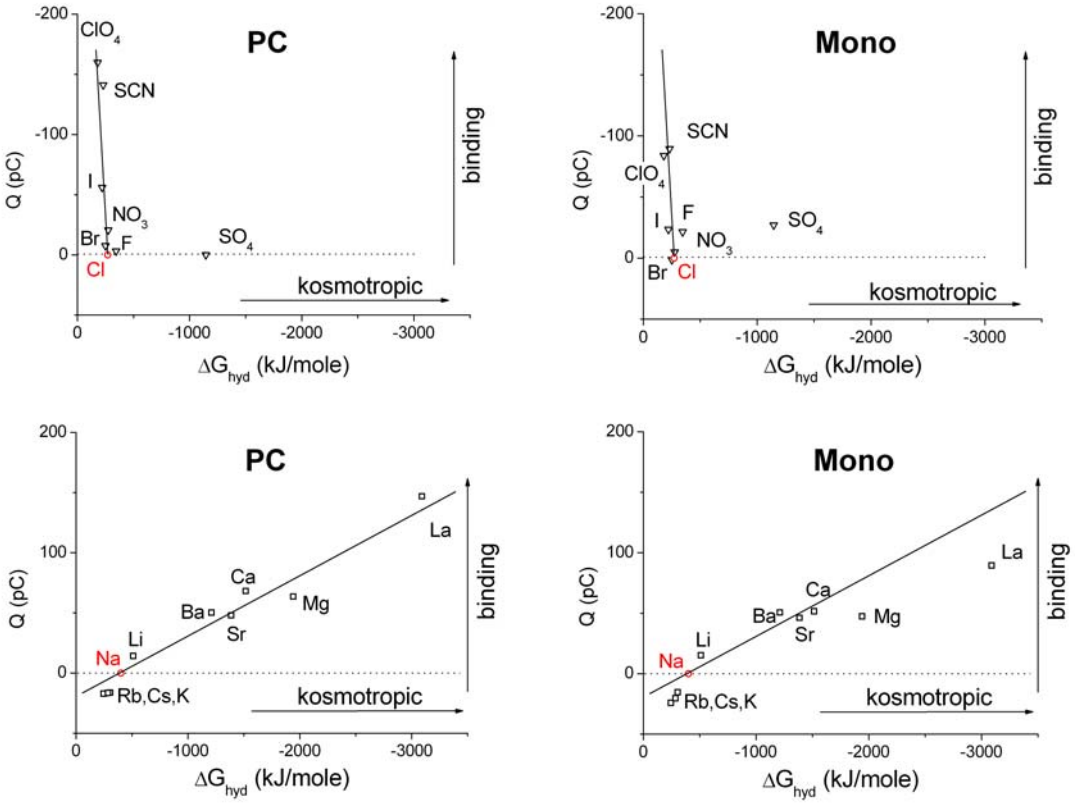

Fig. 7. Charge displacements of different cations and anions on a PC and a Mono membrane.

The figure shows the charge translocated by different anions (open triangles) and cations (open squares) on a diphytanoyl-phosphatidylcholine (PC) and a Monoolein (Mono) membrane. The open red circle indicates the reference ion, which was Na^+ for cations and Cl^- for anions. Ions are classified according to their Gibbs free energies of hydration ΔG_{hyd}.

4.2.4. Concentration Dependence of the Translocated Charge.

Since the translocated charge was strongly ion concentration dependent we determined the saturation behavior for La^{3+}, Mg^{2+}, K^+, ClO_4^- and Br^- on a PC surface. This allowed us to determine an apparent dissociation constant K_D^{app} for the respective ion. The reference solution contained always NaCl at a concentration to keep the Cl^- concentration constant in the cation concentration jumps and the Na^+ concentration constant in the anion concentration jumps (see above). The data were

analyzed using a hyperbolic function $Q_0=Q_0^{max.}c/(c+K_D^{app})$ where *c* is the ion concentration.

4.2.5. Uncompensated Salt Concentration Jumps.

Here the test solution contained buffer plus the indicated salt and the reference solution only buffer. The transient currents recorded in this case comprise contributions from cation and anion. They are strongly dependent on the applied salt. The currents were integrated to yield the translocated charge. From the studied salts, NaSCN, $NaClO_4$ and NaI gave rise to negative charge displacements indicating that the SCN^-, ClO_4^- and I^- anions associate more tightly with the membrane than the accompanying cation Na^+. As for the chlorides always a positive charge displacement is found increasing in the same order as in Fig. 7, $K^+ < Na^+ < Li^+ < La^{3+}$. Here the cations array closer to the membrane than the anions.

4.3. Discussion

4.3.1. Chaotropic Anions are attracted to the Lipid Interface.

If anions are classified according to their free energy of hydration ΔG_{hyd} (Marcus, 1991) a well defined series for the translocated charge is obtained where the anion with the smallest $-\Delta G_{hyd}$ yields the largest negative charge translocation. This means the most hydrophobic or the most chaotropic anion binds best to or at the lipid. These results exactly fit the series obtained for the influence of anions on the dipole potential of PC liposomes (Clarke & Lupfert, 1999). Clarke and Lüpfert explain the reduction of the dipole potential by binding of the chaotropic anion at the positive side of the dipole deep in the lipid headgroup. This is in agreement with our results, which show a large negative charge translocation upon binding of chaotropic anions like ClO_4^-.

4.3.2. Kosmotropic Cations are attracted to the Lipid Interface.

Interestingly, for cations the inverse series is obtained with respect to $-\Delta G_{hyd}$. We found that the higher $-\Delta G_{hyd}$ is, the larger the translocated charge. This means the most hydrophilic or the most kosmotropic cation binds best. Again, our results agree with those obtained for the effect of cations on the lipid dipole potential (Clarke & Lupfert, 1999) but also with an early study of the adsorption of cations to phosphatidylserine liposomes (Eisenberg, 1979). In consequence, we find a more attractive potential for kosmotropic than for chaotropic cations.

4.3.3. PC Membranes can be Anion or Cation Selective.

Up to now we have only ranked ion binding within the group of anions or cations. The polarity of the charge displacements after uncompensated salt concentration jumps, however, indicates whether cations or anions bind preferentially to the membrane. These experiments show that a zwitterionic PC surface (no net charge) depending on the specific ion pair can prefer the cation or the anion. In particular, the strongly chaotropic anions (SCN^- and ClO_4^-) have a higher affinity for the membrane than their Na^+ counter ions, while for the chlorides NaCl and KCl the cations bind stronger. This is unexpected because Hofmeister interactions are generally believed to be dominated by anions (Collins & Washabaugh, 1985). Finally, the uncompensated salt concentration jump experiments also rule out that the specific cation effects (Fig. 7)

are brought about predominantly by extraction of tightly bound Cl^- from the surface (yielding a positive charge displacement), rather than binding of the cations.

4.3.4. Headgroup Charges make a Difference.

The most abundant lipid in an average mammalian cell membrane is phosphatidylcholine (45 – 55%), which comprises a negatively charged phosphate (PO_4^-) group and a positively charged ammonium ($N(CH_3)_3^+$) group. But also the charged sites of many lipid membrane constituents are phosphate and ammonium groups. Consequently, PC is a good prototype lipid for a study of the interaction of ions with a biological membrane. To address the question how these groups determine the interaction of ions with the SSM surface, a membrane composed of the zwitterionic PC is compared to a membrane composed of a lipid with no charged groups (Mono). Additionally, net charged lipids, like the positively charged DOTAP or the negatively charged PG, were investigated.

From the experiments using lipids with different headgroups a clear tendency emerges that cations preferentially bind to the negatively charged PG while anions prefer the positively charged DOTAP headgroup. This is by itself not surprising and the standard Gouy-Chapman electrostatic theory describes accumulation of positive ions at negatively charged surfaces and vice versa. But we have to bear in mind that the observed charge translocations represent the difference to the reference ions Na^+ and Cl^-. In the Gouy-Chapman formalism all ions of identical valency yield the same result and there should be no difference between ClO_4^- and Cl^- or between Na^+ and K^+. However, the effect of charged headgroups could be explained by the increased local cation concentration at the DOPG surface and the increased local anion concentration at the DOTAP surface predicted by the electrostatic interaction. It cannot, however, explain the more efficient binding to zwitterionic PC as compared to uncharged Mono, which is more prominent for the anions than for the cations (Fig. 7). Taken together this seems to be suggestive of a mechanism different from pure electrostatics which modifies ion binding at different lipid headgroups.

4.3.5. Interaction Mechanism of Anions and Cations with a Lipid Interface.

Different physicochemical parameters of the ions like the Gibbs free energy of hydration chosen in this publication have been taken into account to rationalize the ionic sequences. Unfortunately many of these parameters are correlated themselves

(Kunz *et al.*, 2004) so that these procedures are of little help to identify the dominating forces acting between the interface and the ion. It has recently been shown that dispersion forces have to be taken into account at physiological ion concentrations where electrostatic interactions are screened (Kunz *et al.*, 2004) and may be responsible for Hofmeister effects (Bostrom *et al.*, 2002). The relevant parameter determining dispersion forces on ions is the ionic polarizability, which is large for large chaotropic ions (Kunz *et al.*, 2004; Leontidis, 2002) and would predict preferential binding of both, chaotropic cations and anions, in disagreement with our experimental results.

An ion binding mechanism according to the 'principle of matching water affinities' has been proposed by Collins (Collins, 2004; Collins, 2006) which predicts binding of chaotropic ions to chaotropic surface groups and kosmotropic ions to kosmotropic surface groups. Since PO_4^- is strongly kosmotropic (and the putative binding site for cations) and $N(CH_3)_3^+$ is chaotropic (and the putative binding site for anions) this would explain our results on PC. But it cannot account for the fact that a lipid without these residues (Mono) shows the same cation and anion binding series. And it cannot explain either why for various phosphate compounds as well as other anionic surfactants the reversed cation series is found (see. e.g. (Haverd & Warr, 2000) and the literature cited herein). In contrast to these compounds, however, in the present study the phosphate group is chemically linked to ammonium or glycerol groups or consists only of a glycerol headgroup (Mono), and, therefore, the influence of the phosphate group alone is not decisive. We believe, in agreement with the results of Jungwirth and co-workers (Jungwirth & Tobias, 2001; Vrbka *et al.*, 2004) that it is necessary to precisely describe the role of the component that is present in larger excess, namely water. To understand the specific ion effects, it is very probably not sufficient to describe the water as a bulk or as hydration water. The geometry of the water molecules around the ions and headgroups very probably makes the difference. Advances in this direction come from recent molecular dynamics studies of zwitterionic PC membranes (Bockmann *et al.*, 2003; Pandit *et al.*, 2003; Sachs *et al.*, 2004; Sachs & Woolf, 2003) and negatively (Mukhopadhyay *et al.*, 2004; Zhao *et al.*, 2007) or positively (Gurtovenko *et al.*, 2005) charged lipid membranes. For example, simulation of PC membranes show that Cl^- binds slightly weaker than Na^+ (Bockmann *et al.*, 2003; Pandit *et al.*, 2003) and that chaotropic anions bind better than kosmotropic ones to the lipid headgroups (Sachs *et al.*, 2004; Sachs & Woolf, 2003). Both results agree with our experiments.

5. Rapid Activation of MelB

5.1. Introduction

For the analysis of dynamic properties of bacterial secondary active transporters time resolved experiments are essential which probe the pre-steady-state of the system. This requires a rapid perturbation of the initial state of the transporter. Such a perturbation could be achieved, for example, by a concentration jump of an enzymatic ligand or substrate. In the case of surface immobilized enzymes a rapid solution exchange is difficult because of the unstirred layer at the surface (Barry & Diamond, 1984). An additional complication arises from the fact that virtually no technique is available that allows the rapid time resolved analysis of the surface concentration of substrate molecules. However, quantitative temporal information concerning the surface substrate concentration rise is a prerequisite for a proper interpretation of the measured signals as well as for the optimization of the fluidic system.

Here, the transient currents obtained after an ion concentration jump are used as a real-time probe of the local ion concentration at the lipid surface. This makes ion concentration jumps an interesting tool for the analysis of the time course of solution exchange on the SSM surface and enables exploration of different fluidic configurations. In particular, a novel flow geometry (valve-less diverted geometry) based on the idea of Benjamin Dürk (Dueck, 2006) was developed and applied to reinvestigate a rapid electrogenic reaction induced by sugar binding to a bacterial sugar transporter, the melibiose permease (MelB) from *Escherichia coli*. Sugar binding to MelB in the presence of Na^+ is associated with a charge displacement detected after application of a melibiose concentration jump to MelB proteoliposomes immobilized to a SSM (Ganea *et al.*, 2001; Meyer-Lipp *et al.*, 2004). It was proposed that sugar binding displaces charged amino acyl side chains or reorients electrical dipoles, which may account for this electrogenic reaction. Indeed, sugar binding triggers a conformational transition observed by tryptophan fluorescence spectroscopy (Mus-Veteau & Leblanc, 1996; Mus-Veteau *et al.*, 1995), suggesting an electrogenic conformational transition (Meyer-Lipp *et al.*, 2004). However, kinetic information about both processes to strengthen this assignment was not available so far. In particular, because of the limited time resolution of the SSM set-up used for these experiments, only a lower limit of $k > 50\ s^{-1}$ could be assigned to the charge displacement (Ganea *et al.*, 2001; Meyer-Lipp *et al.*, 2004). Here, this reaction is

reanalyzed using the improved time resolution of the valve-less diverter configuration (Fig. 2B) and an iterative least-squares deconvolution algorithm. These developments allowed for the first time a direct kinetic comparison between electrogenic partial reactions and time-resolved fluorescence changes monitored by stopped-flow spectroscopy in MelB. The stopped-flow experiments were performed by Michela Schlüter and they can be found in (Garcia-Celma *et al.*, 2008).

5.2. Results

5.2.1. Calculation of Delay and Concentration Rise Time in an Analytical Approximation.

The cuvette for rapid solution exchange represents a wall jet configuration. After switching the valve, the fastest streamlines need a time t_0 to reach the surface of the SSM. The delay time t_0 defines the starting point of the concentration jump. Subsequently, the average concentration rises with a rise time τ (see Eq. 12). We will consider two limiting cases: Hagen–Poiseuille flow in a cylindrical tube and plug flow. Hagen–Poiseuille flow has a parabolic velocity profile while in plug flow all fluid elements have the same velocity.

For Hagen–Poiseuille flow in a cylindrical tube (flow rate $\dot{V}$, length x, diameter R) the time dependence of the average concentration can be calculated (Pintschovius & Fendler, 1999) and is taken as the substrate concentration at the surface of the SSM $c_s(t)$:

$$c_S(t) = c_0\left(1 - \frac{\tau_{HP}}{t}\right) \qquad t \geq \tau_{HP} \qquad \text{(Eq. 14)}$$

$$\tau_{HP} = \frac{\pi R^2 x}{2\dot{V}} \qquad \text{(Eq. 15)}$$

Here c_0 is the concentration of an arbitrary substrate in the test solution and, τ_{HP} the substrate surface concentration rise time corresponding to a Hagen–Poiseuille flow. Note that in Hagen–Poiseuille flow delay and concentration rise time are identical:

$$t_{0(HP)} = \tau_{HP} = \frac{\pi R^2 x}{2\dot{V}} \qquad \text{(Eq. 16)}$$

As for the ideal plug flow, the concentration rise time is zero (τ_{PF} = 0) and the delay is given by:

$$t_{0(PF)} = \frac{\pi R^2 x}{\dot{V}} \qquad \text{(Eq. 17)}$$

Additionally, the flow needs to cover a characteristic distance called development length L_e to develop from an initial plug flow to the full Hagen–Poiseuille flow profile (Al-Nassri & Unny, 1980; Raja *et al.*, 2000; Washabaugh & Zahn, 1994). The development length L_e is given by $L_e/2R = 0.06Re$, where Re represents the Reynolds number and R is the diameter. Under the flow conditions of our

experiments, L_e covers a range of 53 ─ 210 mm from the minimal (0.7 ml s^{-1}) to the maximal flow rate (2.5 ml s^{-1}). Therefore, a fully developed Hagen–Poiseuille flow profile is never obtained within the dimensions of our flow pathways, and a mixed profile is to be expected.

5.2.2. Experimental Determination of the Concentration Rise Time.

To measure the rise time of the surface substrate concentration (rise time τ) we took advantage of the fact that a rapid cation or anion exchange at millimolar concentrations generates a transient current at a solid-supported membrane (see section 4). The solution exchange protocol used consisted of the sequential application of a reference and a test solution containing buffer plus 100 mM NaCl and buffer plus 100 mM $NaClO_4$, respectively. The rise time τ is obtained from the fitting of the translocated charge with Eq. 12.

Assuming that the interaction of the salts with the surface is rapid compared to the solution exchange process, the displaced charge can be used as a relative measure of the time dependence of the local ion concentration at the surface of the SSM. To rule out that these dependencies are limited by the kinetics of ion/surface interaction, we determined the rise time τ at a given flow condition and geometry using different concentrations and different ions. The same rise time τ within the error limits was determined using ClO_4^- at concentrations from 1 to 100 mM and for 100 mM ClO_4^-, K^+ and Br^- as well as 50 mM Mg^{2+}. These results confirm that the measured rise time τ is not limited by the kinetics of ion/surface interaction and support the assumption that the charge displacement can be used as a reliable probe for the time course of ion surface concentration.

5.2.3. Influence of the Flow Rate and the Diverter–SSM Distance on the Delay t_0 and the Concentration Rise Time τ.

To identify the limiting factors for the concentration rise time at the surface of the SSM, the rise time was experimentally determinated at several flow rates for three different flow configurations (Fig. 8). These configurations mainly differ in the diverter–SSM distance *x*, which represent the length of the pathway shared between test and reference solutions. For the valve-controlled diverted geometries (x = 44 mm and x = 33 mm), the experimental rise times are somewhat smaller than the theoretical prediction of Eq. 15 (Hagen–Poiseuille). To reduce the distance *x* by one

order of magnitude (x = 3.5 mm), a valve-less diverted geometry was used. This allowed concentration rise times as low as 2 ms (Fig. 8). Here, however, the experiment yielded significantly larger rise times than the theory based on Hagen–Poiseuille flow. Probably, in this time range additional factors become limiting like the valve opening time (< 1 ms) or the acceleration of the fluid (~2 ms).

As for the delay t_0, its experimental value was always larger than the calculated delay t_0 for a Hagen–Poiseuille flow (Eq. 16) and coincides with the result expected for a plug flow (Eq. 17). In addition, the pressure versus flow diagram was clearly non-linear, in disagreement with the prediction from a Hagen–Poiseuille flow.

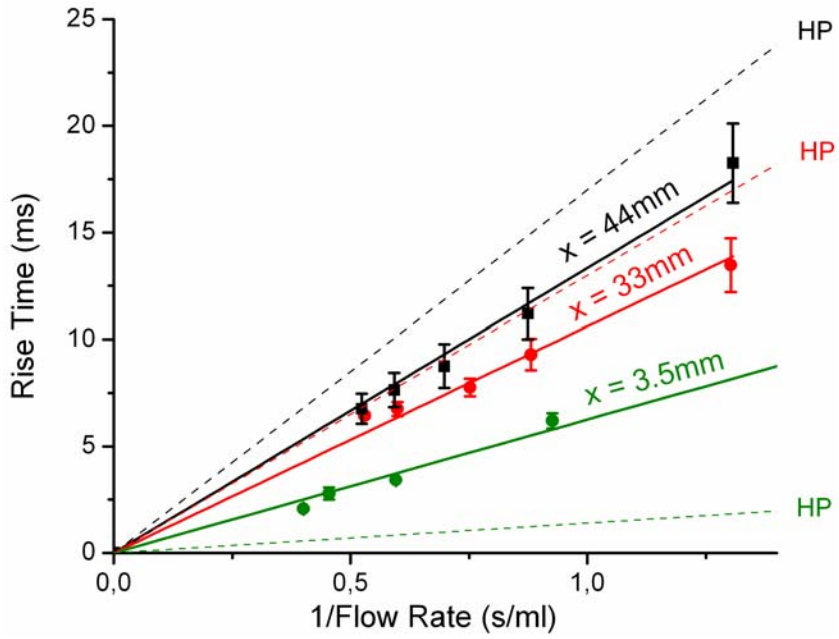

Fig. 8. Concentration rise times for 3 different flow configurations.

The experimentally determined concentration rise time is plotted vs. the reciprocal of the flow rate for three configurations: (i) valve-controlled diverter, Valve V2 = NR161T031, and x = 44 mm (black squares); (ii) valve-controlled diverter, V2 = NR161T031, and x = 33 mm (red circles); (iii) valve-less diverter, V1 = V2 = NR225T011, and x = 3.5 mm (green circles). Tube diameter for all 3 cases d = 1 mm. The concentration rise time τ was determined as described in the text by application of a 100 mM Cl^-/ClO_4^- solution exchange (both solutions were buffered in 50 mM Hepes/Tris at pH 7.0). For statistical analysis, the rise times were determined for three different SSM-electrodes and the error bars represent their standard error (SE). The solid lines are linear fits to the data points. The dashed lines are the theoretical prediction assuming Hagen-Poiseuille flow (see text).

5.2.4. Measurement and Analysis of Charge Translocation in MelB.

The electrogenic activity of MelB can be investigated by adsorbing proteoliposomes to a SSM and applying a substrate concentration jump (Ganea *et al.*, 2001). In the presence Na^+, sugar binding triggers a rapid electrogenic reaction. In previous studies, the value of this rate constant was only estimated to be > 50 s^{-1} due to insufficient time resolution (Ganea *et al.*, 2001; Meyer-Lipp *et al.*, 2004; Meyer-Lipp *et al.*, 2006). This reaction has been re-analyzed using the improved time resolution of the valve-less diverter configuration.

The transient currents recorded after a melibiose concentration jump in the presence and absence of Na^+ are shown in Fig. 9. The dramatic Na^+ dependence of the transient currents demonstrates that they are indeed associated with the enzymatic activity of MelB. In agreement with previous studies, a rising phase followed by a bi-exponential decay towards the base line was observed in both cases (Fig. 9). The fast phase of the decay has been previously assigned to a rapid electrogenic conformational transition triggered by sugar binding, while the slow phase has been assigned to downhill melibiose/Na^+ or melibiose/H^+ symport under conditions of capacitive coupling (Meyer-Lipp *et al.*, 2004). With MelB, we are dealing with an intermediate situation between the two limiting cases described in section 3.2. Here, the response of the capacitive electrode to the current generated by MelB is represented as a bi-exponential decay:

$$I_{Circuit}(t) = A_1 \times Exp\left(-(t-t_0)/\tau_1\right) + A_2 \times Exp\left[-(t-t_0)/\tau_2\right] \qquad \text{(Eq. 18)}$$

The time constant τ_1 reflects a rapid electrogenic conformational transition triggered by sugar binding, and the time constant τ_2 the charging of the proteoliposomes. A_1 and A_2 are the amplitudes of the exponentials, and the current starts at $t = t_0$.

Additionally, the electrogenic response of MelB is affected by the time resolution of the system, which can be described by a transfer function f(t) (Varju, 1977). In our case, the transfer function reflects the time course of the substrate concentration rise time at the SSM surface and it corresponds to the derivative of Eq. 12:

$$f(t) = \frac{3 \times t^2 \times \tau^3}{(t^3 + \tau^3)^2} \qquad \text{(Eq. 19)}$$

Note that the irrelevant parameters Q_0 and t_0 have been set to 1 and 0, respectively. The value of the rise time τ is determined experimentally from the fitting of the charge translocated during a concentration jump of 100 mM $NaClO_4$ against 100 mM NaCl with Eq. 12. For comparison, the transfer function corresponding to the

measurements shown in Fig. 9 has been included in the figure. Clearly, the transfer function decays more rapidly than the signal but is sufficiently slow to distort it.

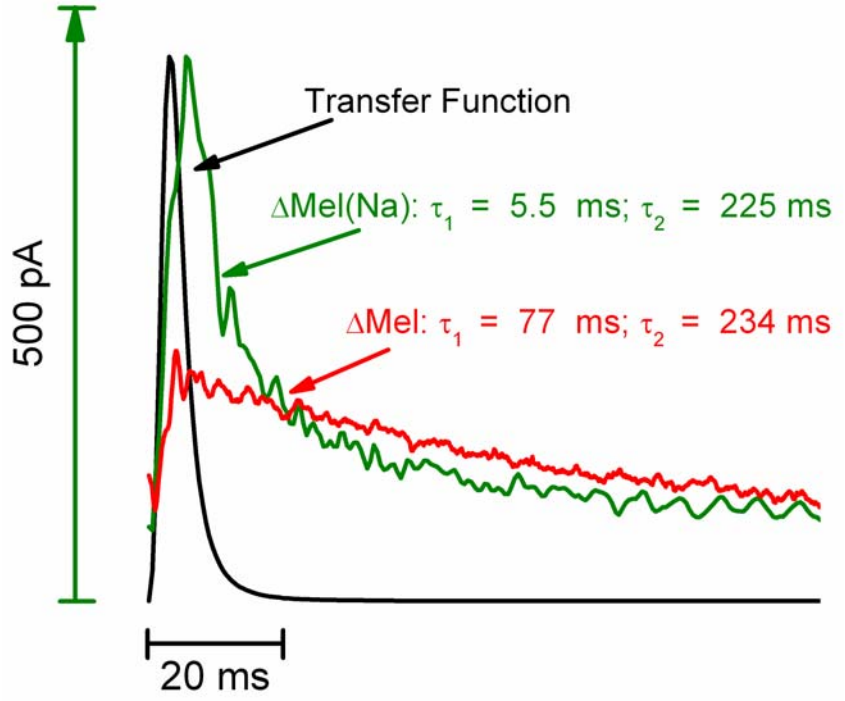

Fig. 9. Transient currents generated by MelB and the transfer function of the system.

The transient currents (average of 6 measurements) generated by the melibiose permease MelB after a melibiose concentration jump in the presence (green) and absence (red) of Na^+ are shown in the figure. The flow rate was set to 1.5 ml s^{-1}. The two time constants (τ_1 and τ_2) are obtained from the fitting of the decay phase to a biexponential decaying function as described in (Ganea *et al.*, 2001). In these fittings, the rising phase was not considered. Solution composition, ΔMel(Na): 100 mM potassium phosphate at pH 7.0, 100 mM KCl, 3 mM NaCl plus 20 mM glucose in the reference and 20 mM melibiose in the test solutions: ΔMel: 100 mM potassium phosphate at pH 7.0, 100 mM KCl plus 20 mM glucose in the reference and 20 mM melibiose in the test solutions. The black line represents the transfer function of the SSM System at the conditions of the experiment.

For a melibiose concentration jump in the presence of sodium, the process of charging of the proteoliposomes is considerable slower than the initial charge translocation ($\tau_2 >> \tau_1$; Fig. 9). Therefore, we will consider that the effect of the charging process on the rate constant of the electrogenic conformational transition is negligible. Under this approximation, the measured output current I(t) can be calculated from the convolution between the response of the equivalent circuit to the

current generated by MelB after a step substrate concentration jump $I_{Circuit}$ and the transfer function of the system f(t) (see also section 3.4):

$$I(t) = \int_{t_0}^{t} f(t-t')I_{Circuit}(t')dt' \qquad \text{(Eq. 20)}$$

Using an appropriate set of values for the parameters A_1, A_2, τ_1, τ_2 and t_0 the output current I(t) can now be numerically calculated by performing the convolution operation shown in Eq. 20. In an iterative least-square deconvolution algorithm, the calculated current is fitted to the measured current to determine the parameters A_1, A_2, τ_1, τ_2 and t_0. The calculated output current and measured current for a typical experiment are shown in Fig. 10. The resulting rate constant for the fast process (k_1 = $1/\tau_1$ = 263 ± 28 s^{-1}) was determined from four different experiments (SSM-electrodes).

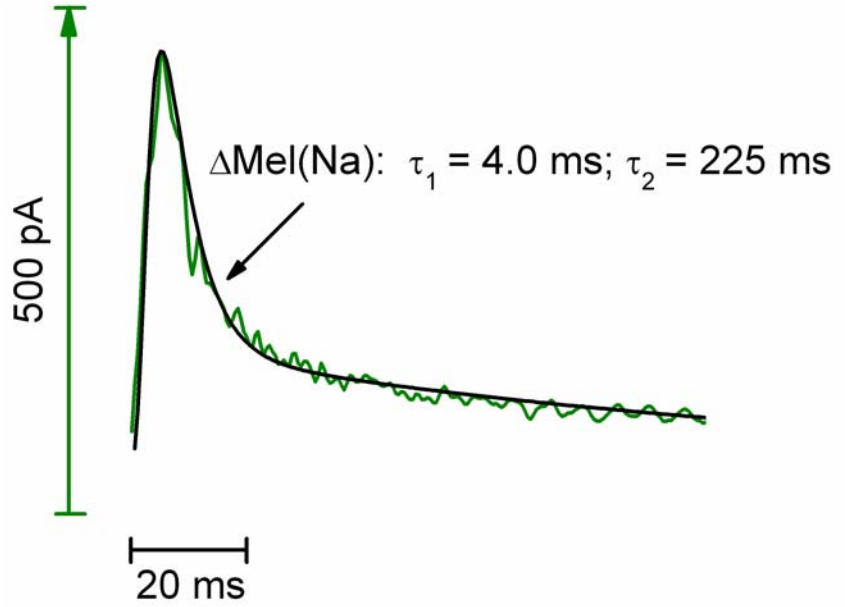

Fig. 10. The result of the iterative least-square deconvolution algorithm.

The transient current generated by MelB after a melibiose concentration jump in the presence of Na^+ is represented in green. As a result of the iterative least-square deconvolution algorithm, the time constants τ_1 and τ_2 are obtained, and they are given in the figure. The black trace corresponds to the calculated current (see text). The experimental conditions are as in Fig. 9.

5.3. Discussion

5.3.1. A New Method for the Experimental Determination of the Time Course of Substrate Surface Concentrations.

In this study we have used the strong interaction of inorganic ions with the lipid surface of an SSM (see section 4) to determine the time course of substrate surface concentrations. Experiments using different salt concentrations and different ions yield identical values and support the assumption that the measured rise times represent the rise time of surface ion concentration. The dependence of the rise time on the technical parameters of the flow system confirms this. The method presented here has the great advantage that it is simple and can be performed on the same sensor that is used for the immobilization of the protein. It, therefore, exactly matches the flow conditions and sensor position used for the activation of the protein on the SSM. This is relevant for time-critical measurements when the deconvolution technique is required to account for the limited time resolution.

Can this approach for ions be generalized for arbitrary charged or uncharged substrates? Charged compounds interact with charged surfaces. In particular they form electric double layers depending on the surface charge. At physiological concentrations (100 mM) a Gouy-Chapman double layer on a biological membrane has a thickness of ~ 1 nm. A typical ion like K^+ diffuses 1 nm in 0.25 ns (using the Einstein relationship $t = \langle x^2 \rangle/(2D)$ with $\langle x^2 \rangle = 10^{-18}$ m^2 and $D = 2 \cdot 10^{-9}$ m^{2}s^{-1}) while the solution exchange is in the millisecond time range. This demonstrates that on the time scale of the solution exchange the double layer is in a rapid kinetic equilibrium with the surface. Therefore, formation of the electrical double layer leads to a modified ionic surface concentration but is not relevant for the time course of surface concentration rise after a concentration jump. In conclusion, the time course of ion surface concentration may be used in a generalized fashion to estimate the rise time of the surface concentration for arbitrary small charged and uncharged substrates.

5.3.2. Rapid Solution Exchange at the SSM using a Wall Jet Geometry.

A simple theoretical model assuming laminar Hagen–Poiseuille flow in a cylindrical tube and an ideal mixer at the end of the tube (Pintschovius & Fendler, 1999) describes the flow conditions surprisingly well (Eqs. 14 to 16). It correctly predicts the linear dependence of the surface concentration rise time on the reciprocal flow rate and even the absolute values are only slightly overestimated. This model, therefore,

can serve as a guide for an improved cuvette design. However, two experimental evidences indicate that the flow cannot be not fully described by a Hagen–Poiseuille model: (i) the flow versus pressure diagram is clearly nonlinear; (ii) the delay times are not in agreement with the predictions of the Hagen–Poiseuille flow model and rather show a plug flow behavior (Eq. 17). Therefore, it seems clear that our flow conditions represent a transit region from plug flow to Hagen–Poiseuille flow. This is to be expected as a fully developed Hagen–Poiseuille flow profile is never obtained within the dimensions of our flow pathways (see section 5.2.1). Importantly, the experiments as well as the theoretical model clearly show that the most important geometrical factor influencing the rise time τ is the length of the common pathway for test and reference solutions i.e., the diverter–SSM distance *x*.

Effective perfusion of the SSM surface relies on the application of high flow rates. On the other hand, fast flow at the surface represents a risk of ablation for the immobilized proteoliposomes because of fluid shear forces. However, this is obviously not the case since proteoliposomes can be investigated on the SSM for hours with only very little decrease in signal. It is concluded that an unstirred layer of at least 200 nm (the dimensions of the proteoliposomes) does indeed exist but represents no serious barrier for a millisecond substrate rise time at the SSM surface.

5.3.3. The Rapid Electrogenic Conformational Transition in MelB

Sugar binding induces a rapid electrogenic reaction in MelB that can be correlated with a conformational transition observed in intrinsic tryptophan fluorescence spectroscopy (Meyer-Lipp *et al.*, 2006; Mus-Veteau *et al.*, 1995). For a kinetic comparison, Michela Schlüter measured the time resolved tryptophan fluorescence in a stopped-flow experiment. The same preparation of MelB proteoliposomes was investigated with the improved cuvette for rapid solution exchange in combination with an iterative least-squares deconvolution algorithm. The rate constants of the fast phase obtained from the time-resolved electrical and fluorescence experiments agree within the error limit. This agreement is a strong argument in favor of a common molecular process behind the fluorescence change and the charge translocation. It supports the previous proposition of a melibiose induced electrogenic conformational transition and assigns a rate constant of $k_1 \sim 250\ s^{-1}$ to it.

6. Electrophysiological Characterization of LacY

6.1. Introduction

The major facilitator superfamily (MFS) is a huge group of evolutionarily related transport proteins. Family members are found in membranes from archaea to the mammalian central nervous system, and they catalyze transport of a wide variety solutes into or out of all cells. Thus, these membrane proteins play critical roles in the physiology (eg. epithelial transport) and pathology (eg. glucose/galactose malabsorption) of living organisms. In addition, they represent major drug targets. One of the best-characterized members of the MFS is the lactose permease (LacY) from *Escherichia coli*, structures of which have been solved recently at atomic resolution (Abramson *et al.*, 2003; Guan *et al.*, 2007; Mirza *et al.*, 2006). Because of the wealth of biochemical and biophysical data available for LacY (reviewed in (Guan & Kaback, 2006; Kaback *et al.*, 2007; Majumdar *et al.*, 2007; Smirnova *et al.*, 2007; Zhou *et al.*, 2008)), it represents an ideal model system for the investigation of the basic principles and molecular details of secondary active transport.

Although it has been known for many years that lactose/H^+ symport catalyzed by LacY is an electrogenic reaction (Patel *et al.*, 1982; West, 1970; West & Mitchell, 1972), and in spite of numerous efforts, LacY has so far resisted all attempts at standard electrophysiological analysis. Despite the *lacy* gene is expressed well in frog oocytes and other eukaryotic cells, LacY remains in the *cis*-Golgi and the peri-nuclear membrane and does not target to the plasma membrane to any extent whatsoever (J. Liu &, H. Ronald Kaback, unpublished information). Here, the first successful electrophysiological study of LacY by using purified, reconstituted proteoliposomes with solid-supported membrane (SSM)-based electrophysiology is presented.

6.2 Results

6.2.1. Downhill Sugar/H^+ Symport generates Transient Currents.

Proteoliposomes containing reconstituted LacY were immobilized on an SSM-coated gold electrode (the sensor), and charge displacement induced by downhill sugar/H^+ symport into the proteoliposomes was detected by capacitive coupling (Schulz *et al.*, 2008). Transport was initiated by a sugar concentration jump using rapid solution exchange. When the sugar reaches the surface of the SSM, a transient current starts abruptly. The time course of the signals is characterized by two distinct phases: a rapid rise to a maximum followed by a much slower decay towards the base line (Fig. 11). Because the decay is not exponential, it was quantified by the decay time from peak to half-maximal current ($\tau_{1/2}$). The maximal value of the peak current is observed after a 50 mM concentration jump of lactose, and the peak currents generated after 50 mM concentration jumps of lactulose and melibiose are ~65 % and ~50 %, respectively, of that recorded with lactose (Fig. 11). However, addition of 50 mM sucrose (Fig. 11), a sugar that is not substrate of LacY, has no effect.

Sugar binding and transport catalyzed by LacY are inactivated by alkylation of Cys148 primarily (Bieseler *et al.*, 1985; Trumble *et al.*, 1984; van Iwaarden *et al.*, 1993). Consistently, no electrical transient is observed after treatment with *N*-ethylmaleimide (NEM).

6.2.2. Varying Lipid to Protein Ratios.

Electrogenic transport by a reconstituted protein leads to transient currents in the capacitively coupled system (Bamberg *et al.*, 1979; Schulz *et al.*, 2008). With wild-type LacY, downhill sugar/H^+ symport into the proteoliposomes generates an inside positive potential, which acts to decelerate the downhill symport reaction catalyzed by LacY, leading to transient currents. However, any conformational transition that displaces charged amino acyl side chains or reorients electrical dipoles also represents an electrogenic transition that may contribute to the transient nature of the currents (see also section 3.2.2). Indeed, melibiose binding triggers an electrogenic conformational transition in the melibiose permease (MelB) from *Escherichia coli* that is a major component of the transient currents observed (Ganea *et al.*, 2001; Meyer-Lipp *et al.*, 2004). To discriminate between downhill sugar/H^+ symport and an

electrogenic conformational transition, experiments were performed with proteoliposomes reconstituted at different lipid to protein ratios (LPR; weight/weight).

As an increase in the LacY particle density clearly leads to a significantly faster decay of the transient currents, the currents observed with wild-type LacY represent mainly charging of the liposome membrane due to downhill sugar/H^+ symport activity.

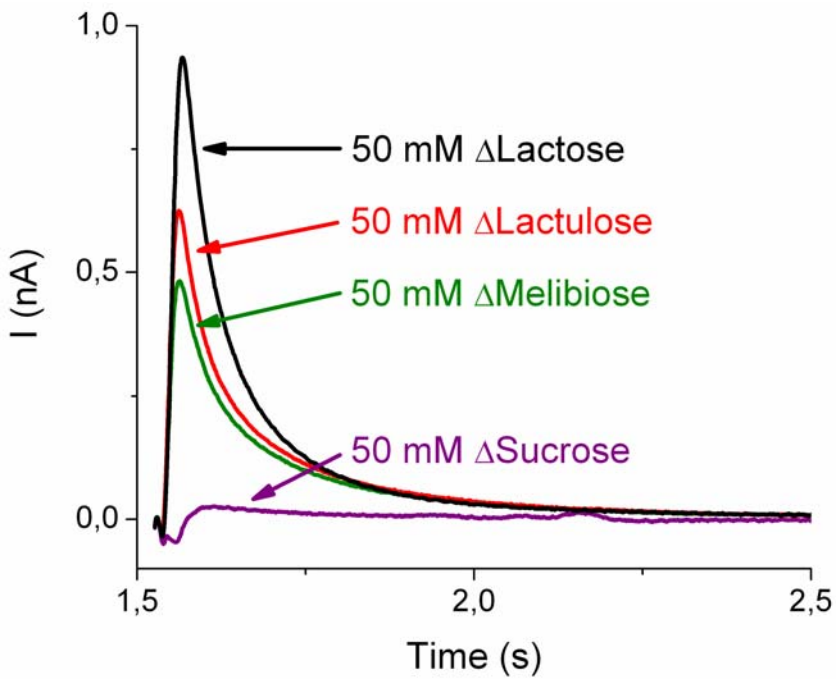

Fig. 11. Transient currents obtained with wild-type LacY.

Transient currents obtained with wild-type LacY proteoliposomes after a 50 mM sugar concentration jump at t = 1.5 s. The traces in black, red, green and violet correspond to concentration jumps of lactose (50 mM; ΔLactose), lactulose (50 mM; ΔLactulose), melibiose (50 mM; ΔMelibiose), and sucrose (50 mM; ΔSucrose), respectively. The nonactivating solution and all activating solutions were prepared in 100 mM potassium phosphate at pH 7.6 plus 1 mM of DTT. All traces shown were recorded from one sensor.

6.2.3. Effect of pH.

Rates of efflux from right-side-out membrane vesicles (Kaczorowski & Kaback, 1979) or proteoliposomes reconstituted with purified LacY (Garcia *et al.*, 1983; Viitanen *et al.*, 1983) showed that the turnover of LacY strongly depend on the pH. Indeed, the shape and magnitude of the transients generated by downhill lactose/H^+ symport are strongly dependent on pH. Considering that the transients correspond to downhill

sugar/H^+ symport activity (see above), they can be approximated by Eqs. 3 to 7 (see section 3.2.1). Indeed, this limiting case predicts that an increase in the turnover results in an increase of the peak current and a faster decay towards the base line, as observed.

Peak currents were investigated at different pH values and lactose concentrations. An increase in pH from 6.6 to 8.5 generates a 5-flod increase in the saturating peak current. Indeed, rates of efflux (i.e., downhill lactose/H^+ symport in the opposite direction) from right-side-out membrane vesicles (Kaczorowski & Kaback, 1979) or proteoliposomes reconstituted with purified LacY (Garcia *et al.*, 1983; Viitanen *et al.*, 1983) exhibit a similar dependence on pH. The half saturating concentration $K_{0.5}$ increases only slightly with the pH. At pH 7.6, a $K_{0.5}$ of 5.3 ± 0.5 mM is obtained, which is close to that of 3.1 ± 0.7 mM determined for downhill lactose/H^+ influx in proteoliposomes reconstituted with purified LacY (Viitanen *et al.*, 1984).

6.2.4. Transient Currents in Mutants.

In order to dissect the overall electrogenic response, mutants of LacY that bind ligand, but do little or no lactose/H^+ symport were utilized. Mutant E325A is specifically defective in all steps involving H^+ release from LacY, but catalyzes exchange and counterflow at least as well as wild-type (Carrasco *et al.*, 1986; Carrasco *et al.*, 1989). Concentration jumps of 50 mM lactose, lactulose or melibiose produce transient currents with virtually identical kinetics and negligible differences in magnitude (Fig. 12A), which are abolished after treatment with NEM. However, the transient currents are ~5-times smaller than those observed for lactose with wild-type LacY and exhibit significantly faster decays followed by shallow negative phases. The negative component represents discharge of the liposome membrane after a rapid charge translocation (see also section 3.2.2). This phenomenon is common for the capacitively coupled system (Schulz *et al.*, 2008) and indicates absence of significant steady-state charge transport across the liposome membrane (i.e., downhill sugar/H^+ symport activity).

Mutant C154G binds sugar as well as wild-type and exhibits extremely low, but significant transport activities (Menick *et al.*, 1987; Menick *et al.*, 1985; Sahin-Toth & Kaback, 2001; Smirnova & Kaback, 2003). Concentration jumps with 50 mM lactose, lactulose or melibiose generate transient currents of comparable magnitude as E325A LacY, which are also abolished by NEM treatment. In contrast to E325A, the magnitude and kinetics of the peak currents recorded with C154G LacY depend on

the sugar utilized (Fig. 12B). Concentration jumps of 50 mM lactose or lactulose trigger transient currents that decay faster compared with the wild-type. Interestingly, a 50 mM melibiose concentration jump, generates the largest peak current with a significantly faster exponential decay followed by a small negative phase.

From the transient currents measured, the kinetics of the true transport currents generated by the mutants can be reconstructed by using an iterative least-squares deconvolution algorithm (see section 5). For E325A LacY, regardless of the sugar used, the transient currents are indistinguishable from the transfer function, indicating that charge translocation is too fast to be resolved by the measurements. In this case, only a lower limit can be estimated for the rate constant of the process (k > 200 s^{-1}). For C154G LacY, the rate constants k for 50 mM concentration jumps of lactose or lactulose are 53 ± 5 s^{-1} or 72 ± 5 s^{-1}, respectively. However, the k for a 50 mM concentration jump of melibiose is too rapid for accurate measurement (k > 200 s^{-1}).

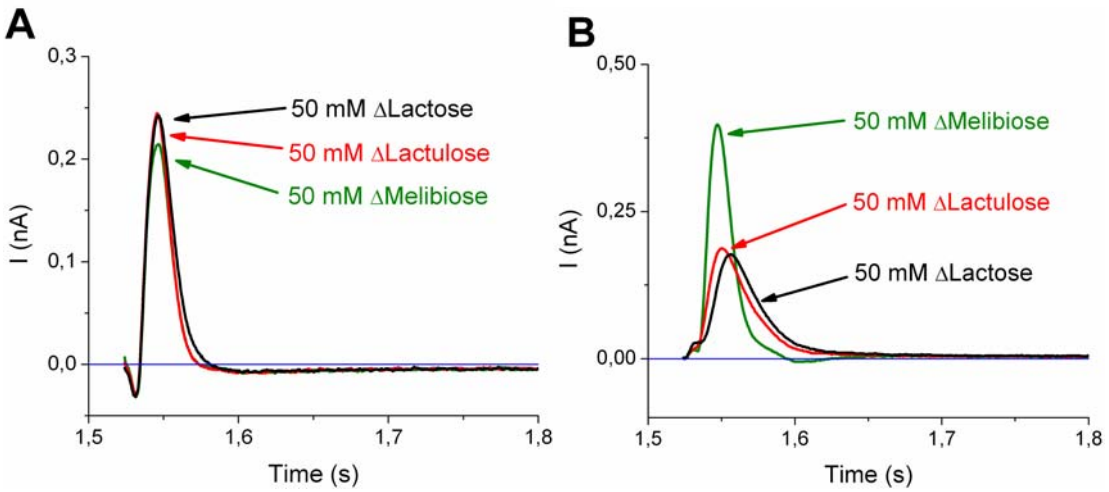

Fig. 12. Transient currents obtained with LacY mutants.

The solution exchange protocol and composition of the solutions was the same as described in Fig. 11. The base line is represented in blue. (***A***) E325A LacY was reconstituted into proteoliposomes and activated with 50 mM concentration jumps of lactose (50 mM; ΔLactose), lactulose (50 mM; ΔLactulose) or melibiose (50 mM; ΔMelibiose) at pH 7.6. All traces exhibit virtually identical kinetics and only small differences in magnitude with an exponential decay towards the base line with a time constant of ~10 ms followed by a shallow negative phase. (***B***) Transient currents obtained with C154G LacY proteoliposomes after 50 mM sugar concentration jumps at pH 7.6. The transient currents corresponding to 50 mM ΔLactose or 50 mM ΔLactulose decay mono-exponentially towards the base line, with time constants of ~20 ms, while the transients observed with 50 mM ΔMelibiose exhibit the largest peak current and a significantly faster exponential decay with a time constant of ~10 ms followed by a small negative phase.

6.3. Discussion

6.3.1. Wild-type LacY.

Reconstitution of LacY using the procedure described previously (Foster *et al.*, 1982; Garcia *et al.*, 1983; Newman *et al.*, 1981) results in proteoliposomes with approximately 85% of the LacY molecules in the right-side-out orientation (i.e., with the periplasmic side facing the exterior of the proteoliposome) (Herzlinger *et al.*, 1984). Therefore, application of a substrate concentration jump corresponds to substrate transport in the physiological direction. All transported sugars trigger positive transient currents, in agreement with the displacement of positive charge (H^+) into the proteoliposomes, as a result of downhill sugar/H^+ symport. From all sugars tested, lactose generates the largest transient current, consistent with it being the most efficiently transported substrate. The currents depend on pH and substrate concentration and are blocked by alkylation with NEM. All these observations strongly support the contention that the transient currents reflect specifically the electrogenic activity of LacY.

Interestingly, the decay of the current observed with MelB after application of a melibiose concentration jump in the presence of Na^+ presents a marked biphasic pattern. A fast phase due to an electrogenic conformational transition triggered by melibiose binding is followed by a slow phase related to downhill melibiose/Na^+ symport (Ganea *et al.*, 2001; Meyer-Lipp *et al.*, 2004). With wild-type LacY, at a similar time resolution, a fast initial current decay is not observed. This is especially apparent in the currents recorded at low transporter density which decay slowly with a $\tau_{1/2}$ = 260 ± 2 ms. Such a behavior can only be explained when the initial reactions, if electrogenic, are slow or if charge translocation occurs late in the LacY reaction cycle. Nevertheless, sugar binding occurs with a rate constant > 50 s^{-1} ruling out a slow initial step. Although this argument is strictly only valid for the mutants, the fact that they are fully capable of sugar binding indicates that the same rate constants apply also to the wild-type. Taken together, our data indicate that the major electrogenic step in wild-type LacY occurs late in the reaction cycle.

6.3.2. LacY Mutants.

The transient currents of the mutant enzyme E325A and C154G LacY differ drastically from the response of the wild-type. They are five to ten times smaller and considerably faster than the transients observed with wild-type LacY. Smaller

transient currents could be interpreted in terms of downhill sugar/H^+ symport with reduced turnover in E325A and C154G LacY. However, this would not only lead to a smaller current amplitude but also to a slower decay (see, for example, the transient currents observed with wild-type LacY at pH 6.6 which are around five times smaller in amplitude and, at the same time, decay five times slower than at pH 8.5). In contrast, the transient currents observed with both mutants at pH 7.5 decay even faster than the transients recorded with wild-type at maximal activity (pH 8.5). This indicates that the currents observed with E325A and C154G LacY are not determined by charging of the liposomes but rather represent electrogenic conformational transitions. The charge translocated in this conformational transition is around 20 times smaller than the charge translocated per turnover by the wild-type. In other words, substrate binding to the mutants induces a charge displacement corresponding to the transport of the equivalent of only ~ 6 % of an elementary charge across the membrane.

Although smaller, these transient currents can be used to estimate binding rate constants for the different sugars and mutants. They range between 50 and > 200 s^{-1} and depend on the nature of substrate and mutant. Recent stopped-flow experiments revealed that the binding of α-NPG (*p*-nitrophenyl α-D-galactopyranoside) to C154G/V331C LacY in detergent micelles is a two step process: a binding step followed by a slower conformational change with a rate constant of 238 s^{-1} detected with fluorescent-labeled protein (Smirnova *et al.*, 2006). Obviously, sugar binding triggers a conformational change with a rate constant similar to that observed in the electrophysiological experiments which may be responsible for the charge translocation observed. Unfortunately, a direct comparison of rate constants is not possible because of the strong interaction of α-NPG with the membrane which generates large electrical artefacts.

6.3.3. Electrogenic Steps in the LacY Reaction Cycle.

Combining the results obtained with wild-type LacY and the transport impaired mutants, there is clear evidence for a major electrogenic step late in the reaction cycle, and a rapid electrogenic reaction during or immediately after sugar binding with a relatively low electrogenicity. It seems unlikely that the latter is a unique property of the E325A and C154G mutants. Most probably this charge translocation also takes place in the wild-type, but is completely masked by its 20-fold greater

charge transport activity. This small charge translocation is only observed under conditions where sugar/H^+ symport is blocked, as in the mutant proteins.

Based on previous observations on the kinetics of LacY (Kaczorowski & Kaback, 1979; Kaczorowski *et al.*, 1979; Robertson *et al.*, 1980; Viitanen *et al.*, 1983) and on our electrophysiological findings we propose that the main electrogenic step corresponds to deprotonation of wild-type LacY in the inward-facing conformation (Fig. 13). In this context, it is notable that: (i) structural, biochemical and biophysical data strongly support the contention that wild-type and C154G LacY are predominantly in an inward-facing conformation (Abramson *et al.*, 2003; Guan *et al.*, 2007; Kaback *et al.*, 2007; Majumdar *et al.*, 2007; Smirnova *et al.*, 2007; Zhou *et al.*, 2008); (ii) the rate of efflux from proteoliposomes reconstituted with purified LacY is strongly influenced by the voltage across the membrane, whereas exchange is completely voltage independent (Garcia *et al.*, 1983); thus, the main electrogenic step is related to protonation/deprotonation of LacY in either the inward- or outward-facing conformations or the return of the empty carrier; (iii) the shape of the transient currents indicates that the main electrogenic step in wild-type LacY occurs late in the reaction cycle (see above). Considering these points, it is likely that the inward-facing deprotonated transporter is the initial state, and that deprotonation corresponds to the main electrogenic step of the transport cycle (Fig. 13). Following this argument, the main electrogenic step would take place at the end of the transport cycle, in agreement with the conclusions obtained from the analysis of the transient currents. As downhill lactose/H^+ symport is specifically inhibited 3- to-4-fold in deuterium oxide, deprotonation is probably not only the main electrogenic step but is also rate limiting (Viitanen *et al.*, 1983).

With C154G LacY, all transport reactions, including equilibrium lactose exchange, are almost abolished (van Iwaarden *et al.*, 1993; van Iwaarden *et al.*, 1991) indicating that the substrate translocation step is blocked. In the absence of substrate this mutant is in an inward-facing conformation and paralyzed in an open conformation on the periplasmic side, but able to close on the cytoplasmic side upon lactose binding (Majumdar *et al.*, 2007; Nie *et al.*, 2008; Smirnova *et al.*, 2007; Zhou *et al.*, 2008). E325A LacY exhibits no active transport whatsoever; however, in contrast to C154G LacY, mutant E325A catalyzes exchange and counterflow at least as well as wild-type LacY, indicating that this mutant is permanently protonated, [i.e. H^+ dissociation is blocked in E325A LacY but binding is normal (Carrasco *et al.*, 1986; Carrasco *et al.*, 1989; Sahin-Toth & Kaback, 2001). In both mutants a rapid but weakly electrogenic reaction with similar magnitude and kinetic properties is seen. This

agrees with our notion that periplasmic H^+ binding is not responsible for the charge translocation observed and that, the rapid initial charge displacement of minor electrogenicity is associated with sugar binding. Possibly the rapid conformational transition following sugar binding (Smirnova *et al.*, 2006) leads to rearrangement of charged residues within LacY (Mirza *et al.*, 2006; Weinglass *et al.*, 2004), which may account for this phenomenon.

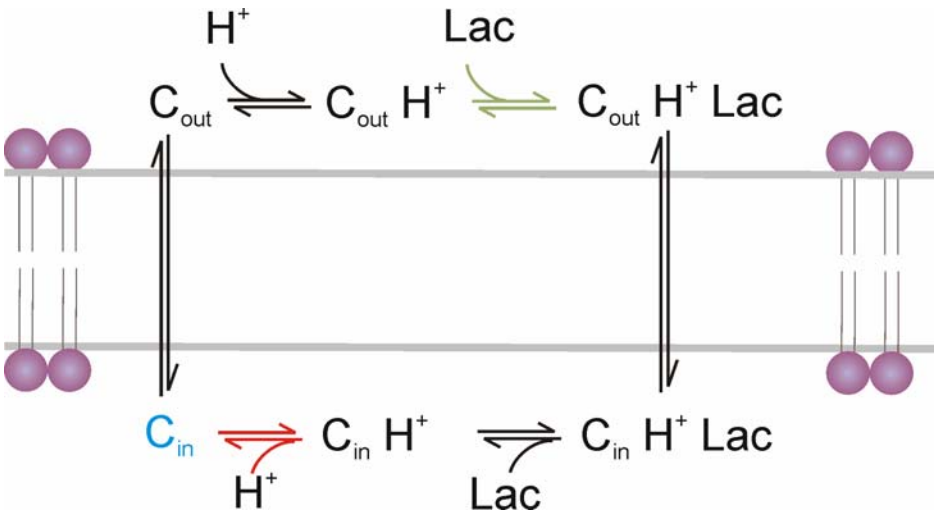

Fig. 13. Transport cycle in LacY.

We propose that the cycle starts with LacY in the configuration C_{in} (represented in blue) and that the main electrogenic step in the transport cycle corresponds to cytoplasmic proton release (red arrows). In addition, it is suggested that a rapid initial charge displacement of minor electrogenicity is associated with sugar binding (green arrows).

7. General Discussion and Perspectives

7.1. Applications and Technical Developments

7.1.1. SSM-Based Electrophysiology

Solid-supported membranes (SSMs) present comparable lipid mobilities, conductivities, and capacitances than black lipid membranes (BLMs) (Florin & Gaub, 1993; Seifert *et al.*, 1993). However, mechanical perturbations, which usually destroy a BLM, do not influence the life-time of a SSM, which is mechanically so stable that solutions may be rapidly exchanged at its surface (Pintschovius & Fendler, 1999). Solid-supported membranes are the principal element of the SSM-based electrophysiology (reviewed in (Ganea & Fendler, 2009; Schulz *et al.*, 2008)). With this electrophysiological technique, proteoliposomes, membrane vesicles, or membrane fragments are adsorbed to an SSM and are activated using a rapid substrate concentration jump. The SSM is then utilized as a capacitive electrode to record the electrogenic response of the transporter. Except for a few rare exceptions, bacterial transporters do not target the plasma membrane of eukaryotic cells, thereby precluding application of standard electrophysiological technology (like two electrode voltage clamp or patch clamp). In contrast, the SSM-based electrophysiology was very successful in the characterization of this type of transporters (Ganea & Fendler, 2009). Indeed, two secondary active transporters (LacY and MelB) from *Escherichia coli* have been electrophysiologically investigated in this dissertation (sections 5 and 6).

7.1.2. Improvements in the Time Resolution

The SSM-based electrophysiology can be utilized not only to measure the continuous electrogenic transport activity of the transporter but also to investigate electrogenic conformational transitions. However, for a proper interpretation of the measured signals as well as for the optimization of the fluidic system, quantitative temporal information concerning the surface substrate concentration rise is a prerequisite. Interestingly, the time course of the transient currents generated after an ion concentration jump is independent of the particular ion or concentration utilized. These observations support the conclusion that the time course of the translocated charge in an ion concentration jump corresponds to the time course of the substrate concentration jump (see section 5). We have, therefore, utilized ion concentration jumps to identify the critical parameters affecting the time resolution and the transfer

function of the system. To recover the rate constants of the underlying charge translocations recorded after activation of the transporter, the transfer function was utilized as an input for a least-square deconvolution algorithm. A novel cuvette design in combination with the least-square deconvolution algorithm allowed the investigation of the rate constant of sugar induced electrogenic conformational transitions in MelB and LacY (sections 5 and 6). With MelB, the kinetics of a sugar induced conformational transition was also measured using stopped-flow tryptophan fluorescence spectroscopy. There, the relaxation time constant obtained for the charge displacement agrees with that determined in the stopped-flow experiments.

7.1.3. Specific Interactions between Ions and Lipid Membranes

The properties of lipid membranes, which represent the most important biological interface between intracellular and extracellular compartments, are essentially modulated by the ionic composition of the surrounding aqueous medium. In a new application of the SSM-technique, the bare SSM has been utilized to investigate the specific interactions between ions and lipid headgroups (section 4). This was achieved by exchanging solutions of different ionic compositions at the surface of a SSM through a flow system. This solution exchange resulted in charge translocations that were interpreted in terms of binding of the ions to the lipid headgroups at the SSM surface. We found that chaotropic anions and kosmotropic cations are attracted to the membrane independent of the membrane composition. In particular, the same behavior was found for lipid headgroups bearing no charge like monoolein. This general trend is modulated by the electrostatic interaction of the ions with the lipid headgroup charge. In our opinion, it is necessary to consider the geometry of the water molecules around the ions and headgroups to understand these effects. Indeed, our experimental results are in agreement with recent molecular dynamic simulations of PC membranes (Bockmann *et al.*, 2003; Pandit *et al.*, 2003; Sachs *et al.*, 2004; Sachs & Woolf, 2003).

7.2. Electrophysiological Characterization of Bacterial Secondary Active Transporters

7.2.1. Positioning the Major Electrogenic Step

In this dissertation, two bacterial secondary active transporters (MelB and LacY) have been electrophysiologically investigated (sections 5 and 6). Their electrogenic responses are, however, very different. Sugar binding to MelB in the presence of Na^+ results in a fast electrogenic conformational transition that is a major component of

the transient currents observed (Ganea *et al.*, 2001; Meyer-Lipp *et al.*, 2004). This initial fast charge translocation indicates that the major electrogenic step in MelB occurs at the beginning of the reaction cycle. In contrast, with wild-type LacY a fast initial current decay is not observed. This was especially apparent in the currents recorded at low transporter density which decay slowly with a $\tau_{1/2}$ = 260 ± 2 ms. Such a behavior can only be explained when the initial reactions, if electrogenic, are slow or if charge translocation occurs late in the LacY reaction cycle. Nevertheless, sugar binding occurs with a rate constant > 50 s^{-1} ruling out a slow initial step (the rate constant for the sugar induced electrogenic conformational transition in MelB was k = 263 $\pm$ 28 s^{-1}). Although this argument is strictly only valid for the mutants, the fact that they are fully capable of sugar binding indicates that the same rate constants apply also to the wild-type. Taken together, our data indicate that the major electrogenic step in wild-type LacY occurs late in the reaction cycle.

7.2.2. The Role of the Orientation

To date, four bacterial secondary active transporters from *Escherichia coli* have been characterized by means of the SSM-based electrophysiology: the melibiose permease MelB (Ganea *et al.*, 2001); the Na^+/ H^+ antiporter (NhaA) (Zuber *et al.*, 2005); the Na^+/Proline transporter (PupP) (Zhou *et al.*, 2004); and, the lactose permease LacY (see section 6). Two of these transporters (MelB and PupP) are inside-out (ISO) in the proteoliposome membrane and present the major electrogenic step early in the reaction cycle. In contrast, LacY and NhaA are right-side out (RSO) in the proteoliposome membrane and present the major electrogenic step late in the reaction cycle. These observations seem to suggest that the orientation of the transporter influences whether the major electrogenic step takes place early or late in the cycle.

7.3. Perspectives

Combining previous observations on the kinetics of LacY (Garcia *et al.*, 1983; Kaczorowski & Kaback, 1979; Kaczorowski *et al.*, 1979; Robertson *et al.*, 1980) with our electrophysiological characterization of this transporter, we propose that the turnover involves at least two electrogenic reactions: (i) a minor reaction that occurs upon sugar binding and is due to a conformational transition in LacY; and (ii) a major reaction due to cytoplasmic release of H^+ during downhill sugar/H^+ symport, which is the limiting step for this mode of transport. The proposed kinetic model could be further investigated with the following experiments:

First, electrogenic conformational transitions induced by sugar binding would be monitored in mutations affecting residues involved in H^+ translocation and coupling, like mutants in the following side chains: Glu-126, Arg-144, Glu-325, Glu-269, Arg-302, and His-322 (Guan & Kaback, 2006; Sahin-Toth *et al.*, 2000). To obtain the rate constants of these electrogenic reactions, experiments would be performed at a better time resolution.

Second, membrane vesicles containing overexpressed LacY can be obtained in a right-side-out (RSO) (Kaback, 1971; Short et al., 1974) or inside-out (ISO) (Reenstra et al., 1980) configuration, while reconstitution of LacY into proteoliposomes leads preferentially to a RSO orientation (Herzlinger et al., 1984). Therefore, use of membrane vesicles would provide an opportunity to study symport electrophysiologically from both sides of the membrane. Furthermore, a proton electrochemical gradient of either polarity can be generated in RSO or ISO vesicles, respectively via the respiratory chain by using appropriate electron donors (Ramos et al., 1976; Reenstra et al., 1980).

Third, although time-dependent fluorescence changes due to sugar binding to LacY have been resolved recently by stopped-flow with *p*-nitrophenyl-α-D-galactopyranoside (α-NPG) (Smirnova *et al.*, 2008; Smirnova *et al.*, 2006), a direct comparison with electrophysiological data has not yet been possible. While the electrophysiological experiments employ reconstituted LacY, purified LacY molecules in detergent micelles have been utilized for the fluorescence experiments. Studies with reconstituted, 2-(4'-maleimidylanilino)naphthalene-6-sulfonic acid (MIANS)-labeled LacY (Smirnova *et al.*, 2008) could be carried out by using stopped-flow in order to directly compare time-resolved electrogenic events and fluorescence changes. Electrogenic conformational transitions could be measured and the rate constants determined, as shown for MelB (see section 5).

Fourth, time-resolved Fourier-transform infrared (trFTIR) difference spectroscopy reveals that water molecules act as cofactors in vectorial H^+ transfer in bacteriorhodopsin (bR) (Garczarek *et al.*, 2005; Wolf *et al.*, 2008). Therefore, it was proposed that transient protonation of an important glutamate residue exposes the protonated water cluster in bR to extracellular solvent, leading to H^+ release to the bulk water (Garczarek *et al.*, 2005; Wolf *et al.*, 2008). Based on the behavior of mutants defective in H^+ transport and coupling, it has been suggested (Guan & Kaback, 2006) that water may also act as a cofactor during the sugar/H^+ symport activity of LacY. More specifically, the side chains involved in H^+ transport do not form a pathway through LacY, but form a network near the apex of the water-filled

cavity and across from the sugar-binding site (Abramson *et al.*, 2003). These side chains may ligand to one or more structured water molecules that become transiently protonated during turnover of LacY, thereby acting as cofactors in H^+ transport. In any event, Glu325 is clearly involved in H^+ release from LacY during lactose/H^+ symport (Guan & Kaback, 2006; Kaback *et al.*, 2001; Sahin-Toth & Kaback, 2001). Fourier-transform infrared experiments could be carried out at different pH values with wild-type and E325A LacY to investigate the putative role of water molecules as cofactors.

In summary, electrophysiological and spectroscopic techniques could be utilized to further investigate structure-function relationships in LacY, with special emphasis on SSM-based electrophysiology. This approach represents a novel means of probing the mechanism of ion-gradient coupled active transport.

8. References

Abramson J, Smirnova I, Kasho V, Verner G, Kaback HR, Iwata S (2003) Structure and mechanism of the lactose permease of Escherichia coli. *Science* 301: 610-615

Adams SR, Tsien RY (1993) Controlling cell chemistry with caged compounds. *Annu Rev Physiol* 55: 755-784

Al-Nassri SA, Unny T (1980) Developing laminar flow in the inlet length of a smooth pipe. *Applied Scientific Research* 36: 313-332

Bamberg E, Apell HJ, Dencher NA, Sperling W, Stieve H, Lauger P (1979) Photocurrents generated by bacteriorhodopsin on planar bilayer membranes. *Biophysics of Structure and Mechanism* 5: 277-292

Barry PH, Diamond JM (1984) Effects of unstirred layers on membrane phenomena. *Physiological Reviews* 64: 763-872

Bieseler B, Prinz H, Beyreuther K (1985) Topological studies of lactose permease of Escherichia coli by protein sequence analysis. *Ann N Y Acad Sci* 456: 309-325

Bockmann RA, Hac A, Heimburg T, Grubmuller H (2003) Effect of sodium chloride on a lipid bilayer. *Biophysical Journal* 85: 1647-1655

Borlinghaus RT, Apell HJ, Lauger P (1988) Fast charge translocations associated with partial reactions of Na,K-ATPase induced by ATP concentration-jump. *Prog Clin Biol Res* 268A: 477-484

Bostrom M, Williams DRM, Ninham BW (2002) Ion specificity of micelles explained by ionic dispersion forces. *Langmuir* 18: 6010-6014

Carrasco N, Antes LM, Poonian MS, Kaback HR (1986) lac permease of Escherichia coli: histidine-322 and glutamic acid-325 may be components of a charge-relay system. *Biochemistry* 25: 4486-4488

Carrasco N, Puttner IB, Antes LM, Lee JA, Larigan JD, Lolkema JS, Roepe PD, Kaback HR (1989) Characterization of site-directed mutants in the lac permease of Escherichia coli. 2. Glutamate-325 replacements. *Biochemistry* 28: 2533-2539

Claessens M, van Oort BF, Leermakers FAM, Hoekstra FA, Stuart MAC (2004) Charged lipid vesicles: Effects of salts on bending rigidity, stability, and size. *Biophys J* 87: 3882-3893

Clarke RJ, Lupfert C (1999) Influence of anions and cations on the dipole potential of phosphatidylcholine vesicles: A basis for the Hofmeister effect. *Biophysical Journal* 76: 2614-2624

Collins KD (2004) Ions from the Hofmeister series and osmolytes: effects on proteins in solution and in the crystallization process. *Methods* 34: 300-311

Collins KD (2006) Ion hydration: Implications for cellular function, polyelectrolytes, and protein crystallization. *Biophys Chem* 119: 271-281

Collins KD, Washabaugh MW (1985) The Hofmeister effect and the behaviour of water at interfaces. *Q Rev Biophys* 18: 323-422

Drachev LA, Jasaitis AA, Kaulen AD, Kondrashin AA, Liberman EA, Nemecek IB, Ostroumov SA, Semenov A, Skulachev VP (1974) Direct measurement of electric current generation by cytochrome oxidase, H+-ATPase and bacteriorhodopsin. *Nature* 249: 321-324

Dueck B (2006) Ein Biosensor fuer die Grundlagenforschung und die pharmakologische Wirkstoffsuche an Ionenkanaelen. *Diplomarbeit*

Eisenberg (1979) Adsorption of Monovalent Cations to Bilayer Membranes Containing Negative Phospholipids. *Bilayer Membranes* 18: 5213-5223

Eisenberg M, Gresalfi T, Riccio T, McLaughlin S (1979) Adsorption of Monovalent Cations to Bilayer Membranes Containing Negative Phospholipids. *Bilayer Membranes* 18: 5213-5223

Fahr A, Lauger P, Bamberg E (1981) Photocurrent kinetics of purple-membrane sheets bound to planar bilayer-membranes. *Journal of Membrane Biology* 60: 51-62

Fendler K, Grell E, Haubs M, Bamberg E (1985) Pump currents generated by the purified Na+K+-ATPase from kidney on black lipid membranes. *Embo J* 4: 3079-3085

Fendler K, Jaruschewski S, Hobbs A, Albers W, Froehlich JP (1993) Pre-steady-state charge translocation in NaK-ATPase from eel electric organ. *J Gen Physiol* 102: 631-666

Florin E-L, Gaub HE (1993) Painted supported lipid membranes. *Biophysical Journal* 64: 375-383

Forbush B, 3rd (1984) Na+ movement in a single turnover of the Na pump. *Proc Natl Acad Sci U S A* 81: 5310-5314

Foster DL, Garcia ML, Newman MJ, Patel L, Kaback HR (1982) Lactose-proton symport by purified lac carrier protein. *Biochemistry* 21: 5634-5638

Frank HS, Evans MW (1945) Free volume and entropy in condensed systems .3. Entropy in binary liquid mixtures - Partial molal entropy in dilute solutions - Structure and thermodynamis in aqueous electrolytes. *J Chem Phys* 13: 507-532

Ganea C, Fendler K (2009) Bacterial transporters: Charge translocation and mechanism. *Biochim Biophys Acta*

Ganea C, Pourcher T, Leblanc G, Fendler K (2001) Evidence for intraprotein charge transfer during the transport activity of the melibiose permease from Escherichia coli. *Biochemistry* 40: 13744-13752

Garcia-Celma JJ, Dueck B, Stein M, Schlueter M, Meyer-Lipp K, Leblanc G, Fendler K (2008) Rapid activation of the melibiose permease MelB immobilized on a solid-supported membrane. *Langmuir* 24: 8119-8126

Garcia-Celma JJ, Smirnova IN, Kaback HR, Fendler K (2009) Electrophysiological characterization of LacY. *Proc Natl Acad Sci U S A*

Garcia ML, Viitanen P, Foster DL, Kaback HR (1983) Mechanism of lactose translocation in proteoliposomes reconstituted with lac carrier protein purified from Escherichia coli. 1. Effect of pH and imposed membrane potential on efflux, exchange, and counterflow. *Biochemistry* 22: 2524-2531

Garczarek F, Brown LS, Lanyi JK, Gerwert K (2005) Proton binding within a membrane protein by a protonated water cluster. *Proc Natl Acad Sci U S A* 102: 3633-3638

Guan L, Kaback HR (2006) Lessons from lactose permease. *Annu Rev Biophys Biomol Struct* 35: 67-91

Guan L, Mirza O, Verner G, Iwata S, Kaback HR (2007) Structural determination of wild-type lactose permease. *Proc Natl Acad Sci U S A* 104: 15294-15298

Gurtovenko AA, Miettinen M, Karttunen M, Vattulainen I (2005) Effect of monovalent salt on cationic lipid membranes as revealed by molecular dynamics simulations. *J Phys Chem B* 109: 21126-21134

Haverd VE, Warr GG (2000) Cation selectivity at air/anionic surfactant solution interfaces. *Langmuir* 16: 157-160

Herrmann TR, Rayfield GW (1978) The electrical response to light of bacteriorhodopsin in planar membranes. *Biophys J* 21: 111-125

Herzlinger D, Viitanen P, Carrasco N, Kaback HR (1984) Monoclonal antibodies against the lac carrier protein from Escherichia coli. 2. Binding studies with membrane vesicles and proteoliposomes reconstituted with purified lac carrier protein. *Biochemistry* 23: 3688-3693

Holloway PW (1973) A simple procedure for removal of Triton X-100 from protein samples. *Anal Biochem* 53: 304-308

Jiskoot W, Teerlink T, Beuvery EC, Crommelin DJ (1986) Preparation of liposomes via detergent removal from mixed micelles by dilution. The effect of bilayer composition and process parameters on liposome characteristics. *Pharm Weekbl Sci* 8: 259-265

Jones G, Dole M (1929) The viscosity of aqueous solutions of strong electrolytes with special reference to barium chloride. *J Am Chem Soc* 51: 2950-2964

Jung H, Tebbe S, Schmid R, Jung K (1998) Unidirectional Reconstitution and Characterization of Purified Na+/Proline Transporter of Escherichia coli&#x2020. *Biochemistry* 37: 11083-11088

Jungwirth P, Tobias DJ (2001) Molecular structure of salt solutions: A new view of the interface with implications for heterogeneous atmospheric chemistry. *J Phys Chem B* 105: 10468-10472

Kaback HR (1971) Bacterial Membranes. In *Methods in Enzymol*, Kaplan NP, Jakoby WB, Colowick NP (eds), Vol. XXII, pp 99-120. New York: Elsevier

Kaback HR, Dunten R, Frillingos S, Venkatesan P, Kwaw I, Zhang W, Ermolova N (2007) Site-directed alkylation and the alternating access model for LacY. *Proc Natl Acad Sci U S A* 104: 491-494

Kaback HR, Sahin-Toth M, Weinglass AB (2001) The kamikaze approach to membrane transport. *Nat Rev Mol Cell Biol* 2: 610-620

Kaczorowski GJ, Kaback HR (1979) Mechanism of lactose translocation in membrane vesicles from Escherichia coli. 1. Effect of pH on efflux, exchange, and counterflow. *Biochemistry* 18: 3691-3697

Kaczorowski GJ, Robertson DE, Kaback HR (1979) Mechanism of lactose translocation in membrane vesicles from *Escherichia coli*. 2. Effect of imposed delta psi, delta pH, and delta mu H+. *Biochemistry* 18: 3697-3704

Kameyama K, Muroya A, Takagi T (1997) Properties of a Mixed Micellar System of Sodium Dodecyl Sulfate and Octylglucoside. *J Colloid Interface Sci* 196: 48-52

Keszthelyi L, Ormos P (1980) Electric signals associated with the photocycle of bacteriorhodopsin. *Acta Biochimica Et Biophysica Hungarica* 15: 152-152

Kunz W, Lo Nostro P, Ninham BW (2004) The present state of affairs with Hofffieister effects. *Curr Opin Colloid Interface Sci* 9: 1-18

Leontidis E (2002) Hofmeister anion effects on surfactant self-assembly and the formation of mesoporous solids. *Curr Opin Colloid Interface Sci* 7: 81-91

Majumdar DS, Smirnova I, Kasho V, Nir E, Kong X, Weiss S, Kaback HR (2007) Single-molecule FRET reveals sugar-induced conformational dynamics in LacY. *Proc Natl Acad Sci U S A* 104: 12640-12645

Marcus Y (1991) Thermodynamics of solvation of ions .5. Gibbs free-energy of hydration at 298.15 K. *J Chem Soc-Faraday Trans* 87: 2995-2999

McCray JA, Herbette L, Kihara T, Trentham DR (1980) A new approach to time-resolved studies of ATP-requiring biological systems; laser flash photolysis of caged ATP. *Proc Natl Acad Sci U S A* 77: 7237-7241

Menick DR, Lee JA, Brooker RJ, Wilson TH, Kaback HR (1987) Role of cysteine residues in the lac permease of Escherichia coli. *Biochemistry* 26: 1132-1136

Menick DR, Sarkar HK, Poonian MS, Kaback HR (1985) cys154 Is important for lac permease activity in Escherichia coli. *Biochem Biophys Res Commun* 132: 162-170

Meyer-Lipp K, Ganea C, Pourcher T, Leblanc G, Fendler K (2004) Sugar binding induced charge translocation in the melibiose permease from Escherichia coli. *Biochemistry* 43: 12606-12613

Meyer-Lipp K, Sery N, Ganea C, Basquin C, Fendler K, Leblanc G (2006) The inner interhelix loop 4-5 of the melibiose permease from Escherichia coli takes part in conformational changes after sugar binding. *J Biol Chem* 281: 25882-25892

Mirza O, Guan L, Verner G, Iwata S, Kaback HR (2006) Structural evidence for induced fit and a mechanism for sugar/H+ symport in LacY. *Embo J* 25: 1177-1183

Miyagishi S, Okada K, Asakawa T (2001) Salt Effect on Critical Micelle Concentrations of Nonionic Surfactants, N-Acyl-N-methylglucamides (MEGA-n). *J Colloid Interface Sci* 238: 91-95

Mukhopadhyay P, Monticelli L, Tieleman DP (2004) Molecular dynamics simulation of a palmitoyl-oleoyl phosphatidylserine bilayer with Na+ counterions and NaCl. *Biophysical Journal* 86: 1601-1609

Mus-Veteau I, Leblanc G (1996) Melibiose Permease of Escherichia Coli - Structural Organization of Cosubstrate Binding Sites as Deduced from Tryptophan Fluorescence Analyses. *Biochemistry* 35: 12053-12060

Mus-Veteau I, Pourcher T, Leblanc G (1995) Melibiose permease of Escherichia coli: substrate-induced conformational changes monitored by tryptophan fluorescence spectroscopy. *Biochemistry* 34: 6775-6783

Nagel G, Fendler K, Grell E, Bamberg E (1987) Na+ currents generated by the purified (Na+ + K+)-ATPase on planar lipid membranes. *Biochim Biophys Acta* 901: 239-249

Newman MJ, Foster DL, Wilson TH, Kaback HR (1981) Purification and reconstitution of functional lactose carrier from Escherichia coli. *J Biol Chem* 256: 11804-11808

Nie Y, Sabetfard FE, Kaback HR (2008) The Cys154-->Gly mutation in LacY causes constitutive opening of the hydrophilic periplasmic pathway. *J Mol Biol* 379: 695-703

Ollivon M, Eidelman O, Blumenthal R, Walter A (1988) Micelle-vesicle transition of egg phosphatidylcholine and octyl glucoside. *Biochemistry* 27: 1695-1703

Ollivon M, Lesieur S, Grabielle-Madelmont C, Paternostre M (2000) Vesicle reconstitution from lipid-detergent mixed micelles. *Biochim Biophys Acta* 1508: 34-50

Pandit SA, Bostick D, Berkowitz ML (2003) Molecular dynamics simulation of a dipalmitoylphosphatidylcholine bilayer with NaCl. *Biophysical Journal* 84: 3743-3750

Patel L, Garcia ML, Kaback HR (1982) Direct measurement of lactose/proton symport in Escherichia coli membrane vesicles: further evidence for the involvement of histidine residue(s). *Biochemistry* 21: 5805-5810

Petrachet HI, Zemb T, Belloni L, Parsegian VA (2006) Salt screening and specific ion adsorption determine neutral-lipid membrane interactions. *Proc Natl Acad Sci U S A* 103: 7982-7987

Pintschovius J, Fendler K (1999) Charge translocation by the Na+/K+-ATPase investigated on solid supported membranes: rapid solution exchange with a new technique. *Biophys J* 76: 814-826

Pourcher T, Bassilana M, Sarkar HK, Kaback HR, Leblanc G (1990) The melibiose/Na+ symporter of Escherichia coli: kinetic and molecular properties. *Philos Trans R Soc Lond B Biol Sci* 326: 411-423

Raja LL, Kee RJ, Deutschmann O, Warnatz J, Schmidt LD (2000) A critical evaluation of Navier-Stokes, boundary-layer, and plug-flow models of the flow and chemistry in a catalytic-combustion monolith. *Catalysis Today* 59: 47-60

Ramos S, Schuldiner S, Kaback HR (1976) The electrochemical gradient of protons and its relationship to active transport in Escherichia coli membrane vesicles. *Proc Natl Acad Sci U S A* 73: 1892-1896

Reenstra WW, Patel L, Rottenberg H, Kaback HR (1980) Electrochemical proton gradient in inverted membrane vesicles from *Escherichia coli*. *Biochemistry* 19: 1-9

Renoncourt A, Vlachy N, Bauduin P, Drechsler M, Touraud D, Verbavatz JM, Dubois M, Kunz W, Ninham BW (2007) Specific alkali cation effects in the transition from micelles to vesicles through salt addition. *Langmuir* 23: 2376-2381

Robertson DE, Kaczorowski GJ, Garcia ML, Kaback HR (1980) Active transport in membrane vesicles from *Escherichia coli*: the electrochemical proton gradient alters the distribution of the *lac* carrier between two different kinetic states. *Biochemistry* 19: 5692-5702

Sachs JN, Nanda H, Petrache HI, Woolf TB (2004) Changes in phosphatidylcholine headgroup tilt and water order induced by monovalent salts: Molecular dynamics simulations. *Biophysical Journal* 86: 3772-3782

Sachs JN, Woolf TB (2003) Understanding the Hofmeister effect in interactions between chaotropic anions and lipid bilayers: Molecular dynamics simulations. *J Am Chem Soc* 125: 8742-8743

Sahin-Toth M, Kaback HR (2001) Arg-302 facilitates deprotonation of Glu-325 in the transport mechanism of the lactose permease from Escherichia coli. *Proc Natl Acad Sci U S A* 98: 6068-6073

Sahin-Toth M, Karlin A, Kaback HR (2000) Unraveling the mechanism of the lactose permease of Escherichia coli. *Proc Natl Acad Sci U S A* 97: 10729-10732

Saier MH (1999) Genome archeology leading to the characterization and classification of transport proteins. *Curr Opin Microbiol* 2: 555-561

Saier MH, Jr. (1998) Molecular phylogeny as a basis for the classification of transport proteins from bacteria, archaea and eukarya. *Adv Microb Physiol* 40: 81-136

Saier MH, Jr. (2000) A functional-phylogenetic classification system for transmembrane solute transporters. *Microbiol Mol Biol Rev* 64: 354-411

Schulz P, Garcia-Celma JJ, Fendler K (2008) SSM-based electrophysiology. *Methods* 46: 97-103

Schurtenberger P, Mazer N, Waldvogel S, Kanzig W (1984) Preparation of monodisperse vesicles with variable size by dilution of mixed micellar solutions of bile salt and phosphatidylcholine. *Biochim Biophys Acta* 775: 111-114

Seddon AM, Curnow P, Booth PJ (2004) Membrane proteins, lipids and detergents: not just a soap opera. *Biochim Biophys Acta* 1666: 105-117

Seifert K, Fendler K, Bamberg E (1993) Charge transport by ion translocating membrane proteins on solid supported membranes. *Biophys J* 64: 384-391

Short SA, Kaback HR, Kohn LD (1974) D-lactate dehydrogenase binding in *Escherichia coli* dld- membrane vesicles reconstituted for active transport. *Proc Natl Acad Sci USA* 71: 1461-1465

Smirnova I, Kasho V, Choe JY, Altenbach C, Hubbell WL, Kaback HR (2007) Sugar binding induces an outward facing conformation of LacY. *Proc Natl Acad Sci U S A* 104: 16504-16509

Smirnova IN, Kaback HR (2003) A mutation in the lactose permease of Escherichia coli that decreases conformational flexibility and increases protein stability. *Biochemistry* 42: 3025-3031

Smirnova IN, Kasho V, Kaback HR (2008) Protonation and sugar binding to LacY. *Proc Natl Acad Sci U S A*

Smirnova IN, Kasho VN, Kaback HR (2006) Direct sugar binding to LacY measured by resonance energy transfer. *Biochemistry* 45: 15279-15287

Trumble WR, Viitanen PV, Sarkar HK, Poonian MS, Kaback HR (1984) Site-directed mutagenesis of cys148 in the lac carrier protein of Escherichia coli. *Biochem Biophys Res Commun* 119: 860-867

Tsuchiya T, Wilson TH (1978) Cation-sugar cotransport in the melibiose transport system of Escherichia coli. *Membr Biochem* 2: 63-79

Ueno M, Tanford C, Reynolds JA (1984) Phospholipid vesicle formation using nonionic detergents with low monomer solubility. Kinetic factors determine vesicle size and permeability. *Biochemistry* 23: 3070-3076

van Iwaarden PR, Driessen AJ, Lolkema JS, Kaback HR, Konings WN (1993) Exchange, efflux, and substrate binding by cysteine mutants of the lactose permease of Escherichia coli. *Biochemistry* 32: 5419-5424

van Iwaarden PR, Driessen AJ, Menick DR, Kaback HR, Konings WN (1991) Characterization of purified, reconstituted site-directed cysteine mutants of the lactose permease of Escherichia coli. *J Biol Chem* 266: 15688-15692

Varju D (1977) Das Faltungsintergral. In *Systemtheorie für Biologen und Mediziner*, pp 40-44. Berlin, Heidelberg, New York: Springer

Viitanen P, Garcia ML, Foster DL, Kaczorowski GJ, Kaback HR (1983) Mechanism of lactose translocation in proteoliposomes reconstituted with lac carrier protein purified from Escherichia coli. 2. Deuterium solvent isotope effects. *Biochemistry* 22: 2531-2536

Viitanen P, Garcia ML, Kaback HR (1984) Purified reconstituted lac carrier protein from Escherichia coli is fully functional. *Proc Natl Acad Sci U S A* 81: 1629-1633

Vrbka L, Mucha M, Minofar B, Jungwirth P, Brown EC, Tobias DJ (2004) Propensity of soft ions for the air/water interface. *Curr Opin Colloid Interface Sci* 9: 67-73

Wallin E, von Heijne G (1998) Genome-wide analysis of integral membrane proteins from eubacterial, archaean, and eukaryotic organisms. *Protein Sci* 7: 1029-1038

Washabaugh AP, Zahn M (1994) Charge Density Enhancement Due to Recirculatory Flow. *IEEE Transactions on Dielectrics & Electrical Insulation* 1: 38-52

Weinglass A, Whitelegge JP, Faull KF, Kaback HR (2004) Monitoring conformational rearrangements in the substrate-binding site of a membrane transport protein by mass spectrometry. *J Biol Chem* 279: 41858-41865

West IC (1970) Lactose transport coupled to proton movements in Escherichia coli. *Biochemical and Biophysical Research Communications* 41: 655-&

West IC, Mitchell P (1972) Proton movements coupled to transport of beta-galactosides into Escherichia coli. *Biochemical Journal* 127: P56-&

Wilson DM, Wilson TH (1987) Cation specificity for sugar substrates of the melibiose carrier in Escherichia coli. *Biochim Biophys Acta* 904: 191-200

Wolf S, Freier E, Gerwert K (2008) How does a membrane protein achieve a vectorial proton transfer via water molecules? *Chemphyschem* 9: 2772-2778

Xu J, Li HL (1995) The chemistry of self-assembled long-chain alkanethiol monolayers on gold. *Journal of Colloid and Interface Science* 176: 138-149

Yazyu H, Shiota-Niiya S, Shimamoto T, Kanazawa H, Futai M, Tsuchiya T (1984) Nucleotide sequence of the melB gene and characteristics of deduced amino acid sequence of the melibiose carrier in Escherichia coli. *J Biol Chem* 259: 4320-4326

Zhao W, Rog T, Gurtovenko AA, Vattulainen I, Karttunen M (2007) Atomic-scale structure and electrostatics of anionic palmitoyloleoylphosphatidylglycerol lipid bilayers with Na+ counterions. *Biophys J* 92: 1114-1124

Zhou A, Wozniak A, Meyer-Lipp K, Nietschke M, Jung H, Fendler K (2004) Charge translocation during cosubstrate binding in the Na+/proline transporter of E-coli. ***J Mol Biol*** **343: 931-942**

Zhou Y, Guan L, Freites JA, Kaback HR (2008) Opening and closing of the periplasmic gate in lactose permease. ***Proc Natl Acad Sci U S A*** **105: 3774-3778**

Zuber D, Krause R, Venturi M, Padan E, Bamberg E, Fendler K (2005) Kinetics of charge translocation in the passive downhill uptake mode of the Na+/H+ antiporter NhaA of Escherichia coli. ***Biochim Biophys Acta*** **1709: 240-250**

9. Summaries

9.1. Summary

A solid-supported membrane (SSM) is an alkanethiol/lipid hybrid membrane with comparable lipid mobility, conductivity, and capacitance than a black lipid membrane (BLM) (Florin & Gaub, 1993; Seifert *et al.*, 1993). However, mechanical perturbations, which usually destroy a BLM, do not influence the life-time of a SSM, which is mechanically so stable that solutions may be rapidly exchanged at its surface (Pintschovius & Fendler, 1999). This key property has been utilized in this thesis to characterize electrophysiologically two bacterial secondary active transporters (MelB and LacY) (sections 5 and 6) as well as to investigate the specific interactions between ions and lipid membranes (section 4). The main achievements are summarized below:

9.1.1. Specific Interaction between Ions and Lipid Headgroups

Since the pioneering studies by Frank Hofmeister and his group in Prague some 130 years ago, specific ion effects have been described in literature in thousand of publications. In particular, the properties of lipid membranes, which represent the most important biological interface between intracellular and extracellular compartments, are essentially modulated by the ionic composition of the surrounding aqueous medium. To investigate specific interactions between ions and lipid membranes, solutions of different ionic composition were exchanged at the surface of a SSM through a flow system. This solution exchange resulted in charge translocations that were interpreted in terms of binding of the ions to the lipid headgroups at the SSM surface. Ions were classified relative to a reference ion, which was sodium (for cations) and chloride (for anions). In agreement with previous studies on the influence of ions on the dipole potential of diphytanoyl-phosphatidylcholine (PC) liposomes (Clarke & Lupfert, 1999), we found that chaotropic anions and kosmotropic cations are attracted to the PC membrane. Interestingly, this trend was also observed for a lipid bearing no charge (like monoolein). In experiments with positively charged lipids (DOTAP) and negatively charged lipids (DOPG), we found that this general trend is modulated by the electrostatic interaction of the ions with the lipid headgroup charge.

The 'principle of matching water affinities' proposed by Collins (Collins, 2004; Collins, 2006) predicts binding of chaotropic ions to chaotropic surface groups (like the ammonium group) and kosmotropic ions to kosmotropic surface groups (like the phosphate group). Although this principle would explain our results with PC, it cannot explain why a lipid without these headgroups exhibits the same trend or why for various phosphate compounds as well as other anionic surfactants the reversed cation series is found (Haverd & Warr, 2000). In our opinion, it is necessary to consider the geometry of the water molecules around the ions and headgroups to understand these effects. Indeed, our experimental results are in agreement with recent molecular dynamic simulations of PC membranes where it was shown that Cl^- binds slightly weaker than Na^+ (Bockmann *et al.*, 2003; Pandit *et al.*, 2003) and that chaotropic anions bind better than kosmotropic ones to the lipid headgroups (Sachs *et al.*, 2004; Sachs & Woolf, 2003).

9.1.2. Time Resolved Experiments

Time resolved experiments are essential for the analysis of dynamic properties of bacterial secondary active transporters. Such experiments require a rapid perturbation of the initial state of the transporter, for example, with a rapid substrate concentration jump. Therefore, quantitative temporal information concerning the substrate concentration rise is a prerequisite for a proper interpretation of the measured signals as well as for the optimization of the fluidic system. Interestingly, the time course of the transient currents generated after an ion concentration jump is independent of the particular ion or concentration utilized. These observations support the conclusion that the time course of the translocated charge in an ion concentration jump corresponds to the time course of the substrate concentration jump. Indeed, the translocated charge depends on the flow rate of the experiments and the technical parameters of the flow system. Therefore, ion concentration jumps were utilized to identify and quantify the critical parameters affecting the time resolution and the transfer function of the system. Under the flow conditions of the experiment, it is expected that a fully developed Hagen – Poiseuille flow is never obtained within the dimension of our flow pathways. Consistently, the experimental data indicate that an intermediate situation between the plug flow and the Hagen – Poiseuille flow regimes is observed.

Sugar binding in the presence of Na^+ to the melibiose permease (MelB) from *Escherichia coli*, results in a fast electrogenic conformational transition (Ganea *et al.*,

2001; Meyer-Lipp *et al.*, 2004). However, because of the limited time resolution of theses experiments, only a lower limit of $k > 50\ s^{-1}$ could be assigned to the charge displacement. A novel cuvette design in combination with a least-square de-convolution algorithm allowed the reinvestigation and accurate determination of this electrogenic conformational transition. Furthermore, the rate constant obtained from the electrical measurements is very similar to that obtained from a ligand-induced conformational change measured by stopped-flow tryptophan fluorescence spectroscopy. Both findings indicate that upon sugar binding MelB undergoes an electrogenic conformational transition with a rate constant k of ~ 250 s^{-1}.

The lactose permease (LacY) from *Escherichia coli* was electrophysiologically investigated with the same novel cuvette design utilized for MelB. With LacY, two mutants (E325A and C154G) were utilized to investigate electrogenic conformational transitions triggered by sugar binding (see section 9.1.3.). The least-square deconvolution algorithm was again utilized to recover the rate constants (k) of these conformational transitions. However, for E325A LacY, the electrogenic conformational transitions are too fast to be resolved. For C154G LacY, the rate constants of the electrogenic conformational transitions triggered by 50 mM concentration jumps of lactose or lactulose are $53 \pm 5\ s^{-1}$ and $72 \pm 5\ s^{-1}$, respectively.

9.1.3. Electrophysiological Characterization of LacY

One of the best-characterized secondary active transporters is the lactose permease (LacY) from *Escherichia coli*. Because of the wealth of structural, biophysical, and biochemical data available for LacY (reviewed in (Guan & Kaback, 2006; Kaback *et al.*, 2001), it represents an ideal model system for the investigation of the basic principles and molecular details of secondary active transport. However, LacY (as well as many other bacterial membrane transporters) do not target to the plasma membrane in frog oocytes or other eukaryotic cells, thereby precluding application of standard electrophysiological technology. Here, the first successful electrophysiological study of LacY by using purified, reconstituted proteoliposomes with SSM-based electrophysiology is presented. Downhill sugar/H^+ symport into proteoliposomes reconstituted with purified wild-type LacY generates transient currents measured by capacitive coupling with an SSM-electrode. The transient currents observed depend on the sugar substrate utilized, and they are completely blocked by alkylation of Cys148 with *N*-ethylmaleimide (NEM) (Bieseler *et al.*, 1985; Trumble *et al.*, 1984; van Iwaarden *et al.*, 1993). Thus, the transients are specifically

due to the electrogenic activity of LacY. The time course of the transients is characterized by two distinct phases: a rapid rise to a maximum followed by a much slower decay towards the base line.

Downhill sugar/H^+ symport into the proteoliposomes generates an inside positive potential, which acts to decelerate the downhill symport reaction, leading to transient currents. However, any conformational transition that displaces charged amino acyl side chains or reorients electrical dipoles also represents an electrogenic process that may contribute to the transient nature of the currents. To discriminate between these two possibilities, experiments were performed with proteoliposomes reconstituted at lipid to protein ratios (LPR) of 10 and 5. An electrogenic conformational transition is expected to yield identical time constants for decay of the transients at different particle densities. In contrast, charging of the liposomal membrane by downhill sugar/H^+ symport should lead to decreasing time constants at increasing protein densities. We found that an increase in the protein density results in a significantly faster decay of the transients. Therefore, the transient currents observed for wild-type LacY represent mainly charging of the liposome membrane due to downhill sugar/H^+ symport.

The electrical transients observed with wild-type LacY are strongly dependent on ambient pH: an overall increase in pH from 6.6 to 8.5 causes a five-fold increase in the magnitude of the peak current, in agreement with rates of efflux from right-side-out membrane vesicles (Kaczorowski & Kaback, 1979) or proteoliposomes reconstituted with purified LacY (Garcia *et al.*, 1983; Viitanen *et al.*, 1983). Furthermore, the half saturating concentration increases only slightly with the pH, and its value is close to the value determined for downhill lactose/H^+ influx in proteoliposomes reconstituted with purified LacY (Viitanen *et al.*, 1984).

To dissect the overall electrogenic response, mutants of LacY that bind ligand, but do little or no lactose/H^+ symport were utilized. Mutant E325A is specifically defective in all steps involving H^+ release from LacY, but catalyzes exchange and counterflow at least as well as wild-type (Carrasco *et al.*, 1986; Carrasco *et al.*, 1989). With E325A LacY, concentration jumps with different galactopyranosides induce transient currents with virtually identical kinetics and negligible differences in magnitude. These transient currents are also abolished after treatment with NEM. However, the transient currents are ~5-times smaller than those observed with wild-type LacY. Mutant C154G binds sugar as well as wild-type but exhibits extremely low transport activities (Menick *et al.*, 1987; Menick *et al.*, 1985; Sahin-Toth & Kaback, 2001; Smirnova & Kaback, 2003). In contrast to mutant E325A, the magnitude and kinetics

of the peak currents recorded with C154G LacY depend on the substrate utilized. Nevertheless, the same amount of translocated charge is observed with both mutants (only 6% of the total charge displacement observed with wild-type LacY). Importantly, the time course of the transient currents is significantly faster with both mutant proteins relative to the wild-type. Therefore, these transients are not associated with residual symport activity, but to electrogenic conformational transitions triggered by sugar binding. It is proposed that downhill substrate/H^+ symport in LacY involves at least two electrogenic reactions: (i) a minor electrogenic reaction that occurs upon sugar binding and is due to a conformational transition in LacY; and (ii) a major electrogenic reaction probably due to cytoplasmic release of H^+ during downhill sugar/H^+ symport, which is the limiting step for this mode of transport. This interpretation is in agreement with wealth of biochemical and biophysical data.

9.2. Zusammenfassung

Eine festkörperunterstützte Membran (SSM: *solid-supported membrane*) ist eine Alkanthiol-/Lipid-Mischmembran mit einer vergleichbaren Lipidmobilität, Leitfähigkeit und elektrischen Kapazität wie eine schwarze Lipidmembran (BLM: *black lipid membrane*) (Florin & Gaub, 1993; Seifert *et al.*, 1993). Jedoch beeinflussen mechanische Störungen, die normalerweise eine BLM zerstören, die Lebensdauer der SSM nicht, da diese mechanisch so stabil ist, dass Lösungen auf ihrer Oberfläche schnell ausgetauscht werden können (Pintschovius & Fendler, 1999). Diese wichtige Eigenschaft wurde in dieser Doktorarbeit genutzt, um zwei bakterielle sekundäre aktive Transporter (MelB and LacY) elektrophysiologisch zu charakterisieren (Sektionen 5 und 6) und die spezifischen Wechselwirkungen zwischen Ionen und Lipidmembranen zu untersuchen (Sektion 4). Die wichtigsten Ergebnisse sind im Folgenden zusammengefasst:

9.2.1. Spezifischen Wechselwirkungen zwischen Ionen und Lipidmembranen

Seit den ersten Studien von Frank Hofmeister und seiner Gruppe in Prag vor etwa 130 Jahren wurden spezifische Ioneneffekte in tausenden von Veröffentlichungen beschrieben. Insbesondere werden die Eigenschaften von Lipidmembranen, die die wichtigste biologische Schnittstelle zwischen dem Zellinneren und dem Zelläußeren darstellen, durch die ionische Zusammensetzung des umgebenden wässrigen Mediums beeinflusst. Um die spezifischen Wechselwirkungen zwischen Ionen und Lipidmembranen zu untersuchen, wurden Lösungen mit verschiedenen ionischen Zusammensetzungen durch ein Durchflusssystem auf der SSM-Oberfläche ausgetauscht. Dieser Lösungsaustausch resultierte in Ladungsverschiebungen, die hinsichtlich der Bindung der Ionen an die Lipid-Kopfgruppen auf der SSM-Oberfläche interpretiert wurden. Die Ionen wurden in Bezug auf ein Referenzion klassifiziert, und zwar Natrium (für Kationen) und Chlorid (für Anionen). Wir werden im Folgenden die Begriffe chaotropisch und kosmotropisch verwenden, die sich auf die Wechselwirkung zwischen Wassermolekülen und Ionen beziehen: kosmotropische Ionen sind „Wasserstruktur-Macher“ und chaotropische Ionen sind „Wasserstruktur-Brecher“. Übereinstimmend mit früheren Studien über den Einfluss von Ionen auf das Dipolpotential von Phosphatidylcholin(PC)-Liposomen (Clarke & Lupfert, 1999), fanden wir heraus, dass die chaotropischen Anionen und kosmotropischen Kationen von der PC-Membran angezogen werden. Interessanterweise konnte dieser Trend auch bei einem nicht geladenen Lipid (wie Monoolein) beobachtet werden. Bei Experimenten mit positiv geladenen Lipiden (DOTAP) und negativ geladenen Lipiden

(DOPG) fanden wir heraus, dass dieser generelle Trend durch elektrostatische Wechselwirkungen der Ionen mit Ladungen auf der Lipid-Kopfgruppe beeinflusst wird.

Das von Collins vorgeschlagene Prinzip der 'gleichen Wasseraffinitäten' (*'the principle of matching water affinities'*) (Collins, 2004; Collins, 2006) sagt die Bindung von chaotropischen Ionen an chaotropische Lipidgruppen (wie die Ammoniumgruppe) und kosmotropischen Ionen an kosmotropische Lipidgruppen (wie die Phosphatgruppe) voraus. Obwohl dieses Prinzip unsere Ergebnisse mit PC erklären würde, kann es nicht erklären, warum ein Lipid ohne diese Kopfgruppe den gleichen Trend aufweist oder warum man bei verschiedenen Phosphatzusammensetzungen und anderen Anionen-Tensiden die umgekehrte Reihenfolge der Kationen vorfindet (Haverd & Warr, 2000). Wir sind der Meinung, dass es notwendig ist, die Geometrie der Wassermoleküle um die Ionen und Kopfgruppen herum zu berücksichtigen, um diese Effekte zu verstehen. Tatsächlich stimmen unsere Versuchsergebnisse mit neuesten molekulardynamischen Simulationen von PC-Membranen überein, die gezeigt haben, dass Cl^- etwas schwächer bindet als Na^+ (Bockmann *et al.*, 2003; Pandit *et al.*, 2003) und dass chaotropische Anionen besser an Lipid-Kopfgruppen binden als kosmotropische (Sachs *et al.*, 2004; Sachs & Woolf, 2003).

9.2.2. Zeitaufgelöste Experimente

Zeitaufgelöste Experimente sind fundamental für die Analyse der dynamischen Eigenschaften von bakteriellen sekundären aktiven Transportern. Solche Experimente erfordern eine schnelle Störung des Ausgangszustandes der Transporter, z.B. durch einen schnellen Substratkonzentrationssprung. Deshalb sind quantitative zeitliche Informationen, die den Anstieg der Substratkonzentration betreffen, eine Voraussetzung für eine genaue Interpretation der gemessenen Signale und die Optimierung des Durchflusssystems. Interessanterweise ist der Zeitverlauf von transienten Messströmen, die nach Ionenkonzentrationssprüngen auftreten, unabhängig vom speziellen Ion oder der verwendeten Konzentration. Diese Beobachtungen stützen die Schlussfolgerung, dass der Zeitverlauf der Ladungsverschiebung in einem Ionenkonzentrationssprung dem Zeitverlauf eines Substratkonzentrationssprungs entspricht. Tatsächlich hängt die Ladungsverschiebung von der Durchflussrate der Experimente und den technischen Parametern des Durchflusssystems ab. Deshalb wurden Ionenkonzentrationssprünge verwendet, um die kritischen Parameter zu identifizieren und zu quantifizieren, die die Zeitauflösung und die Transferfunktion des Systems

beeinflussen. Unter den spezifischen Durchflussbedingungen des Experiments wird erwartet, dass unter unseren Strömungsbedigungen nie eine voll entwickelte Hagen-Poiseuille Strömung erreicht wird. Übereinstimmend damit deuten die experimentellen Daten darauf hin, dass ein Zwischenzustand zwischen einer idealen "plug flow" und der Hagen-Poiseuille Strömung beobachtet werden kann.

Die Zuckerbindung an die Melibiose Permease (MelB) von *Escherichia coli* in Gegenwart von Na^+ resultiert in einer elektrogenen Konformationsänderung (Ganea *et al.*, 2001; Meyer-Lipp *et al.*, 2004). Aufgrund der begrenzten Zeitauflösung dieser Experimente könnte der Reaktionsgeschwindigkeitskonstante dieser Konformationsänderung jedoch nur ein Wert von mindestens $k > 50\ s^{-1}$ zugeordnet werden. Ein neues Küvettendesign, in Verbindung mit einem Dekonvolutionsalgorithmus nach der Methode der kleinsten Fehlerquadrate, erlaubte die erneute Erforschung und akkurate Bestimmung dieser Konformationsänderung. Desweiteren ist die Geschwindigkeitskonstante, die sich aus den elektrischen Messungen ergeben hat, sehr ähnlich derjenigen, die aus Messungen von substratinduzierten Konformationsänderungen mit „stopped-flow" Tryptophan-Fluoreszenz-Spektroskopie resultiert. Beide Ergebnisse lassen darauf schließen, dass MelB bei Zuckerbindung eine elektrogene Konformationsänderung mit einer Reaktionsgeschwindigkeitskonstante von $k \sim 250\ s^{-1}$ durchmacht.

Die Lactose Permease (LacY) von *Escherichia coli* wurde mit Hilfe des gleichen neuen Küvettendesigns, das bereits bei MelB eingesetzt wurde, elektrophysiologisch untersucht. Mit LacY wurden zwei Mutanten (E325A und C154G) verwendet, um eine durch Zuckerbindung ausgelöste, elektrogene Konformationsänderung zu untersuchen (siehe Sektion 9.2.3.). Hierbei wurde erneut der Dekonvolutionsalgorithmus nach der Methode der kleinsten Fehlerquadrate verwendet, um die Reaktionsgeschwindingkeitskonstante (k) dieser Konformationsänderung herauszufinden. Jedoch ist für E325A LacY die elektrogene Konformationsänderung für eine exakte Bestimmung zu schnell. Für C154G LacY ist die Reaktionsgeschwindingkeitskonstante (k) für 50 mM Konzentrationssprung von Laktose oder Laktulose $53 \pm 5\ s^{-1}$ beziehungsweise $72 \pm 5\ s^{-1}$.

9.2.3. Elektrophysiologische Untersuchung von LacY

Eine der am besten charakterisierten sekundären aktiven Transporter ist die Lactose Permease (LacY) von *Escherichia coli*. Dank einer Vielzahl an verfügbaren strukturellen, biophysischen und biochemischen Daten für LacY (Guan & Kaback, 2006; Kaback *et al.*, 2001) stellt sie ein ideales Modellsystem zur Erforschung der Grundprinzipien und der molekularen Details der sekundären aktiven Transporter

dar. Nichtsdestotrotz kann LacY (so wie auch viele andere bakterielle Membran-Transporter) in die Plasma-Membran von Froscheizellen oder in andere eukaryotische Zellen nicht exprimiert werden. Deshalb war bisher die standardmäßige elektrophysiologische Untersuchung von LacY nicht möglich. Hier wird die erste erfolgreiche elektrophysiologische Studie von LacY unter Einsatz aufgereinigter, in Proteoliposomen rekonstituierter Proteine, mit SSM-basierter Elektrophysiologie gezeigt. Der „bergab“ Zucker/Protonen-Symport in Proteoliposomen, die mit dem aufgereinigten Wildtyp LacY rekonstituiert wurden, generiert transiente Messströme, die durch kapazitive Kopplung mit einer SSM-Elektrode gemessen werden. Die beobachteten transienten Messströme hängen von den Zuckersubstraten ab und werden vollständig durch die Alkylierung von Cystein 148 mit N-Äthylmaleimid (NEM: *N-Ethylmaleimide*) blockiert (Bieseler *et al.*, 1985; Trumble *et al.*, 1984; van Iwaarden *et al.*, 1993). Nach Substratzugabe erhielt man transiente Ströme aufgrund der elektrogenen Aktivität von LacY. Der Zeitverlauf der Transienten ist durch zwei verschiedene Phasen charakterisiert: ein schneller Anstieg auf die Stromspitze, gefolgt von einem deutlich langsameren Abfall hin zur Basislinie.

Der „bergab“ Zucker/Protonen-Symport in Proteoliposomen hinein generiert ein inneres positives Potenzial, was eine verlangsamte „bergab“ Symport-Reaktion hervorruft, die zu transienten Messströmen führt. Jedoch stellt jede Konformationsänderung, die geladene Aminosäureseitenketten verlagert oder elektrische Dipole umorientiert, auch einen elektrogenen Prozess dar, der zu der transienten Eigenschaft der Messströme beitragen kann. Um zwischen diesen beiden Möglichkeiten zu unterscheiden wurden Experimente mit Proteoliposomen, die mit unterschiedlichen Lipid- zu Protein- Verhältnissen von LPR 10 oder 5 (LPR: *Lipid to protein ratio*) rekonstituiert wurden, durchgeführt. Es wird erwartet, dass eine elektrogene Konformationsänderung identische Zeitkonstanten für den Abfall der Transienten bei verschiedenen Partikeldichten ergibt. Dagegen sollte das Laden der Liposommembran durch einen „bergab“ Zucker/Protonen-Symport zu abnehmenden Zeitkonstanten bei zunehmender Partikeldichte führen. Wir haben herausgefunden, dass eine Zunahme der Proteindichte in einem wesentlich schnelleren Abfall der Transienten resultiert. Daher stellen die für den Wildtyp LacY beobachteten transienten Ströme hauptsächlich eine Ladung der Liposommembran aufgrund des „bergab“ Zucker/Protonen-Symports dar.

Die elektrischen Transienten, die beim Wildtyp LacY beobachtet wurden, hängen stark vom pH-Wert ab: Ein gesamter Anstieg des pH-Werts von 6,6 auf 8,5 verursacht eine fünffache Zunahme des Werts der Stromspitze, in Übereinstimmung

mit den Effluxraten von RSO (RSO: *right-side-out*) Membranvesikeln (Kaczorowski & Kaback, 1979) oder Proteoliposomen, die mit aufgereinigter LacY rekonstituiert wurden (Garcia *et al.*, 1983; Viitanen *et al.*, 1983). Außerdem erhöht sich die Halbsättigungskonzentration nur leicht bei steigendem pH-Wert. Ihr Wert ist ähnlich wie derjenige, der beim „bergab" Zucker/Protonen-Symport in LacY Proteoliposomen, gemessen wurde (Viitanen *et al.*, 1984).

Um die allgemeine elektrogene Reaktion zu analysieren wurden Mutanten von LacY, die Ligand binden, aber wenig oder keinen Lactose/Protonen-Transport machen, verwendet. Die Mutante E325A weist einen Defekt bei allen Schritten, die die H^+ Abgabe von LacY involvieren, auf. E325A LacY katalysiert „exchange" und „counterflow" mindestens genauso gut wie der Wildtyp (Carrasco *et al.*, 1986; Carrasco *et al.*, 1989). Bei Verwendung von E325A LacY induzieren Konzentrationssprünge mit unterschiedlichen Galactopyranosiden transiente Ströme mit nahezu identischer Kinetik. Diese Ströme verschwinden nach Behandlung mit NEM. Jedoch sind die transienten Ströme fünfmal kleiner als diejenigen, die beim Wildtyp LacY beobachtet wurden. Die Mutante C154G bindet Zucker genauso gut wie der Wildtyp, aber zeigt extrem niedrige Transportaktivitäten (Menick *et al.*, 1987; Menick *et al.*, 1985; Sahin-Toth & Kaback, 2001; Smirnova & Kaback, 2003). Im Gegensatz zur Mutante E325A hängen die Größe und die Kinetik der transienten Ströme, die bei C154G LacY erfasst wurden, vom verwendeten Substrat ab. Nichtsdestotrotz kann man bei beiden Mutanten die gleiche Ladungsverschiebung beobachten (nur 6% der gesamten Ladungsverschiebung, die beim Wildtyp LacY beobachtet wurde). Wichtig ist, dass der Zeitverlauf der transienten Ströme wesentlich schneller bei den beiden mutierten Proteinen im Vergleich zum Wildtyp LacY ist. Deshalb entstehen die Transienten nicht aufgrund einer Rest-Transportaktivität, sondern aufgrund einer elektrogenen Konformationsänderung, ausgelöst durch Zuckerbindung. Es wird vermutet, dass der „bergab" Zucker/Protonen-Symport bei LacY mindestens zwei elektrogene Reaktionen involviert: (i) eine schwach elektrogene Reaktion, die aufgrund der Zuckerbindung erfolgt und einer elektrogenen Konformationsänderung in LacY zuzuschreiben ist; und (ii) eine stark elektrogene Reaktion, die vermutlich auf eine zytoplasmische Abgabe von H^+ während des „bergab" Zucker/Protonen-Symports zurückzuführen ist, was den ratenlimitierenden Schritt für diese Art von Transport darstellt. Diese Interpretation stimmt überein mit einer Vielzahl an biochemischen und biophysischen Daten.

Acknowledgements

I wish to thank Prof. Dr. Klaus Fendler for the three challenging projects and for his excellent and detailed supervision of my work. His help and support inside and outside the laboratory have been crucial for the successful development of the different projects. Furthermore, I appreciate very much his encouragement and good advices for my future academic career.

I am very grateful to Prof. Dr. Ernst Bamberg for giving me the chance to work in the Department of Biophysical Chemistry at the Max-Planck-Institute of Biophysics, and for the great interest and support to my work.

I would like to thank Distinguished Prof. Dr. H. Ronald Kaback (University of California, Los Angeles) for the very helpful suggestions to my work, especially in the reconstitution of LacY into proteoliposomes. His enthusiasm and new ideas were of great help in the successful electrophysiological characterization of LacY.

To Dr. Vladimir Kasho and Dr. Irina Smirnova from the laboratory of Distinguished Prof. Dr. H. Ronald Kaback I would like to say many thanks for kindly providing me with purified LacY and for fruitful discussions.

I am very grateful to Prof. Dr. Werner Kunz for his help and support to our work on the specific interactions between ions and lipid headgroups and for helpful discussions.

I would like to thank Prof. Gérard Leblac for providing our laboratory with bacterial strains and plasmids encoding MelB as well as for his support to the project about the rapid activation of MelB.

To Benjamin Dueck, Martin Stein, Michela Schlüter, and Kerstin Meyer-Lipp, I would like to say many thanks for their contributions to the project about the rapid activation of MelB proteoliposomes immobilized on a SSM. Michela Schlüter is also acknowledged for the first guide around the labs and showing me the stopped-flow technique.

I would like to thank Dr. Winfried Hasse for the excellent freeze–fracture micrographs of the reconstituted LacY proteoliposomes and Andre Bazzone for excellent help with the electrophysiological characterization of LacY mutants.

I thank especially Dr. Anca Poppescu and Prof. Constanta Ganea for their enthusiasm, exchange of constructive ideas, and friendship.

To Dr. Sebastian Richers, I would like to say many thanks for helpful discussions about protein purification, for patiently practicing German with me, and for his nice friendship.

I am very grateful to Dr. Klaus Hartung, Dr. Christian Bamann, and Dr. Robert E. Dempski for fruitful discussions

I would like to thank Lina Hatahet for excellent assistance in the laboratory.

To Heidi Bergemann, thank you so much for all the help during the past years!

Helga Volk receives my sincere thanks for her tremendous help with posters and figures.

I would like to say many thanks to Solveigh McCormack and Rosemarie Schmidtell for their help in the library.

I would like to acknowledge the Deutsche Forschungsgemeinschaft (projects SFB 807 and 447), as well as the Max Planck Gesellschaft for supporting the research.

I thank especially all group members of the group leaded by Prof. Dr. Klaus Fendler, past and present, for stimulating discussions in our Friday's seminar and for their great help in the laboratory.

I am very grateful to all the group members of the Department of Biophysical Chemistry, past and present, for your friendship and for all the good moments we have had together.

I would like specially thank Melanie Alt for more than five wonderful years of relationship. I would like to thank also her family and mine for their support.

List of Publications

Publications not included in this dissertation:

- Garcia-Celma JJ, Cross A (2004) Stokes or Newton? Decide yourself. Orginal Title: "¿Stokes o Newton? Decidelo tu mismo". Revista Española de Fisica 18: 36-39

This publication reflects a research performed as a student in Physics at the University of Valencia.

- Aguilella-Arzo M, Garcia-Celma JJ, Cervera J, Alcaraz A, Aguilella VM (2007) Electrostatic properties and macroscopic electrodiffusion in OmpF porin and mutants. *Bioelectrochemistry* **70:** 320-327

This publication reflects a research performed as post-graduate student at the University Jaume I.

Publications included in this dissertation:

- Garcia-Celma JJ, Hatahet L, Kunz W, Fendler K (2007) Specific anion and cation binding to lipid membranes investigated on a solid supported membrane. *Langmuir* **23:** 10074-10080

- Garcia-Celma JJ, Dueck B, Stein M, Schlueter M, Meyer-Lipp K, Leblanc G, Fendler K (2008) Rapid activation of the melibiose permease MelB immobilized on a solid-supported membrane. *Langmuir* **24:** 8119-8126

- Schulz P, Garcia-Celma JJ, Fendler K (2008) SSM-based electrophysiology. *Methods* 46: 97-103

- Garcia-Celma JJ, Smirnova IN, Kaback HR, Fendler K (2009) Electrophysiological characterization of LacY. *Proc Natl Acad Sci U S A*

Contributions to the Manuscripts

1) Specific Anion and Cation Binding to Lipid Membranes investigated on a Solid-Supported Membrane

Designed the research with Klaus Fendler.

Measured the datasets shown in the different figures with the exception of Figure 4.

Analyzed the data with Klaus Fendler.

Wrote the manuscript with Klaus Fendler and Werner Kunz.

2) Rapid Activation of MelB Immobilized on a Solid-Supported Membrane

Designed the research with Benjamin Dueck, Michela Schlueter, and Klaus Fendler.

Measured the data shown in Figure 3, Figure 4 (the data corresponding to the valve-less diverted geometry), Figure 5, and Figure 6A.

Developed the least-square deconvolution algorithm

Analyzed the data with Klaus Fendler.

Wrote the manuscript with Klaus Fendler.

3) SSM-based electrophysiology

Measured the data shown in Figure 7.

Wrote the manuscript with Klaus Fendler and Patrick Schulz.

4) Electrophysiological Characterization of LacY

Designed the research with Klaus Fendler.

Measured all the data shown in the figures and tables.

Analyzed the data with Irina N. Smirnova, Klaus Fendler, and H. Ronald Kaback.

Wrote the manuscript with Irina N. Smirnova, Klaus Fendler, and H. Ronald Kaback.

Curriculum Vitae

PERSONAL INFORMATION

Surname, Name	**GARCÍA-CELMA, Juan-José**
Address	**Obere Hainstr. 2A, 61440 Oberursel, Germany**
Telephone	**+49 (0) 15156367131**
e-mail	juanjose.garciacelma@gmail.com
Nationality	Spanish
Date and place of birth	**04.01.1980 (Tortosa, Spain)**

EXPERIENCE

01/2006 – Present	**Ph.D. Student** at the Max-Planck-Institute of Biophysics, Frankfurt
01/2006 – Present	**International Max Planck Research School for Structure and Function of Biological Membranes** at the Max-Planck-Institute of Biophysics, Frankfurt
09/2003 – 10/2005	**Post-graduate student** at the University Jaume I, Castellon

EDUCATION

10/1998 – 06/2003	**Studies in Physics** at the University of Valencia, Spain - ***First prize*** on "Laboratory Award 2001" for the best new designed laboratory experiment (shared with Dr. Ana Cros Stoetter) - ***Collaboration Fellowship*** on optical fibers (2003) - ***Degree on Physics*** in June 2003, average grade: between 2 and 1
09/1994 – 06/1998	**Secondary School,** Caravaca de la Cruz, Spain Scientific branch

SELECTED PRESENTATIONS

2009	**"Biophysical Society Annual Meeting"** Oral Presentation
2008	**"Mechanical and Electrical Properties of Artificial and Cellular membranes", Gomadingen, Germany** Oral Presentation
	"Transporters 2008", Murten, Switzerland Oral Presentation

LANGUAGE SKILLS

Spanish Mother Tongue

English Fluent

German Good command

Appendix: Publications

Specific Anion and Cation Binding to Lipid Membranes Investigated on a Solid Supported Membrane

Juan J. Garcia-Celma,[†] Lina Hatahet,[†] Werner Kunz,[‡] and Klaus Fendler*[,†]

Department of Biophysical Chemistry, Max Planck Institute of Biophysics, D-60438 Frankfurt, Germany, and Institute of Physical and Theoretical Chemistry, University of Regensburg, D-93040 Regensburg, Germany

Received April 24, 2007. In Final Form: June 20, 2007

Ion binding to a lipid membrane is studied by application of a rapid solution exchange on a solid supported membrane. The resulting charge displacement is analyzed in terms of the affinity of the applied ions to the lipid surface. We find that chaotropic anions and kosmotropic cations are attracted to the membrane independent of the membrane composition. In particular, the same behavior is found for lipid headgroups bearing no charge, like monoolein. This general trend is modulated by electrostatic interaction of the ions with the lipid headgroup charge. These results cannot be explained with the current models of specific ion interactions.

Introduction

Many processes in surface science, colloid science, and biophysics critically depend on the choice of the background salt in a way that goes beyond the description by the Gouy−Chapman mean-field theory. While this theory would predict the same behavior for all ions of the same valency, "specific" effects for different ions of the same charge are found which in many cases follow a more or less well-defined sequence, the so-called Hofmeister series (for reviews, see Cacace[1] or Collins[2]). The nature of the ionic interactions with the surfaces leading to these Hofmeister phenomena is still under debate (for reviews, see Kunz[3] or Leontidis[4]). Many different concepts have been introduced over the years to account for specific ion effects. To mention only the most recent, ionic dispersion or van der Waals forces acting on the ions at the interface[5−8] or the concept of matching water affinities[9,10] have been proposed. However, none of these theories led to a satisfactory explanation of the observed effects on a broad scale, although the MD simulations by Jungwirth and co-workers[11,12] are most promising. Not only are their results on the air−water interface fairly predictive, but they also take into account the influence of ion polarizability on the water structure, which is probably the key point for the understanding of Hofmeister effects.

Lipid membranes represent the most important biological interface. They not only contain the whole transport and sensory machinery of the cell, but also are important for a large number of mechanical tasks like cell adhesion, fusion, growth, and migration. Here, the ionic composition of the aqueous medium plays a significant role, essentially modulating the properties of the lipid membrane like the surface potential,[13] the dipole potential,[14] the structure and dynamics of the lipid molecules[15,16] or intermembrane forces,[17] the transition from micelles to vesicles,[18] and the swelling of vesicles.[19] A convenient model system for a biological membrane is a solid supported lipid membrane (SSM). SSMs have found a broad application as rugged carriers for membrane proteins. Imbedded or attached to this membrane, their activity can be assessed by a variety of methods like IR spectroscopy, electrochemistry, or electrical measurements.[20−22] Here, we have used an SSM to study ion

* To whom correspondence should be addressed. Fax: (+) 49 69 6303-2002. E-mail: klaus.fendler@mpibp-frankfurt.mpg.de.

[†] Max Planck Institute of Biophysics.

[‡] University of Regensburg.

(1) Cacace, M. G. The Hofmeister series: salt and solvent effects on interfacial phenomena. *Q. Rev. Biophys.* **1997**, *30* (3), 241−277.

(2) Collins, K. D.; Washabaugh, M. W. The Hofmeister effect and the behaviour of water at interfaces. *Q. Rev. Biophys.* **1985**, *18*, 323−422.

(3) Kunz, W.; Lo Nostro, P.; Ninham, B. W. The present state of affairs with Hofffieister, effects. *Curr. Opin. Colloid Interface Sci.* **2004**, *9* (1−2), 1−18.

(4) Leontidis, E. Hofmeister anion effects on surfactant self-assembly and the formation of mesoporous solids. *Curr. Opin. Colloid Interface Sci.* **2002**, *7* (1−2), 81−91.

(5) Ninham, B. W.; Yaminsky, V. Ion Binding and Ion Specificity - the Hofmeister Effect and Onsager and Lifshitz Theories. *Langmuir* **1997**, *13* (7), 2097−2108.

(6) Bostrom, M.; Williams, D. R. M.; Ninham, B. W. Ion specificity of micelles explained by ionic dispersion forces. *Langmuir* **2002**, *18* (16), 6010−6014.

(7) Bostrom, M.; Williams, D. R. M.; Ninham, B. W. Special ion effects: Why the properties of lysozyme in salt solutions follow a Hofmeister series. *Biophys. J.* **2003**, *85* (2), 686−694.

(8) Bostrom, M.; Williams, D. R. M.; Stewart, P. R.; Ninham, B. W. Hofmeister effects in membrane biology: The role of ionic dispersion potentials - art. no. 041902. *Phys. Rev. E* **2003**, *6804* (4 Part 1), 1902.

(9) Collins, K. D. Ions from the Hofmeister series and osmolytes: effects on proteins in solution and in the crystallization process. *Methods* **2004**, *34* (3), 300−311.

(10) Collins, K. D. Ion hydration: Implications for cellular function, polyelectrolytes, and protein crystallization. *Biophys. Chem.* **2006**, *119* (3), 271−281.

(11) Jungwirth, P.; Tobias, D. J. Molecular structure of salt solutions: A new view of the interface with implications for heterogeneous atmospheric chemistry. *J. Phys. Chem. B* **2001**, *105* (43), 10468−10472.

(12) Vrbka, L.; Mucha, M.; Minofar, B.; Jungwirth, P.; Brown, E. C.; Tobias, D. J. Propensity of soft ions for the air/water interface. *Curr. Opin. Colloid Interface Sci.* **2004**, *9* (1−2), 67−73.

(13) Eisenberg, M.; Gresalfi, T.; Riccio, T.; McLaughlin, S. Adsorption of Monovalent Cations to Bilayer Membranes Containing Negative Phospholipids. *Bilayer Membr.* **1979**, *18* (23), 5213−5223.

(14) Clarke, R. J.; Lüpfert, C. Influence of anions and cations on the dipole potential of phosphatidylcholine vesicles: A basis for the Hofmeister effect. *Biophys. J.* **1999**, *76* (5), 2614−2624.

(15) Sachs, J. N.; Nanda, H.; Petrache, H. I.; Woolf, T. B. Changes in phosphatidylcholine headgroup tilt and water order induced by monovalent salts: Molecular dynamics simulations. *Biophys. J.* **2004**, *86* (6), 3772−3782.

(16) Zhao, W.; Rog, T.; Gurtovenko, A. A.; Vattulainen, I.; Karttunen, M. Atomic-scale structure and electrostatics of anionic palmitoyloleoylphosphatidylglycerol lipid bilayers with Na+ counterions. *Biophys. J.* **2007**, *92* (4), 1114−1124.

(17) Petrachet, H. I.; Zemb, T.; Belloni, L.; Parsegian, V. A. Salt screening and specific ion adsorption determine neutral-lipid membrane interactions. *Proc. Natl. Acad. Sci. U.S.A.* **2006**, *103* (21), 7982−7987.

(18) Renoncourt, A.; Vlachy, N.; Bauduin, P.; Drechsler, M.; Touraud, D.; Verbavatz, J. M.; Dubois, M.; Kunz, W.; Ninham, B. W. Specific alkali cation effects in the transition from micelles to vesicles through salt addition. *Langmuir* **2007**, *23* (5), 2376−2381.

(19) Claessens, M.; van Oort, B. F.; Leermakers, F. A. M.; Hoekstra, F. A.; Stuart, M. A. C. Charged lipid vesicles: Effects of salts on bending rigidity, stability, and size. *Biophys. J.* **2004**, *87* (6), 3882−3893.

10.1021/la701188f CCC: $37.00
Published on Web 08/24/2007

binding to a lipid surface, applying an electrophysiological detection technique. We have analyzed the charge translocation after the rapid exchange of various cations and anions on a lipid surface of different composition and interpreted this in terms of binding of the ions in the lipid headgroup region.

Using the painting technique employed in this study, defect-free bimolecular alkanethiol/lipid hybrid membranes may be formed from virtually every lipid.[23] These films have been shown to exhibit physical properties very similar to free-standing lipid membranes such as a comparable lipid mobility, conductivity, and capacitance.[23,24] The thickness determined previously by surface plasmon spectroscopy of 4.1 nm[23] agrees within experimental error with the dimensions expected for an octadecyl mercaptan/diphytanoyl phosphatidylcholine hybrid bilayer, suggesting a conventional bilayer-like order of the lipid layer. Taken together, all experimental evidence available argues for a lipid surface very similar to that of a free-standing lipid membrane.

A solid supported membrane represents a model system for a lipid membrane with the additional benefit of being mechanically so stable that solutions may be rapidly exchanged at its surface. When solutions of different ionic composition are exchanged, a charge displacement can be registered via the supporting gold electrode that represents the relaxation of the different ions in their respective equilibrium positions. As a fist approximation, electrodes detect charge movements within one Debye length's distance, which is ∼1 nm at 100 mM ionic strength. This is also roughly the dimension of the lipid headgroup. We can, therefore, state that the SSM technique registers charge displacements in the immediate headgroup region. According to recent molecular dynamics studies, this is also where ions accumulate.[25,26]

The charge displacements measured on the SSM have been used to obtain information about the relative distribution of cations and anions. Ions are characterized relative to a reference ion, which was Na^+ for cations and Cl^- for anions. A positive charge displacement after a cation exchange or a negative charge displacement after an anion exchange means that the average equilibrium position of the ions is closer to the underlying electrode than that of Na^+ (for cations) or of Cl^- (for anions) and/or that more ions reside in this position. This is frequently called "binding", and we will use this term in the following, keeping in mind that it can be anything between a diffuse accumulation in or very close to the lipid headgroup up to specific binding at a well-defined binding site.[4]

Materials and Methods

Chemicals. Activating and nonactivating solutions contained 10 mM Tris/Hepes pH 7.0 plus salt. The lipid film-forming solutions were as follows: diphytanoyl phosphatidylcholine 1.5% (w/v) in *n*-decane, dioleoyl phosphatidyl glycerol 1.5% in *n*-decane, dioleoyl trimethylammonium propane 1.5% in *n*-decane (synthetic lipids from Avanti Polar Lipids Inc., Pelham, USA), and monoolein 1.5% in *n*-decane or squalene (1-oleoyl-*rac*-glycerol from Sigma-Aldrich, St. Louis, USA). A 1 mM octadecyl mercaptan (C_{18}-mercaptan, Aldrich, Steinheim, Germany) solution in ethanol was used for the incubation of the gold electrodes.

SSM Setup. The SSM was prepared by linking an alkanethiol (octadecyl mercaptan) monolayer to a gold electrode deposited on a glass support and covering it with a lipid monolayer. The alkanethiol monolayer forms spontaneously when the freshly gold coated electrode is incubated for 6 h in an ethanolic 1 mM octadecyl mercaptan solution. The lipid monolayer is deposited using a painting technique where a small amount of the film-forming solution is applied to the electrode. The electrode is then mounted in a flow-through cuvette with an inner volume of 17 μL. The monolayer forms spontaneously when the SSM is rinsed with buffer in the cuvette. The planar membrane formed has an area of ∼0.8 mm^2. The gold electrode is connected to an amplifier; the reference electrode is a Ag/AgCl electrode separated from the solution by a salt bridge. For details of the setup, see refs 21 and 27.

Measuring Procedure. The experiments were carried out at room temperature (22 °C). After the formation of the SSM, its capacitance and conductance were determined until they became constant after a waiting time of ∼90 min. Typical values were 300−500 nF/cm^2 for the capacitance and 50−100 nS/cm^2 for the conductance. A typical solution exchange protocol consists of three phases with a duration of 0.5 or 1 s each: (1) reference solution, (2) test solution, and (3) reference solution. The data recording and the solution exchange were controlled via computer as described in ref 27. Electrical signals are observed at the concentration jumps taking place at the beginning (on-signal) and at the end (off-signal) of phase 2. Only the on-signal will be used throughout our analysis.

Analysis of the Currents. The transient currents after the concentration jump were numerically integrated to calculate the displaced charge $Q(t)$ and fitted with an empirical model function

$$Q(t) = Q_0 \frac{(t - t_0)^3}{(t - t_0)^3 + \tau^3}$$

The delay t_0 and the rise time τ represent the time needed for the solution to flow from the terminal valve to the SSM and the rise time of the concentration at its surface, respectively. They had values of $t_0 \approx 54$ ms after switching to the test solution and $\tau \approx 10$ ms. Q_0 represents the total charge displacement generated when ions with different propensities to "bind" to the membrane are exchanged. For the purposes of this paper, only the parameter Q_0 was relevant and was evaluated.

Results

In the solution exchange process, two solutions of different composition were applied to the surface, the test solution and the reference solution, both of which were buffered with 10 mM TRIS/Hepes at pH 7.0. The test solution contained the salt of interest, and the reference solution contained NaCl, which was used as an internal reference. NaCl is a popular reference, since Hofmeister effects often show a sign inversion at Na^+ and Cl^-.[2] To generate pure cation concentration jumps, a constant Cl^- concentration was used throughout the experiment, i.e., for a monovalent cation X, the test solution contained the same concentration of XCl as the reference solution NaCl. For a divalent or trivalent cation, the concentrations were $^1/_2$ and $^1/_3$ of the NaCl concentration. For pure anion concentration jumps, the Na^+ concentration was kept constant using an equivalent procedure. This guaranteed that the observed effect was only due to the anion or the cation to be investigated. A slightly different protocol was used for the data shown in Figure 5 where uncompensated

(20) Naumann, R.; Schmidt, E. K.; Jonczyk, A.; Fendler, K.; Kadenbach, B.; Liebermann, T.; Offenhausser, A.; Knoll, W. The peptide-tethered lipid membrane as a biomimetic system to incorporate cytochrome c oxidase in a functionally active form. *Biosens. Bioelectron.* **1999**, *14* (7), 651−662.

(21) Pintschovius, J.; Fendler, K. Charge translocation by the Na+/K+-ATPase investigated on solid supported membranes: Rapid solution exchange with a new technique. *Biophys. J.* **1999**, *76* (2), 814−826.

(22) Ataka, K.; Richter, B.; Heberle, J. Orientational control of the physiological reaction of cytochrome c oxidase tethered to a gold electrode. *J. Phys. Chem.* B **2006**, *110* (18), 9339−9347.

(23) Florin, E.-L.; Gaub, H. E. Painted supported lipid membranes. *Biophys. J.* **1993**, *64*, 375−383.

(24) Seifert, K.; Fendler, K.; Bamberg, E. Charge transport by ion translocating membrane proteins on solid supported membranes. *Biophys. J.* **1993**, *64* (2), 384−91.

(25) Bockmann, R. A.; Hac, A.; Heimburg, T.; Grubmuller, H. Effect of sodium chloride on a lipid bilayer. *Biophys. J.* **2003**, *85* (3), 1647−1655.

(26) Sachs, J. N.; Woolf, T. B. Understanding the Hofmeister effect in interactions between chaotropic anions and lipid bilayers: Molecular dynamics simulations. *J. Am. Chem. Soc.* **2003**, *125* (29), 8742−8743.

(27) Zhou, A.; Wozniak, A.; Meyer-Lipp, K.; Nietschke, M.; Jung, H.; Fendler, K. Charge translocation during cosubstrate binding in the Na+/proline transporter of *E. coli*. *J. Mol. Biol.* **2004**, *343* (4), 931−942.

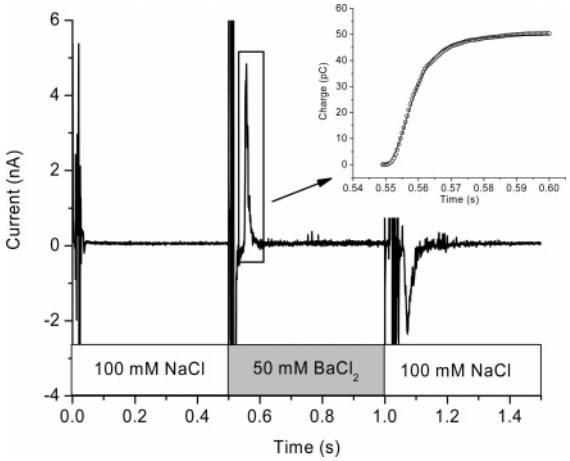

Figure 1. Flow protocol and signal analysis. As an example for the recorded transient currents, the charge translocation after a $BaCl_2$ concentration jump on a PC membrane is shown. The integrated signal with a fit according to the equation given in the text is shown in the inset.

salt concentration jumps were used and the reference solution contained only buffer.

Figure 1 shows a typical transient current after an ion concentration jump. The example in Figure 1 represents a 50 mM Ba^{2+} concentration jump (or more precisely a solution exchange of 100 mM NaCl vs 50 mM $BaCl_2$) at an SSM formed from diphytanoyl phosphatidylcholine (PC). The current is integrated, yielding the charge which, after a short delay, rises rapidly with a time constant of ~10 ms to a maximal value. This time constant represents the Ba^{2+} concentration rise time at the surface of the SSM. The signal is fitted (see Figure 1) as described in the Material and Methods section, yielding the total charge displacement Q_0. In the following, we will analyze Q_0 as a function of different ions, ion concentrations, and composition of the SSM.

Dependence of the Charge Translocation on the Nature of the Applied Cation or Anion. 100 mM salt concentration jumps of different cations and anions generated transient currents that were strongly dependent on the nature of the applied ion. In Figure 2, the translocated charge is plotted for the different anions and cations and for two different lipids, diphytanoyl phosphatidylcholine (PC) and monoolein (Mono). The ions are classified according to their respective free energies of hydration.[28] NaCl was taken as a reference point and, therefore, shows up at $Q_0 = 0$. Positive values represent ions that create a movement of positive charge to the membrane (or negative charge away from the membrane); negative values represent ions that create a movement of negative charge to the membrane (or positive charge away from the membrane) when exchanged for NaCl.

In the case of the cations, the data show an approximately linear dependence on the hydration energy, forming three isolated patches for monovalent, divalent, and trivalent cations. The translocated charge yields the following series (for PC): $La^{3+} > Ca^{2+} > Mg^{2+} > Ba^{2+} > Sr^{2+} > Li^+ > Na^+ > K^+, Rb^+, Cs^+$. The anions show the reverse behavior with respect to the free energy of hydration. Here, the following series for the translocated charge is obtained (for PC): $ClO_4^- > SCN^- > I^- > NO_3^- > Br^- > F^- > Cl^- = SO_4^-$. For Mono, the same general trend is obtained, although not all positions of the individual ions are conserved.

Interaction of the Different Cations and Anions with Different Lipid Headgroups. To test the influence of the chemical nature of the lipid headgroup, we determined the charge translocation using different lipids in the hybrid lipid bilayer on the solid support. Dioleoyl trimethylammonium propane (DOTAP) is a lipid with a positively charged headgroup, diphytanoyl phosphatidylcholine (PC) is zwitterionic, monooleoyl glycerol (Mono) is uncharged, and dioleoyl phosphatidyl glycerol (DOPG) carries a negative charge. All lipids were prepared in *n*-decane; Mono was also used in squalene (Mono-squal) to assess the influence of the solvent. Bilayers formed from Mono in squalene have been reported to contain very little solvent.[29] In the case of PC, the phytanoyl instead of the oleoyl fatty acid chains were used, because diphytanoyl PC is the standard lipid used in SSM applications.[21,30,31]

To investigate the effect of functional sites in the headgroup, we determined the complete anion and cation series for PC and for Mono (in *n*-decane). PC bears a negative phosphate (PO_4^-) and a positive trimethyl ammonium ($N(CH_3)_3^+$) group, which Mono does not have. Interestingly, a nearly identical pattern is obtained for PC and Mono as shown in Figure 2. The only differences observed are a ~50% lower binding for the extremely chaotropic anions (ClO_4^-, SCN^-, and I^-) and the extremely kosmotropic cations (La^{3+}, Ca^{2+}, and Mg^{2+}). Also, F^- and SO_4^{2-} seem to bind somewhat better to the Mono than to the PC surface.

For a broader scan of different surfaces, two cations and two anions were chosen and were applied at a concentration of 100 mM: the chaotropic ions K^+, Br^-, and ClO_4^-, and the kosmotropic cation La^{3+}. Reference ions were Na^+ and Cl^- as described above. The translocated change in all cases is displayed in Figure 3. As expected, cations generate a larger charge displacement at a negative surface, while anions do that at a positive one. The zwitterionic PC represents an intermediate case, and the uncharged Mono shows the least effect. It is, however, interesting to note that cations as well as anions interact with at significant efficiency with the lipid Mono, although it has neither $N(CH_3)_3^+$ nor PO_4^- groups. This rules out the possibility of specific binding to those groups as a major cause of the interaction.

The effect of the charged headgroup is most pronounced for the anions, ClO_4^- as well as Br^-. However, La^{3+} also shows a clear tendency for preferential binding, in this case to the negative PG surface. The behavior of K^+ is less drastic. Here, the observed charge translocation is negative, meaning K^+ binds less than the reference ion Na^+ in all considered lipid surfaces (see Figure 3). If the surface concentration of Na^+ and K^+ is increased by electrostatic interaction with the negative PG surface, a larger translocated charge is expected (see concentration dependence in Figure 4A), as is indeed observed.

Concentration Dependence of the Translocated Charge. Since the translocated charge was strongly ion concentration dependent, we determined the saturation behavior for La^{3+}, Mg^{2+}, K^+, ClO_4^-, and Br^- on a PC surface. This allowed us to determine an apparent dissociation constant K_D^{app} for the respective ion. The reference solution always contained NaCl at a concentration to keep the Cl^- concentration constant in the cation concentration jumps and the Na^+ concentration constant in the anion concentration jumps (see above). The concentration dependence

(28) Marcus, Y. Thermodynamics of solvation of ions. 5. Gibbs free energy of hydration at 298.15 K. *J. Chem. Soc., Faraday Trans.* **1991**, *87*, 2995−2999.

(29) Dilger, J. P.; Benz, R. Optical and electrical properties of thin monoolein lipid bilayers. *J. Membr. Biol.* **1985**, *85* (2), 181−9.

(30) Kelety, B.; Diekert, K.; Tobien, J.; Watzke, N.; Dorner, W.; Obrdlik, P.; Fendler, K. Transporter assays using solid supported membranes: a novel screening platform for drug discovery. *Assay Drug Dev. Technol.* **2006**, *4* (5), 575−82.

(31) Tadini-Buoninsegni, F.; Bartolommei, G.; Moncelli, M. R.; Guidelli, R.; Inesi, G. Pre-steady state electrogenic events of Ca2+/H+ exchange and transport by the Ca2+-ATPase. *J. Biol. Chem.* **2006**, *281*, (49), 37720−37727.

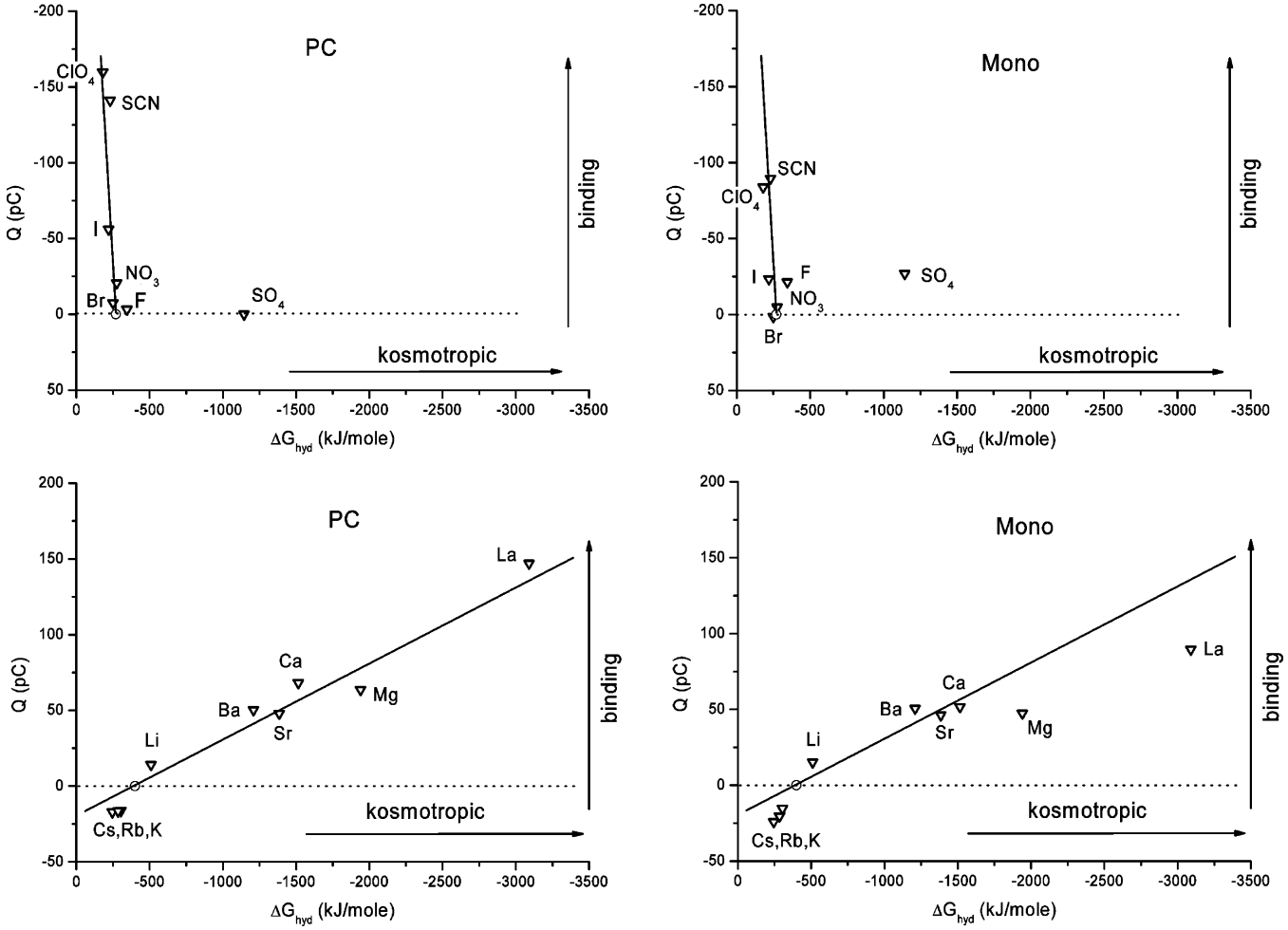

Figure 2. Charge displacements of different anions and cations on a PC (phosphatidylcholine) and a Mono (monoolein) membrane. The open circle indicates the reference ions Na or Cl. Ions are classified according to their Gibbs free energies of hydration ΔG_{hyd}.

is shown in Figure 4. The data were analyzed using a hyperbolic function $Q_0 = Q_0^{max} c/(c + K_D^{app})$ where c is the ion concentration.

The apparent dissociation constant K_D^{app} and the saturation value of the displaced charge Q_0^{max} are compiled in Table 1. Within the group of cations, binding affinity and displaced charge increase drastically with ionic charge. Trivalent La^{3+}, for instance, has an apparent dissociation constant of 13 μM. In general, the cations bind with a higher affinity than the anions. However, the largest value for the displaced charge is measured for the anion ClO_4^-. Br^- showed an approximately linear dependence up to a concentration of 100 mM. Therefore, for this ion, only a lower bound for the parameters K_D^{app} and Q_0^{max} could be given. This agrees with the very low affinity 5 M reported previously for Br^- binding to lipids with PC headgroups.[17]

Uncompensated Salt Concentration Jumps. Here, the test solution contained buffer plus the indicated salt and the reference solution contained only buffer. The transient currents recorded in this case comprise contributions from cation and anion. They are strongly dependent on the applied salt. The currents were integrated to yield the translocated charge and are shown in Figure 5. The saturation values of these traces represent the total charge displacement Q_0. From the studied salts, NaSCN, $NaClO_4$, and NaI gave rise to negative charge displacements indicating that the SCN^-, ClO_4^-, and I^- anions associate more tightly with the membrane than the accompanying cation Na^+. On the other hand, Cl^- presented an affinity for the membrane lower than Na^+. Remarkably, although the translocated charge changes from positive to negative, the sequence shown in Figure 2 is preserved. As for the chlorides, a positive charge displacement is always found increasing in the same order as in Figure 2, $K^+ < Na^+ < Li^+ < La^{3+}$. Here, the cations array closer to the membrane than the anions. Furthermore, the charge translocated by La^{3+} is two times higher than that by Na^+, although the applied concentration was only $^1/_3$ of that of Na^+. Last but not least, these uncompensated salt concentration jumps also show that, although cations bind to the membrane, the effect of changing between monovalent anions is more pronounced than that of changing between monovalent cations (see Figure 2).

To test whether a different saturation behavior of cations and anions (Table 1) could lead to a different sequence in uncompensated salt concentration jumps, we repeated the measurement at 1 M ion concentrations (0.33 mM $LaCl_3$). The same sequence as at 100 mM concentration was obtained. In particular, the sign of the charge displacements of the different salts was not altered, indicating that also at high concentrations cations and anions have a comparable effect.

Discussion

The most abundant lipid in an average mammalian cell membrane is phosphatidylcholine (45−55%), which comprises a negatively charged phosphate (PO_4^-) group and a positively charged ammonium ($N(CH_3)_3^+$) group. In addition, the charged sites of the other lipid membrane constituents are exclusively phosphate and ammonium groups. Consequently, PC is a good prototype lipid for a study of the interaction of ions with a biological membrane. To address the question of how these groups

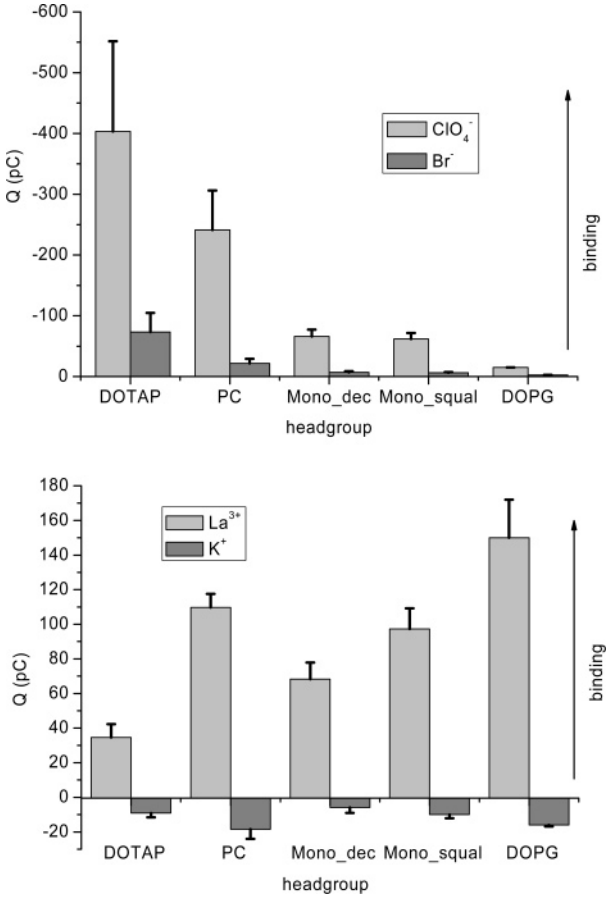

Figure 3. Charge translocation of selected anions (upper panel) and cations (lower panel) on different membranes: dioleoyl trimethylammonium propane (DOTAP), diphytanoyl phosphatidylcholine (PC), monoolein in decane (Mono_dec), monoolein in squalene (Mono_squal), and dioleoyl phosphatydylglycerol (DOPG).

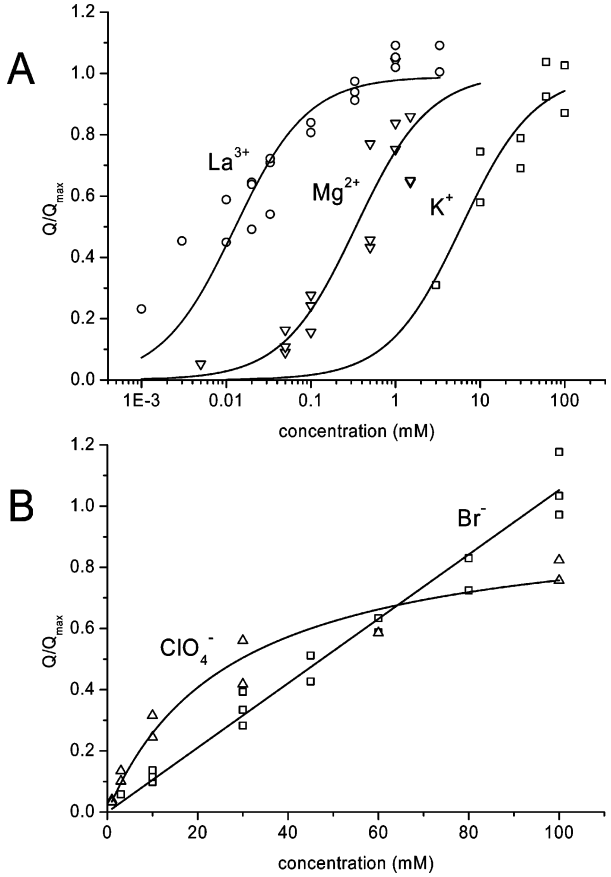

Figure 4. Concentration dependence of the translocated charge of selected cations (A) and anions (B) on a PC membrane. The solid lines are hyperbolic fits to the data. For each ion, 2 to 3 different samples were measured and normalized to the saturation value of the hyperbolic fit. In the case of Br^-, only a linear dependence was found, and for normalization, the value at 100 mM was used.

determine the interaction of ions with the surface, we have compared the PC membrane with a membrane composed of a lipid with no charged groups (Mono).

In addition, lipid headgroups with a net charge, positively charged DOTAP and negatively charged PG, were investigated.

Chaotropic Anions Are Attracted to the Lipid Interface. If anions are classified according to their free energy of hydration ΔG_{hyd}, a well-defined series for the translocated charge is obtained where the anion with the smallest $-\Delta G_{hyd}$ yields the largest negative charge translocation. This means the most hydrophobic or the most chaotropic anion binds best to or in the lipid interface (the classifications chaotropic and kosmotropic are used here in the sense of water structure breaker and water structure maker, respectively). These results exactly fit the series obtained for the influence of anions on the dipole potential of PC liposomes.[14] Clarke and Lüpfert[14] explain the reduction of the dipole potential by binding of the chaotropic anion at the positive side of the dipole deep in the lipid headgroup. This is in agreement with our results which show a large negative charge translocation upon binding of chaotropic anions like ClO_4^-.

Interpretation of these relative measurements in terms of interaction forces requires an absolute reference point. Assuming that the interaction of Cl^- with the surface is negligible (Cl^- in general has only a small Hofmeister effect[2]), the results indicate that chaotropic anions like ClO_4^- experience a stronger attractive potential at the lipid interface than kosmotropic anions like F^-.

Kosmotropic Cations Are Attracted to the Lipid Interface. Interestingly, for cations the inverse series is obtained in our measurements, with the cation with the highest $-\Delta G_{hyd}$ yielding the largest charge translocation, which is positive in this case. This means that the most hydrophilic or the most kosmotropic cation binds best. Again, our results agree with those obtained for the effect of cations on the lipid dipole potential[14] but also with an early study of the adsorption of cations to phosphatidylserine liposomes.[13] In consequence, we find a more attractive potential for kosmotropic than for chaotropic cations. This agrees with recent MD simulations showing that sodium (kosmotropic) possesses a higher affinity than potassium (chaotropic) to a protein surface. There, however, carboxylic groups are proposed to be mainly responsible for this effect.[32]

Since only monovalent anions were used, a comparison with only the monovalent cations seems appropriate. The overall tendency is the same, but it is evident that the effect of monovalent

Table 1. Apparent Dissociation Constants K_D^{app} and Displaced Charge Q_0^{max} for Different Ions on a PC Membrane ($n = 2-3$; See Figure 4)

	K_D^{app}	Q_0^{max}
La^{3+}	$13 \pm 2\ \mu M$	134 ± 5 pC
Mg^{2+}	0.34 ± 0.06 mM	59 ± 4 pC
K^+	6 ± 1.2 mM	-7.7 ± 1 pC
ClO_4^-	27 ± 6 mM	-180 ± 10 pC
Br^-	> 100 mM	< -17 pC

(32) Vrbka, L.; Jungwirth, P.; Bauduin, P.; Touraud, D.; Kunz, W. Specific ion effects at protein surfaces: A molecular dynamics study of bovine pancreatic trypsin inhibitor and horseradish peroxidase in selected salt solutions. *J. Phys. Chem. B* **2006**, *110* (13), 7036−7043.

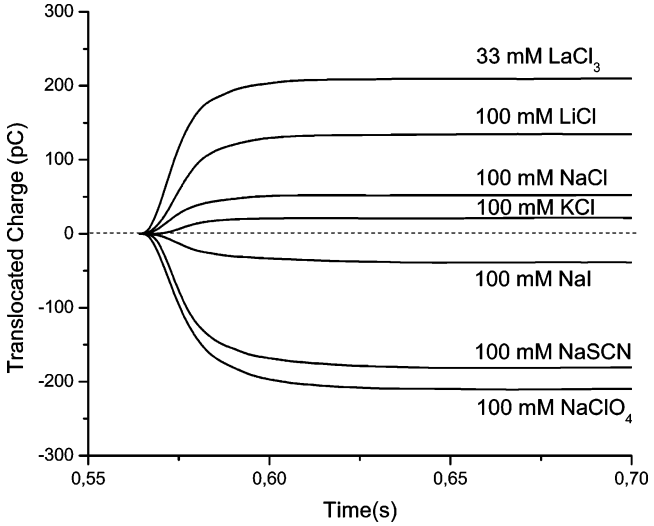

Figure 5. Translocated charge after uncompensated concentration jumps of different salts on a PC membrane. The traces were obtained by integration of the measured transient currents. At $t = 0.5$ s, the buffer solution was exchanged for a solution containing the buffer plus the indicated salt.

cations is only 20% (PC) and 50% (Mono) of the anion effect. This is not surprising, because anion Hofmeister effects are generally larger than those of cations, very probably because of the bigger anion size and polarizability.[3]

Apparent dissociation constants and maximal displaced charge (see Figure 4 and Table 1) show the same tendency as displayed by the data of Figure 2. The most kosmotropic cation and the most chaotropic anion bind best and displace more charge. The largest charge displacement (180 pC) was measured for the ClO_4^- anion at saturating conditions representing only ~1 elementary charge per 1000 lipid molecules (using a membrane area of 0.8 mm^2 and lipid molecular area of ~0.5 nm^2).[33] This is a small number of ions per lipid even if one takes into account that the charge displacement represents only the difference between ClO_4^- and Cl^- average positions and may indicate that the charge displacement is heavily shielded by the polar environment of the lipid headgroup region.

PC Membranes Can Be Anion or Cation Selective. Up to now, we have only ranked ion binding within the group of anions or cations. The polarity of charge displacement after uncompensated salt concentration jumps (Figure 5), however, indicates whether cations or anions bind preferentially to the membrane. Effects of similar magnitude are found for the group of monovalent ion pairs, but they can be of either positive or negative polarity depending on the specific ion pair. Here, it has to be stressed that for a comparison of cations and anions not only specific ion interactions but also electrostatic forces originating from surface and lipid dipole potential play a role. These experiments show that a zwitterionic PC surface (no net charge) depending on the specific ion pair can prefer the cation or the anion. In particular, considering the ion pairs NaSCN and $NaClO_4$, the strongly chaotropic anions have a higher affinity for the membrane than their counterions Na^+, while for the chlorides NaCl and KCl, the cations bind more strongly. This is unexpected, because Hofmeister interactions are generally believed to be dominated by anions.[2] Finally, the uncompensated salt concentration jump experiments also rule out that the specific cation effects (Figure 2) are brought about predominantly by extraction of tightly bound Cl^- from the surface (yielding a positive charge displacement), rather than binding of the cations.

Headgroup Charges Make a Difference. From the experiments using lipid with different headgroups, a clear tendency emerges that cations preferentially bind to the negatively charged PG, while anions prefer the positively charged DOTAP headgroup. This is by itself not surprising, and the standard Gouy−Chapman electrostatic theory describes accumulation of positive ions at negatively charged surfaces, and vice versa. However, we have to bear in mind that the observed charge translocations represent the difference to the reference ions Na^+ and Cl^-. In the Gouy−Chapman formalism, all ions of identical valency yield the same result, and there should be no difference between ClO_4^- and Cl^- and between Na^+ and K^+. However, the effect of charged headgroups could be explained by the increased local cation concentration at the DOPG surface and the increased local anion concentration at the DOTAP surface predicted by the electrostatic interaction. It can not, however, explain the more efficient binding to zwitterionic PC as compared to uncharged Mono, which is more prominent for the anions than for the cations (Figure 3). Taken together, this seems to be suggestive of a mechanism different from pure electrostatics which modifies ion binding at different lipid headgroups.

Interaction Mechanism of Anions and Cations with a Lipid Interface. The question now arises: What kind of mechanism leads to the characteristic series observed for cations and anions? It is clear that the charge translocation after cation or anion exchange represents a typical Hofmeister series with the surprising property that the cation series is reversed with respect to the anion series. A similar behavior has previously been observed with electrochromic dyes, which are believed to report on the dipole potential of the lipid headgroups.[14] This rules out that the peculiar behavior is specific for the SSM/gold electrode sandwich used in our study.

Moreover, the same characteristic behavior is observed for a variety of different lipid headgroups: zwitterionic, positively charged, negatively charged, and uncharged. All show a preferential binding of the chaotropic anion and the kosmotropic cation. This is true even if only the monovalent ions are considered. It is, therefore, unlikely that the observed effect is specific binding to a binding site such as cation binding to the phosphate group of phospholipids as suggested previously.[14]

Different physicochemical parameters of the ions like the Gibbs free energy of hydration chosen in this publication have been taken into account to rationalize the ionic sequences. Unfortunately, many of these parameters are correlated themselves,[3] so that these procedures are of little help to identify the dominating forces acting between the interface and the ion. It has recently been shown that dispersion forces have to be taken into account at physiological ion concentrations where electrostatic interactions are screened[3] and may be responsible for Hofmeister effects.[8] The relevant parameter determining dispersion forces on ions is the ionic polarizability, which is large for large chaotropic ions[3,4] and would predict preferential binding of both chaotropic cations and anions, in disagreement with our experimental results.

An ion binding mechanism according to the "principle of matching water affinities" has been proposed by Collins[9] which predicts binding of chaotropic ions to chaotropic surface groups and kosmotropic ions to kosmotropic surface groups. Since PO_4^- is strongly kosmotropic (and the putative binding site for cations) and $N(CH_3)_3^+$ is chaotropic (and the putative binding site for anions), this would explain our results on PC. However, it cannot account for the fact that a lipid without these residues (Mono) shows the same cation and anion binding series. And it cannot

(33) Almeida, P. F. F.; Winchil, L. C.; Vaz, L.; Thompson, T. E. Lateral Diffusion in the Liquid Phases of Dimyristoylphosphatidylcholine/Cholesterol Lipid Bilayers: A Free Volume Analysis. *Biochemistry* **1992**, *31*, 6739−6747.

explain either why for various phosphate compounds as well as other anionic surfactants the reversed cation series is found (see, e.g., ref 34 and the literature cited herein). In contrast to these compounds, however, in the present study the phosphate group is chemically linked to ammonium or glycerol groups or consists only of a glycerol headgroup (Mono), and, therefore, the influence of the phosphate group alone is not decisive. We believe, in agreement with the results of Jungwirth and co-workers,[11,12] that it is necessary to precisely describe the role of the component that is present in large excess, namely, water. To understand the specific ion effects, it is very probably not sufficient to describe the water as a bulk or as hydration water. The geometry of the water molecules around the ions and headgroups very probably makes the difference, just as this geometry explains why protons have a significant propensity to the air−water interface, a phenomenon that cannot be explained in a bulk model.[35] That there must be a specific hydration around glycerol headgroups was recently found for short-chain glycerol,[36] and first attempts to simulate choline were published also recently.[32]

Considering all these points, we think that it would be an over-interpretation to discuss the results in more detail. In the past, numerous results on specific ion effects were published, and in each paper, a possible explanation was proposed. However, all these interpretations were pure speculations that were done a posteriori. What we need now is a forward and predictive model, and we hope that the data presented here can serve as an experimental reference for such calculations. Advances in that direction come from recent MD studies of zwitterionic PC membranes[15,25,26,37] and negatively[16,38] or positively[39] charged lipid membranes. For example, simulation of PC membranes show that Cl^- binds slightly weaker than Na^+ [25,37] and that chaotropic anions bind better than kosmotropic ones to the lipid headgroups.[15,26] Both results agree with our experiments.

Conclusion

Ion binding to an SSM as a model system for a biological membrane has been studied, and the general characteristics have been determined. Cations and anions both show specific binding but in an oppositely directed Hofmeister series independent of the composition of the lipid membrane. This may indicate that regarding the interaction with the lipid surface the free energy of hydration or the classification of the ions in terms of chaotropicity or kosmotropicity plays a different role for anions and cations. Different interactions may be operative for cations and anions, or specific interactions for a given ion/surface residue pair may have to be taken into account as well as the detailed geometry of water molecules around these pairs. A unified mechanistic model for ion binding to the lipid interface is not available at present. Further progress in understanding the mechanistic origin of this unexpected experimental behavior is expected from molecular modeling studies.

Acknowledgment. The authors thank E. Bamberg for helpful discussions and support of this work.

LA701188F

(34) Haverd, V. E.; Warr, G. G. Cation selectivity at air/anionic surfactant solution interfaces. *Langmuir* **2000**, *16* (1), 157−160.

(35) Mucha, M.; Frigato, T.; Levering, L. M.; Allen, H. C.; Tobias, D. J.; Dang, L. X.; Jungwirth, P. Unified molecular picture of the surfaces of aqueous acid, base, and salt solutions. *J. Phys. Chem. B* **2005**, *109* (16), 7617−7623.

(36) Queste, S.; Bauduin, P.; Touraud, D.; Kunz, W.; Aubry, J. M. Short chain glycerol 1-monoethers - a new class of green solvo-surfactants. *Green Chem.* **2006**, *8* (9), 822−830.

(37) Pandit, S. A.; Bostick, D.; Berkowitz, M. L. Molecular dynamics simulation of a dipalmitoylphosphatidylcholine bilayer with NaCl. *Biophys. J.* **2003**, *84* (6), 3743−3750.

(38) Mukhopadhyay, P.; Monticelli, L.; Tieleman, D. P. Molecular dynamics simulation of a palmitoyl-oleoyl phosphatidylserine bilayer with Na+ counterions and NaCl. *Biophys. J.* **2004**, *86* (3), 1601−1609.

(39) Gurtovenko, A. A.; Miettinen, M.; Karttunen, M.; Vattulainen, I. Effect of monovalent salt on cationic lipid membranes as revealed by molecular dynamics simulations. *J. Phys. Chem. B* **2005**, *109* (44), 21126−21134.

Rapid Activation of the Melibiose Permease MelB Immobilized on a Solid-Supported Membrane

Juan J. Garcia-Celma,[†] Benjamin Dueck,[†] Martin Stein,[†] Michela Schlueter,[†] Kerstin Meyer-Lipp,[†,‡] Gerard Leblanc,[‡] and Klaus Fendler*[,†]

Department of Biophysical Chemistry, Max Planck Institute of Biophysics, D-60438 Frankfurt, Germany, and Institut de Biologie et Technologies-Saclay, CEA-Saclay, F-91191 Gif sur Yvette, France

Received February 8, 2008. Revised Manuscript Received April 17, 2008

Rapid solution exchange on a solid-supported membrane (SSM) is investigated using fluidic structures and a solid-supported membrane of 1 mm diameter in wall jet geometry. The flow is analyzed with a new technique based on specific ion interactions with the surface combined with an electrical measurement. The critical parameters affecting the time course of the solution exchange and the transfer function describing the time resolution of the SSM system are determined. The experimental data indicate that solution transport represents an intermediate situation between the plug flow and the Hagen−Poiseuille laminar flow regime. However, to a good approximation the rise of the surface concentration can be described by Hagen−Poiseuille flow with ideal mixing at the surface of the SSM. Using an improved cuvette design, solution exchange as fast as 2 ms was achieved at the surface of a solid-supported membrane. As an application of the technique, the rate constant of a fast electrogenic reaction in the melibiose permease MelB, a bacterial (*Escherichia coli*) sugar transporter, is determined. For comparison, the kinetics of a conformational transition of the same transporter was measured using stopped-flow tryptophan fluorescence spectroscopy. The relaxation time constant obtained for the charge displacement agrees with that determined in the stopped-flow experiments. This demonstrates that upon sugar binding MelB undergoes an electrogenic conformational transition with a rate constant of $k \approx 250\ s^{-1}$.

Introduction

Solid-supported membranes (SSM) represent model systems for a lipid membrane with the additional benefit of being so mechanically stable that solutions may be rapidly exchanged at the surface. SSMs have found broad application as rugged carriers for membrane proteins. Because these proteins are imbedded in or attached to this membrane, their activity can be assessed by a variety of methods such as fluorescence, Raman and IR spectroscopy, electrochemistry, impedance analysis, and electrical measurements.[1−8] For the analysis of the dynamic properties of these membrane proteins, time-resolved experiments that probe the presteady state of the system are essential. This requires rapid perturbation of the initial state, which in many cases is a concentration jump of an enzymatic ligand or substrate. In the case of surface-immobilized enzymes, rapid solution exchange is difficult because of the unstirred layer at the surface.[9] Furthermore, virtually no technique is available that allows for the rapid time-resolved analysis of the surface concentration of substrate molecules. However, quantitative temporal information concerning the surface substrate concentration rise is a prerequisite for the proper interpretation of the measured signals as well as for the optimization of the fluidic system.

It has been shown recently that the specific interaction of inorganic ions with lipid membranes can be studied using the SSM technique.[10] When solutions of different ionic composition are exchanged, charge displacement can be registered via the supporting gold electrode. This translocated charge represents the relaxation of the different ions in their respective equilibrium positions. As a first approximation, the SSM technique registers charge displacements in the immediate headgroup region.[10] Therefore, the measurement of these charge displacements can be used as a real-time probe of the local ion concentration at the lipid surface. This makes ion concentration jumps an interesting tool for the analysis of the time course of solution exchange on the SSM surface and enables the exploration of different fluidic configurations. In our study, the relevant structural elements for rapid surface concentration exchange were identified, and on the basis of this information, a novel cuvette with a superior time resolution was designed.

Electrophysiological analysis of bacterial transporters is difficult because, except in a few rare cases, these transporters cannot be investigated using standard electrophysiology. Time-resolved electrophysiological characterization of eukaryotic transporters is also difficult. Because the turnover of transporters is low ($<100\ s^{-1}$ in most cases), $\sim 10^4$ to 10^5 transporters are required to generated a measurable signal. This can be obtained only in a "giant patch" or a "whole cell" configuration, both of which have an inherently low time resolutions in solution-exchange experiments. Electrogenic transport proteins have recently been shown to be readily measurable by adsorbing proteoliposomes or membrane fragments containing the protein

* To whom correspondence should be addressed. Fax: (+) 49 69 6303-2002. E-mail: klaus.fendler@mpibp-frankfurt.mpg.de.
[†] Max Planck Institute of Biophysics.
[‡] CEA-Saclay.

(1) Ataka, K.; Richter, B.; Heberle, J. *J. Phys. Chem. B* **2006**, *110*, 9339–9347.
(2) Friedrich, M. G.; Giebeta, F.; Naumann, R.; Knoll, W.; Ataka, K.; Heberle, J.; Hrabakova, J.; Murgida, D. H.; Hildebrandt, P. *Chem. Commun.* **2004**, 2376–2377.
(3) Giess, F.; Friedrich, M. G.; Heberle, J.; Naumann, R. L.; Knoll, W. *Biophys. J.* **2004**, *87*, 3213–3220.
(4) Heyse, S.; Stora, T.; Schmid, E.; Lakey, J. H.; Vogel, H. *Biochim. Biophys. Acta* **1998**, *1376*, 319–338.
(5) Michalke, A.; Galla, H. J.; Steinem, C. *Eur. Biophys. J.* **2001**, *30*, 421–429.
(6) Naumann, R.; Schmidt, E. K.; Jonczyk, A.; Fendler, K.; Kadenbach, B.; Liebermann, T.; Offenhausser, A.; Knoll, W. *Biosens. Bioelectron.* **1999**, *14*, 651–662.
(7) Pintschovius, J.; Fendler, K. *Biophys. J.* **1999**, *76*, 814–826.
(8) Robelek, R.; Lemker, E. S.; Wiltschi, B.; Kirste, V.; Naumann, R.; Oesterhelt, D.; Sinner, E. K. *Angew. Chem., Int. Ed.* **2007**, *46*, 605–8.
(9) Barry, P. H.; Diamond, J. M. *Physiol. Rev.* **1984**, *64*, 763–872.
(10) Garcia-Celma, J. J.; Hatahet, L.; Kunz, W.; Fendler, K. *Langmuir* **2007**, *23*, 10074–10080.

10.1021/la800428h CCC: $40.75
Published on Web 06/24/2008

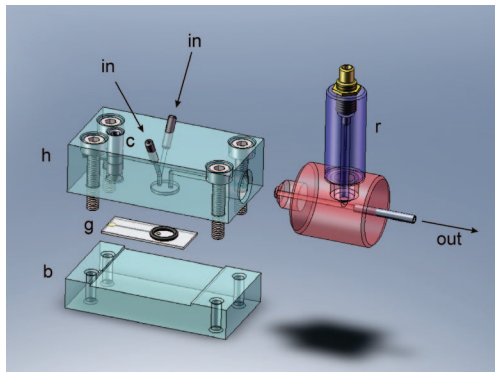

Figure 1. Explosion view of the fast solution-exchange cuvette for valveless diverter flow geometry. The cuvette head (h) and base (b) are made out of Plexiglas. Inlet (in) and outlet (out) bores have a diameter of 1 mm. The reference electrode assembly (r) is placed in the outlet pathway. The cuvette volume is cylindrical and 0.75 mm deep with an internal volume of 17 μL (net volume with O-ring mounted). The SSM is formed on a gold-coated glass slide (g) and has a diameter of 1 mm. It is connected to the contact pad via a 0.2-mm-wide contact strip. Contact to the amplifier is made through a spring contact pin (c). When mounted, the SSM is centered under the inlet bore.

of interest to an SSM.[11–16] The charge translocation of these transport proteins can be measured by rapidly supplying the substrate and measuring the electrical current generated by the transport process. Therefore, for bacterial as well as for eukaryotic transport proteins, the SSM offers the unique opportunity to perform electrophysiological studies with a high time resolution.

In this study, we investigate a rapid reaction induced by sugar binding to a bacterial sugar transporter, the melibiose permease (MelB). Sugar binding to MelB in the presence of Na^+ is associated with a charge displacement that can be detected using proteoliposomes adsorbed to an SSM and applying a melibiose concentration jump.[17] This electrogenic reaction was associated with a conformational transition observed by tryptophan fluorescence spectroscopy[18,19] suggesting an electrogenic conformational transition.[20] However, kinetic information about both processes to strengthen this assignment is not yet available. In particular, because of the limited time resolution of the SSM setup used for these experiments, only a lower bound of $k > 50$ s^{-1} could be assigned to the charge displacement.[20] Here we reanalyze this reaction using the improved time resolution of the valveless diverter configuration (Figure 2B) and an iterative least-squares deconvolution algorithm. In parallel, stopped-flow spectroscopy is employed to obtain time-resolved information about the conformational transition monitored by tryptophan fluorescence. This allows for the first time a direct kinetic comparison of both processes and a determination of rate constants.

Materials and Methods

Chemicals. The lipid-film-forming solution of 1.5% in *n*-decane contained diphytanoyl phosphatidylcholine (PC, synthetic, Avanti Polar Lipids Inc., Pelham, AL) and octadecylamine (60:1 wt/wt, 98%, Riedel-de-Haen AG, Seelze-Hannover, Germany). A 1 mM octadecyl mercaptan (C_{18}-mercaptan, Aldrich, Steinheim, Germany) solution in ethanol was used for the incubation of the gold electrodes. The Cl^-/ClO_4^- solution-exchange experiments were performed in 50 mM Hepes(Tris) pH 7.0 buffer, and the melibiose permease measurements were performed in 100 mM KH_2PO_4(KOH) pH 7.0 (KP_i) buffer.

SSM Setup. The electrodes were prepared by a lithographic process on a 1-mm-thick 9 × 22 mm^2 borofloat glass chip (Fraunhofer Institut Schicht and Oberflächentechnik, Braunschweig, Germany). The 100-nm-thick gold structure consists of a 1-mm-diameter circular active area that is connected to a contact pad via a thin contact strip (Figure 1). The SSM is formed on the active area by linking an alkanethiol (octadecyl mercaptan) monolayer to the gold electrode by a 6 h incubation in a 1 mM ethanolic octadecyl mercaptan solution. The lipid monolayer is deposited using a painting technique where a small amount of the film -forming solution is applied to the electrode. The glass chip with SSM is mounted in a flow-through cuvette with an inner volume of 17 μL. The monolayer forms spontaneously when the electrode is rinsed with buffer in the cuvette. The planar membrane has an area of ~0.8 mm^2. The gold electrode is connected to an amplifier, and the reference electrode is an Ag/AgCl electrode separated from the solution by a salt bridge (Figure 2). Two different flow geometries have been studied: valve-controlled (Figure 2A) and valveless (Figure 2B) diverter geometries. The diverter−SSM distance (i.e., the common pathway for test and reference solutions between terminal valve V_2 and SSM (Figure 2A) or between confluence point and SSM (Figure 2B)) is critical for the concentration rise time. Unless otherwise specified, this pathway is a cylindrical tube of 1-mm-diameter made from polyethylene (Figure 2A) or Plexiglass (Figure 2B). For details of the setup, see also refs 7 and 21.

Measuring Procedure. The experiments were carried out at room temperature (22 °C). After the formation of the SSM, its capacitance and conductance were determined until they became constant after a waiting time of ~90 min. Typical values were 300−500 nF/cm^2 for the capacitance and 50−100 nS/cm^2 for the conductance. A typical solution-exchange protocol consists of three phases (Figure 2) with a duration of 0.5 or 1 s each: (1) reference solution, (2) test solution, and (3) reference solution. Solution flow is controlled via valves V_1 and V_2 (different types of valves, NResearch, West Caldwell, NJ). For fast switching, the valves were driven with a voltage of 17 V, which is slightly larger than the specified value (12 V). For the valveless diverter configuration, the timing of V_1 and V_2 was experimentally adjusted to synchronize the opening of V_2 exactly with the closing of V_1. Electrical signals are observed at the concentration jumps taking place at the beginning (on signal) and at the end of phase 2 (off signal). Only the on signal (exchange from reference to test solution) will be used throughout our analysis.

Determination of Delay and Rise Times. The transient currents after a 100 mM NaCl/$NaClO_4$ solution exchange were numerically integrated, and the translocated charge was fitted with an empirical model function:[10]

$$Q(t) = Q_0 \frac{(t - t_0)^3}{(t - t_0)^3 + \tau^3} \quad (1)$$

The delay t_0 and the rise time τ represent the time needed for the test solution to reach the SSM after opening its pathway and the rise time of the concentration at its surface, respectively. The charge Q_0 corresponds to the total displaced charge during the solution exchange. For the purposes of this article, only parameters t_0 and τ were relevant and were evaluated. Before fitting, the time axis of the displaced

(11) Fendler, K.; Klingenberg, M.; Leblanc, G.; Depont, J. J. H. H. M.; Kelety, B.; Dörner, W.; Bamberg, E. Transport Proteins on Solid Supported Membranes: From Basic Research to Drug Discovery. In *Thin Film Biosensors*; Mirsky, V. M., Ed.; Springer: New York, 2004.
(12) Meyer-Lipp, K.; Sery, N.; Ganea, C.; Basquin, C.; Fendler, K.; Leblanc, G. *J. Biol. Chem.* **2006**, *281*, 25882–25892.
(13) Pintschovius, J.; Fendler, K.; Bamberg, E. *Biophys. J.* **1999**, *76*, 827–836.
(14) Zuber, D.; Krause, R.; Venturi, M.; Padan, E.; Bamberg, E.; Fendler, K. *Biochim. Biophys. Acta* **2005**, *1709*, 240–250.
(15) Tadini-Buoninsegni, F.; Bartolommei, G.; Moncelli, M. R.; Guidelli, R.; Inesi, G. *J. Biol. Chem.* **2006**, *281*, 37720–37727.
(16) Tadini-Buoninsegni, F.; Nassi, P.; Nediani, C.; Dolfi, A.; Guidelli, R. *Biochim. Biophys. Acta* **2003**, *1611*, 70–80.
(17) Ganea, C.; Pourcher, T.; Leblanc, G.; Fendler, K. *Biochemistry* **2001**, *40*, 13744–13752.
(18) Mus-Veteau, I.; Leblanc, G. *Biochemistry* **1996**, *35*, 12053–12060.
(19) Mus-Veteau, I.; Pourcher, T.; Leblanc, G. *Biochemistry* **1995**, *34*, 6775–83.
(20) Meyer-Lipp, K.; Ganea, C.; Pourcher, T.; Leblanc, G.; Fendler, K. *Biochemistry* **2004**, *43*, 12606–12613.
(21) Zhou, A.; Wozniak, A.; Meyer-Lipp, K.; Nietschke, M.; Jung, H.; Fendler, K. *J. Membr. Biol.* **2004**, *343*, 931–942.

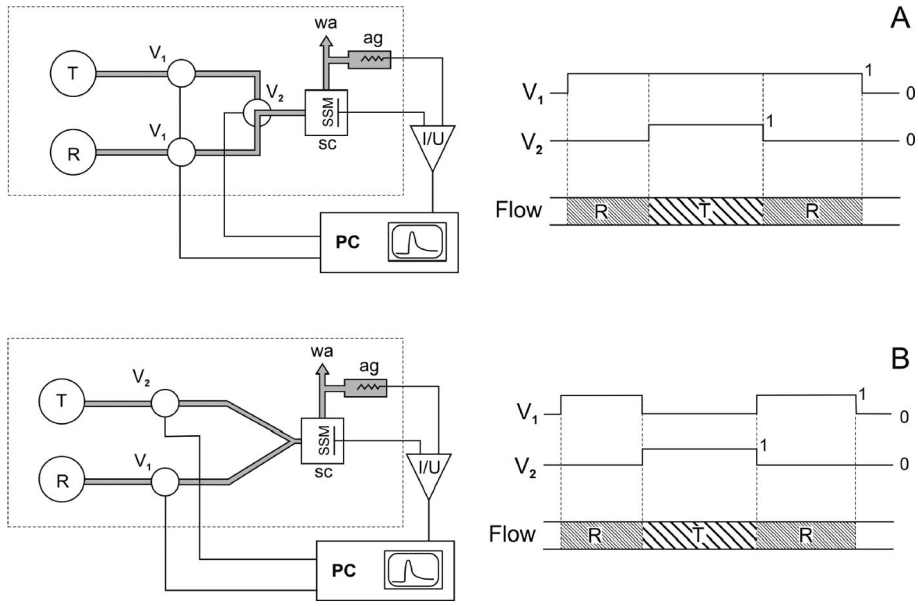

Figure 2. Flow configuration, valve timing, and flow protocol for the two employed diverter geometries. The current is measured with reference to an Ag/AgCl electrode (ag) and amplified by a current/voltage converter (I/U). Valves are controlled and current is recorded by computer (PC). After passing through the cuvette, the solutions are directed to a waste container (wa). (A) Valve-controlled diverter geometry. The two pressurized containers with reference (R) and test (T) solutions are connected to the cuvette (sc) via a 2-way isolation valve V_1 and a 3-way isolation valve V_2 or a 3 × 3-way isolation valve V_2. Opening valve V_1 initiates the flow of R. Subsequently, when V_2 is switched on, T is directed to the cuvette. (B) Valveless diverter geometry. The cuvette is equipped with a y-shaped double inlet bore (Figure 1). The two pressurized containers are now connected to the cuvette via 2-way isolation valves $V_1 = V_2$. Opening valve V_1 initiates the flow of R. Subsequently, simultaneously opening V_2 and closing V_1 directs T into the cuvette.

charge was shifted by subtracting the fluid pathway switching time (0.5 s) plus a valve-switching delay (7.5 ms for NR225T031, 3.5 ms for NR116T011, or 15 ms for NR360T331) from the time values.

Measurement and Analysis of Rapid Charge Displacements in MelB. His-tagged Cys-less MelB was prepared and reconstituted as described.[17] The SSM was formed as described above. Proteoliposomes containing MelB were allowed to adsorb to the SSM[17] for a period of ∼90 min. Transient currents were generated by activating the transporter by a melibiose concentration jump in the presence or absence of Na^+. The solution-exchange protocol consisted of three phases of 0.5 s duration each, in which test and reference solutions were applied to the SSM with adsorbed proteoliposomes (Figure 2). The flow rate was set to 1.5 mL s^{-1}.

To determine the true relaxation times of the current generated by MelB from the measured current, the limited time resolution of the measurements had to be taken into account. Therefore, an iterative least-squares deconvolution algorithm has been developed. The convolution of the input function $I_p(t)$ and the transfer function $f(t)$ describing the time resolution of the SSM system was numerically calculated using the discrete fast Fourier transform algorithm implemented in Mathematica 5.2. For this purpose, the Fourier transform of $f(t)$ is multiplied by the Fourier transform of $I_p(t)$. Then, the inverse Fourier transform of the product yields the output function $I(t)$.[22]

Stopped-Flow Fluorimetric Measurements of MelB. Stopped-flow experiments were carried out using an SF-61DX2 stopped-flow spectrofluorimeter (Hi-Tech Scientific Ltd., Salisbury, U.K.). Intrinsic tryptophan fluorescence was monitored ($\lambda_{ex} = 297$ nm, $\lambda_{em} > 320$ nm) using a 100 W short arc mercury−Xe lamp. The fluorescence was detected at right angles to the incident light beam using a WG320 cutoff filter and an R928 multialkali side-on photomultiplier. The dead time of the instrument was 1.7 ± 0.2 ms[23].

(22) Marko, H., Faltungssatz. In *Methoden der Systemtheorie*, Springer: Berlin Heidelberg New York, 1977; pp 95−108.

Results

Calculation of Delay and Concentration Rise Time in an Analytical Approximation. The cuvette for rapid solution exchange represents a wall jet configuration. After the valve is switched, the fastest streamlines need a time t_0 to reach the surface of the SSM. The delay time t_0 defines the starting point of the concentration jump. Subsequently, the average surface concentration rises with a rise time τ. We consider two limiting cases: Hagen−Poiseuille laminar flow in a cylindrical tube and plug flow. Hagen−Poiseuille flow has a parabolic velocity profile, whereas in plug flow all fluid elements have the same velocity. For simplicity, it is assumed that an "ideal mixer" is placed at the cuvette inlet, generating a uniform inflow of solution with a concentration equal to the average concentration across the cross section of the inlet.

For Hagen−Poiseuille laminar flow in a cylindrical tube (flow rate $\dot{V}$, length x, diameter R), the time dependence of the average concentration can be calculated[7] and is taken as the substrate concentration at the surface of the SSM, $c_s(t)$,

$$c_S(t) = c_0\left(1 - \frac{\tau}{t}\right) \qquad t \geq \tau \tag{2}$$

with $\tau = \{\pi R^2 x\}/\{2\dot{V}\}$.

Here c_0 is the concentration of an arbitrary substrate in the test solution. Note that in Hagen−Poiseuille flow the delay and concentration rise time are identical:

$$\tau = t_0 = \frac{\pi R^2 x}{2\dot{V}} \tag{3}$$

Because in plug flow all solution elements in the flow travel at the same velocity, the delay is given by

$$t_0 = \frac{\pi R^2 x}{\dot{V}} \tag{4}$$

whereas the concentration rise time in ideal plug flow is zero.

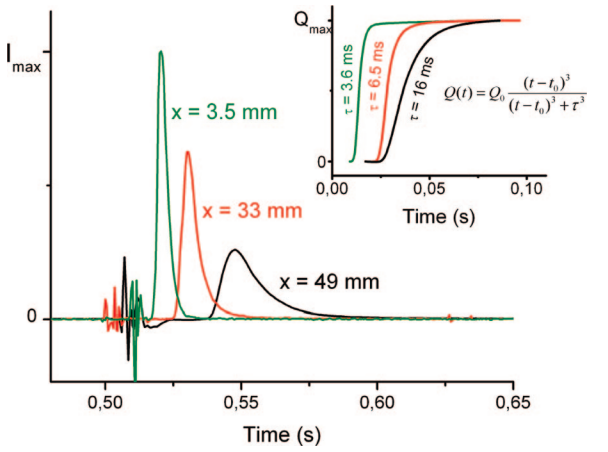

Figure 3. Transient currents generated after 100 mM Cl^-/ClO_4^- solution exchange for three different flow geometries. Solution composition: 50 mM Hepes/Tris pH 7.0, 100 mM NaCl in the reference solution and 100 mM $NaClO_4$ in the test solution. The currents were normalized to equal translocated charge. At $t = 0.5$ s, the fluid pathway was switched from reference to test solution. The flow rate was set to 1.6 mL s^{-1}. Black trace: valve-controlled diverter geometry with V_1 = 2-way isolation valve NR225T011, V_2 = 3 × 3-way isolation valve NR360T331, diverter−SSM distance $x = 49$ mm, tube diameter $d = 1.6$ mm. Red trace: valve-controlled diverter geometry, V_1 = 2-way isolation valve NR225T011, V_2 = 3-way isolation valve NR161T031, $x = 33$ mm, $d = 1$ mm. Green trace: valveless diverter geometry, $V_1 = V_2$ = 2-way isolation valve NR225T011, $x = 3.5$, $d = 1$ mm. (Inset) Integrated current = translocated charge for the three different flow geometries. The charge was fitted using the equation given in the Figure,and the concentration rise time τ was determined.

Experimentally, the concentration rises more steeply than predicted by the hyperbolic dependence of Hagen−Poiseuille flow. Indeed, the dependence could be well approximated by the modified hyperbolic dependence of eq 1. Therefore, the experiments seem to represent an intermediate situation between Hagen−Poiseuille and plug flow, and the equations derived above represent a useful benchmark for the analysis of the experimental flow behavior.

Experimental Determination of Delay and Concentration Rise Time. To measure the rise time of the substrate concentration, we took advantage of the fact that a rapid cation or anion exchange at millimolar concentrations generates a transient current at a solid-supported lipid membrane.[10] Assuming that the interaction of the salts with the surface is rapid compared to the solution-exchange process, the displaced charge can be used as a relative measure of the time dependence of the local ion concentration at the surface of the SSM.

The solution-exchange protocol used in these experiments consisted of the sequential application of a reference and a test solution as detailed in Materials and Methods. In a typical experiment, the reference solution contained buffer plus 100 mM NaCl, and the test solution contained buffer plus 100 mM $NaClO_4$. The strong interaction of the perchlorate anions with the SSM created negative transient currents[10] that were analyzed for the determination of the concentration rise time. ClO_4^- was used because it creates large currents and because of its low affinity compared to that of other ions.[10] Very high affinity ions such as La^{3+} were observed to yield slightly reduced values for the concentration rise time (data not shown).

Typical recorded currents for three different configurations at the same flow rate are shown in Figure 3. At $t = 0.5$ s, the fluid pathway was switched from reference to test solution. As indicated in the figure, these configurations differ mainly in the diverter–SSM distance x. The distance x represents the length of the pathway shared by the test and reference solutions. By varying the length of the connecting tube between the terminal valve and the cuvette, two different values ($x = 49$ and 33 mm) could be implemented for the valve-controlled diverter geometry. An even shorter distance was possible only in the valveless diverter geometry ($x = 3.5$ mm). Note also that for the $x = 49$ mm configuration the tube diameter was different ($d = 1.6$ mm) from that of the other two cases ($d = 1$ mm). Furthermore, a 3 × 3-way isolation valve was used in position V_2, allowing an uninterrupted flow in both pathways. This corresponds to the "classical" configuration employed in previous work.[7,21]

The fast transients observed at $t = 0.50 - 0.52$ s are valve-switching artifacts. Depending on x, the test solution reached the SSM at $t = 0.52 - 0.54$ s, creating transient currents of different amplitudes (5 − 18 nA) and shapes. Because currents obtained with different configurations cannot be directly compared with respect to amplitude, the currents in Figure 3 are normalized to equal displaced charge. Then the currents were numerically integrated (Figure 3 inset) to obtain the displaced charge. Finally, the fit with eq 1 yielded the concentration rise time τ and the delay time t_0 (Materials and Methods).

As will be shown below, the rise time τ clearly depends on the flow conditions in a reasonable and systematic fashion. To further rule out that these dependencies are limited by the kinetics of ion/surface interaction, we determined τ at a given flow condition and geometry using different concentrations and different ions. The same rise time within the error limits was determined using ClO_4^- at concentrations from 1 to 100 mM and for 100 mM ClO_4^-, K^+, and Br^- as well as 50 mM Mg^{2+} (Supporting Information). These results confirm that the measured rise time τ is not limited by the kinetics of ion/surface interaction and support the assumption that the charge displacement can be used as a reliable probe of the time course of the ion surface concentration.

Influence of Technical Parameters of the Flow System on the Rise Time. For rapid surface solution exchange, wall jet geometry with an active surface of ~1 mm^2 was employed (Figure 1). To identify the limiting factors for the concentration rise time at the surface of the SSM, the rise time was experimentally determined under a number of different conditions. In particular, the following technical parameters were varied: (1) the flow rate of the solution; (2) the length, diameter, and material (Teflon, Tygon) of the connecting tube; (3) the flow pathway design (valve-controlled diverter, valveless diverter); and (4) the type of electromagnetic valve.

The flow rate was varied by applying pressure to the solution containers. At pressures of 0.2 to 1 bar, flow rates from ~0.7 to ~2.5 mL s^{-1} were obtained. Interestingly, the pressure versus flow diagram was clearly nonlinear, indicating non-laminar flow conditions (Supporting Information). A concentration jump was applied, and the delay and rise time were measured. With increasing flow rate $\dot{V}$, the delay t_0 and the rise time τ of the integrated charge decreased. As predicted by eq 3, the delay t_0 and the rise time τ are both functions of the reciprocal flow rate and are both plotted as such in Figure 4. In all cases, linear graphs were obtained for t_0 as well as for τ. The experimentally determined delay was always larger than the calculated delay t_0 for Hagen−Poiseuille flow (Figure 4A, dashed lines labeled HP) and coincides with the result for plug flow (dashed lines labeled PF). This, as well as the nonlinear flow versus pressure diagram, indicates that the system is not in a state of pure laminar flow.

Figure 4B is a compilation of the experimental results for the surface concentration rise time τ for different flow geometries.

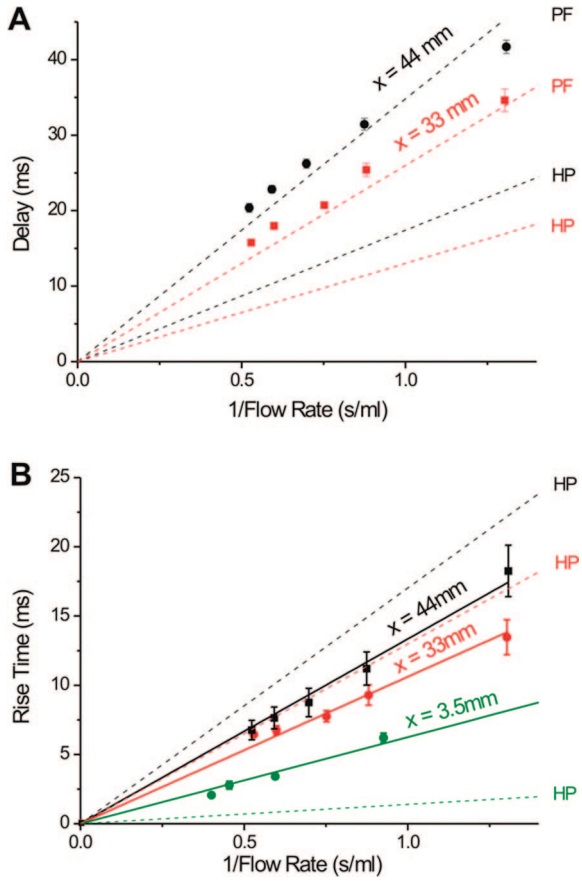

Figure 4. Flow properties using three different flow configurations: (black) valve-controlled diverter, valve V_2 = NR161T031, x = 44 mm; (red) valve-controlled diverter, V_2 = NR161T031, x = 33 mm; (green) valveless diverter $V_1 = V_2$ = NR225T011, x = 3.5 mm. Tube diameter for all three cases d = 1 mm. (A) Delay t_0 was determined as described in the text by application of 100 mM Cl^-/ClO_4^- solution exchange. For the solution composition, see Figure 3. The delay is plotted vs the reciprocal flow rate. The dashed lines are the theoretical predictions (see text) assuming Hagen−Poiseuille flow (HP) or plug flow (PF). (B) Concentration rise time at different flow rates. The solid lines are linear fits to the data points. The dashed lines are the theoretical prediction assuming Hagen−Poiseuille flow (see text).

When plotted versus the reciprocal flow rate, linear graphs were obtained within the error limits. The influence of the diverter−SSM distance x on the rise time was investigated by using different tube lengths between the terminal valve and cuvette. A 25% reduction of x yielded an ~25% reduction of the rise time, in agreement with eq 3. For the valve-controlled diverter geometries, the experimental rise times are somewhat smaller than the theoretical prediction of eq 3, assuming Hagen−Poiseuille flow and an ideal mixer at the cuvette entrance (dashed lines labeled HP in Figure 4B).

In addition, the following parameters have been tested, and these data are all available as Supporting Information. (1) A larger diameter of the tube (1.6 mm) from terminal valve to the cuvette was examined. In agreement with eq 3, the rise time nearly doubled. (2) The effect of acceleration of the volume in the fluid pathway was not found to be significant. This was studied by comparing the "classical" configuration using a 3 × 3-way isolation valve (see the description of Figure 3) characterized by uninterrupted flow with a single 3-way valve as used in Figure 4. (3) It has been discussed that for certain tube materials a "slip" condition is realized, leading to a plug flow profile. We have, therefore, compared Teflon and Tygon tubes but observed no difference in the rise time.

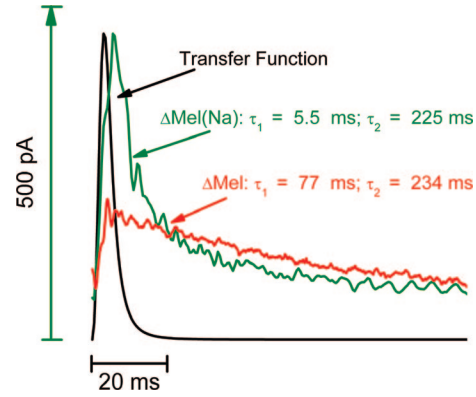

Figure 5. Transient currents (average of six measurements) generated by the melibiose permease MelB after a melibiose concentration jump in the presence (green) and absence (red) of Na^+. The flow rate was set to 1.5 mL s^{-1}. The two time constants representing the decay of the current are given, but the rising phase was not considered. The solution composition for ΔMel(Na) was 100 mM Kpi pH 7.0, 100 mM KCl, and 3 mM NaCl plus 20 mM glucose in the reference and 20 mM melibiose in the test solutions. The solution composition for ΔMel was 100 mM KP_i pH 7.0 and 100 mM KCl plus 20 mM glucose in the reference and 20 mM melibiose in the test solutions. The black line represents the transfer function of the SSM system under the conditions of the experiment.

The experiments described above stress the importance of a short diverter−SSM distance x. However, the construction requirements of the cuvette and valve prevent a much shorter distance than ~33 mm using the conventional flow pathway as shown in Figure 2A. We have, therefore, used valveless diverter geometry (Figures 1 and 2B) to reduce the distance by 1 order of magnitude (x = 3.5 mm). Here, switching of the flow is accomplished upstream of the diverter. Although this requires proper timing of the flow protocol to prevent unwanted mixing of reference and test solutions before the experiment is started, the design allowed a considerable improvement in time resolution. Concentration rise times as low as 2 ms could be obtained at the surface of the SSM (Figure 4B). However, here the experiments yielded significantly larger rise times than did the theory based on Hagen−Poiseuille flow. This indicates that, in this time range, additional factors become limiting, such as the valve opening time (<1 ms) or the time for the acceleration of the fluid (~2 ms).

Measurement and Analysis of Charge Translocation in Melibiose Permease. Sugar binding to melibiose permease (MelB) in the presence of Na^+ is associated with a rapid electrogenic step. This reaction can be detected by the application of a melibiose concentration jump to proteoliposomes immobilized on an SSM.[17] Here, we reanalyzed this reaction using the improved time resolution of the valveless diverter configuration. Figure 5 shows the transient currents recorded after a rapid solution exchange. A flow rate of 1.5 mL s^{-1} was chosen, corresponding to a rise time of the SSM surface concentration of 4.0 ms (Figure 4B). Although higher flow rates are possible, the mechanical artifacts produced by the valve prevented the reliable measurement of the time course of the transient current at flow rates above 1.6 mL s^{-1}. (Note that the MelB-generated currents are more than 10 times smaller than the currents used for the determination of the rise time of the SSM surface concentration in Figures 3 and 4.)

The melibiose concentration jump was performed in the presence and absence of Na^+. A rising phase followed by a biexponentially decaying transient current was observed in both cases (Figure 5). The fast phase of the decay has been previously assigned to an electrogenic conformational transition, and the

slow phase has been assigned to the stationary turnover of the enzyme under conditions of capacitive coupling.[20] Here, only the fast electrogenic conformational transition will be discussed. In the absence of Na^+, its time constant was considerably slower. This has been reported before[17] and probably corresponds to H^+/melibiose cotransport. The dramatic Na^+ dependence of the transient currents demonstrates that they are indeed associated with the enzymatic activity of MelB.

For a linear system, the limited time resolution of a measurement can be described by a transfer function $f(t)$.[24] The output current $I(t)$ is a convolution of the transfer function and the input current $I_p(t)$ (which in our case is the current generated by MelB):

$$I(t) = \int_0^t f(t - t')I_p(t')\,dt' \tag{5}$$

In the SSM measurement, the transfer function is determined by the substrate concentration rise at the SSM surface. It is the first derivative of the step function response of the system.[24] As outlined above, the step function response of the system can be measured using the integrated charge generated by the anion concentration jumps (Figure 3). The corresponding function is eq 1; consequently, the transfer function is its derivative:

$$f(t) = \frac{3t^2\tau^3}{(t^3 + \tau^3)^2} \tag{6}$$

(Note that the irrelevant parameters Q_0 and t_0 have been set to 1 and 0, respectively.) Because the time constant τ has been determined for different flow rates and configurations, the transfer function for a specific experiment may be calculated using eq 6. Finally, the output current can be obtained by solving the convolution equation (eq 5). For comparison, the transfer function for the measurement of Figure 5 has been included in the Figure. Clearly, the transfer function decays more rapidly than the signal but is sufficiently slow to distort it.

To obtain the current generated by MelB $I_p(t)$, the reverse operation has to be performed. For this purpose, the current $I_p(t)$ is assumed to be biexponential:

$$I_p(t) = A_1 e^{-\frac{t - t_0}{\tau_1}} + A_2 e^{-\frac{t - t_0}{\tau_2}} \tag{7}$$

Using an appropriate set of values for parameters A_1, A_2, τ_1, τ_2, and t_0, the output current $I(t)$ can now be numerically calculated by performing the convolution defined by eqs 5–7 as described in Materials and Methods. In an iterative least-squares algorithm, the output current $I(t)$ is fitted to the measured current to determine the parameters A_1, A_2, τ_1, τ_2, and t_0. The calculated output current and measured current for a typical experiment are shown in Figure 6A. The resulting time constants for the fast process τ_1 and the slow process τ_2 were determined from four different experiments and are summarized in Table 1.

Stopped-Flow Fluorescence Measurements. The sugar-induced electrogenic reaction can be correlated with a conformational change observed in intrinsic tryptophan fluorescence spectroscopy.[12,19] For a kinetic comparison, we have measured the time-resolved tryptophan fluorescence in a stopped-flow experiment. A typical fluorescence recording obtained after mixing a proteoliposomal suspension with a melibiose-containing solution is shown in Figure 6B. The data are an average of seven different traces recorded in one experiment. They were fitted using a biexponential model function. Four independent stopped-flow experiments were made and analyzed. The results for the time constants τ_1 and τ_2 are included in the Table for comparison with the electrical measurements. In particular, the time constants for the fast process agree within the error limits.

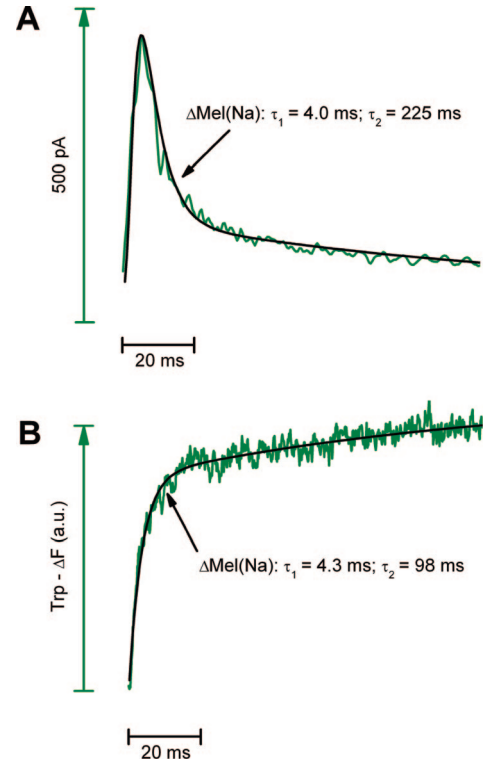

Figure 6. (A) Transient current generated after a melibiose concentration jump in the presence of Na^+ (green). Experimental conditions are the same as in Figure 5. The trace in black corresponds to the final result of the iterative deconvolution algorithm (see text). Time constants for this specific experiment are given in the Figure. (B) Time-resolved tryptophan fluorescence of MelB after mixing of the proteoliposomes with a melibiose-containing solution in the presence of Na^+ (green). The data were fitted with a biexponential function (black). Time constants for this specific experiment are given in the Figure. Two solutions were mixed in a 1:1 ratio. Solution 1 consisted of 20 μg/mL proteoliposomes preincubated with 5 mM NaCl, and 40 mM glucose, and 100 mM KP_i pH 7.0. Solution 2 consisted of 5 mM NaCl, and 40 mM melibiose, and 100 mM KP_i pH 7.0.

Table 1. Comparison of the Time Constants for the Fast and the Slow Components Determined from the Current Measurements at the SSM and from Stopped-Flow Tryptophan Fluorescence Measurements

	current	fluorescence
fast component τ_1 (ms)	3.8 ± 0.4	4.2 ± 0.4
slow component τ_2 (ms)	219 ± 12	90 ± 17

It is interesting that a slow phase (τ_2) is observed in the fluorescence as well as in the electrical measurements. The meaning of that phase is still unclear. As far as the electrical measurements are concerned, this phase has been shown to be related to transporter turnover.[17] Whether its time course is determined by transporter kinetics or by charging of the liposomes is still open. These two possibilities are relevant for electrical and fluorescence experiments because both were performed with the same preparation of proteoliposomes.

Discussion

New Method for the Experimental Determination of the Time Course of Substrate Surface Concentrations. In this study, we have used the strong interaction of inorganic ions

(23) Kane, D. J.; Fendler, K.; Grell, E.; Bamberg, E.; Taniguchi, K.; Froehlich, J. P.; Clarke, R. J. *Biochemistry* **1997**, *36*, 13406–13420.

(24) Varju, D., Das Faltungsintergral. In *Systemtheorie für Biologen und Mediziner*; Springer: Berlin, Heidelberg, NY, 1977; pp 40−44.

with the lipid surface of an SSM to determine the time course of substrate surface concentrations. Experiments using different salt concentrations and different ions (Supporting Information) yield identical values and support the assumption that the measured rise times represent the rise time of surface ion concentration. The dependence of the rise time on the technical parameters of the flow system confirms this. The method presented here has the great advantage that it is simple and can be performed on the same sensor that is used for the immobilization of the protein. It, therefore, exactly matches the flow conditions and sensor position used for the activation of the protein on the SSM. This is relevant for time-critical measurements when the deconvolution technique is required to account for the limited rise time of the surface substrate concentration.

Can this approach for ions be generalized for arbitrary charged or uncharged substrates? Charged compounds interact with charged surfaces. As a result, they form electrical double layers depending on the surface charge. At physiological concentration (100 mM), a Gouy−Chapman double layer on a biological membrane has a thickness of ∼1 nm. A typical ion such as K^+ diffuses 1 nm in 0.25 ns (using the Einstein relationship $t = \langle x^2\rangle/(2D)$ with $\langle x^2\rangle = 10^{-18}$ m^2 and $D = 2 \times 10^{-9}$ m^2 s^{-1}) whereas the solution exchange is in the millisecond time range. This demonstrates that on the time scale of the solution exchange the double layer is in rapid kinetic equilibrium with the surface. Therefore, the formation of the electrical double layer leads to a modified ionic surface concentration but is not relevant to the time course of the rise in surface concentration after a concentration jump. In conclusion, the time course of ion surface concentration may be used in a generalized fashion to estimate the rise time of the surface concentration for arbitrary small charged and uncharged substrates.

Rapid Solution Exchange at the SSM Using Wall Jet Geometry. Because the concentration rise time can be measured using the technique described above, different flow configurations aiming at optimal solution exchange at the SSM surface were investigated. Indeed, the wall jet geometry allows rapid solution exchange at the surface of an SSM. A simple theoretical model assuming laminar Hagen−Poiseuille flow in a cylindrical tube and an ideal mixer at the end of the tube describes the flow conditions surprisingly well. It correctly predicts the linear dependence of the rise time of the surface concentration on the reciprocal flow rate, and even the absolute values are only slightly overestimated. This model, therefore, can serve as a guide for improved cuvette design.

A closer look at the experiments, however, reveals indications for nonlaminar flow behavior. First, the flow versus pressure diagram of the system is clearly nonlinear. Second, the delay times are not in agreement with the predictions of the laminar flow model but rather show plug flow behavior. Indeed, an analysis of the Reynolds number (*Re*) shows that the onset of turbulence is to be expected at high flow rates. Laminar flow in a cylindrical tube is obtained for a Reynolds number of $Re < 2000$.[25] At the maximal flow rate of 2.5 mL s^{-1} used in our experiments, a Reynolds number of $Re = 2\bar{u}R/\nu = 3200$ is obtained (mean velocity $\bar{u} = 3.2$ m s^{-1}, tube radius $R = 0.5$ mm, kinematic viscosity of water $\nu = 10^{-6}$ m^2 s^{-1}), which is clearly above the critical value. A second concept to be considered is the so-called development length L_e. Over this characteristic distance, the flow develops in the tube from an initial plug flow to the full Hagen−Poiseuille flow profile.[26–28] The development length is given by $L_e/2R = 0.06Re$ and covers a range of 53–210 mm from the minimal (0.7 mL s^{-1}) to the maximal flow rate (2.5 mL s^{-1}) of our experiments. Therefore, a fully developed Hagen−Poiseuille flow profile is never obtained with the dimensions of our flow pathways. All things considered, it seems clear that our flow conditions represent a transit region from laminar to turbulent and from plug flow to Hagen−Poiseuille flow. It is therefore not surprising that the delay times show plug flow behavior and that the concentration rise time is always somewhat shorter than the prediction by the Hagen−Poiseuille law. Incidentally, this also indicates the direction of further improvement of the time resolution, namely, large Reynolds numbers.

The experiments as well as the theoretical model clearly show that the most important geometrical factor influencing the rise time at the surface is the length of the common pathway for test and reference solutions (i.e., the distance between the terminal valve or the diverter point and the SSM). On the basis of this insight, a cuvette with improved performance has been designed, allowing a time resolution as low as 2 ms at a pressure of 1 bar. Further improvement could come from an increased flow rate (higher pressure). However, pressure above 1 bar requires special equipment and makes handling the setup difficult.

Effective perfusion of the SSM surface relies on the application of high flow rates. On the other hand, fast flow at the surface represents a risk of ablation for the immobilized proteoliposomes because of fluid shear forces. However, this is obviously not the case because proteoliposomes can be investigated on the SSM for hours with only a very small decrease in signal. It is concluded that an unstirred layer of at least 200 nm (the dimensions of the proteoliposomes) does indeed exist but represents no serious barrier for a millisecond substrate rise time at the SSM surface.

Rapid Electrogenic Reaction during Melibiose Transport of the Melibiose Permease MelB. Transporters are fascinating molecular machines that effectuate the rapid and selective translocation of substrate molecules across the cell membrane. This is in general a complex sequence of partial reactions taking place on a millisecond to microsecond time scale. Techniques for their analysis, therefore, require a time resolution of milliseconds or faster. It is demonstrated above that substrate application to surface-immobilized protein in a few milliseconds is possible. Using the improved flow geometry and advanced signal analysis, we have determined the rate constant of a partial reaction in the transport cycle of a bacterial transporter, the melibiose permease MelB from *Escherichia coli*.

MelB is a sugar cotransporter from *E. coli* that is driven by the favorable Na^+, Li^+, or H^+ electrochemical gradient to drive cell accumulation of galactosides.[29] It has been shown to perform an electrogenic reaction after substrate (melibiose) application.[20] This electrogenic process was associated with a conformational transition observed by tryptophan fluorescence spectroscopy,[18,19] suggesting an electrogenic conformational transition.[20] However, rapid kinetic information about the two processes to strengthen this assignment was not available.

We have reinvestigated the melibiose-induced fluorescence change and charge translocation using instrumentation with sufficient time resolution to determine the temporal behavior. For the fluorescence measurement, standard stopped-flow equipment was

(25) Jirka, G. H., *Einführung in die Hydromechanik*; Universitätsverlag Karlsruhe: Karlsruhe, 2007.

(26) Al-Nassri, S. A.; Unny, T. *Appl. Sci. Res.* **1980**, *36*, 313–332.

(27) Raja, L. L.; Kee, R. J.; Deutschmann, O.; Warnatz, J.; Schmidt, L. D. *Catal. Today* **2000**, *59*, 47–60.

(28) Washabaugh, A. P.; Zahn, M. *IEEE Trans. Dielectr. Electr. Insul.* **1994**, *1*, 38–52.

(29) Leblanc, G.; Bassilana, M.; Pourcher, T. Na^+, H^+ or Li^+-Coupled Melibiose Symport in *E. coli*. In *Molecular Basis of Biomembrane Transport*; Palmieri, F., Quagliariello, E., Ed.; Elsevier Science Publishers B. V.: Amsterdam, 1988; pp 53−62.

employed whereas the electrical measurement was performed with the improved cuvette for rapid solution exchange in combination with an iterative least-squares deconvolution algorithm. The time constants of the fast phases determined with both techniques agree within the error limit (Table 1). This is a strong argument in favor of a common molecular process behind the fluorescence change and the charge translocation. It supports the previous proposition of a melibiose-induced electrogenic conformational transition and assigns a rate constant of $k \approx 250\ s^{-1}$ to it.

Acknowledgment. We thank C. Kremin for helpful discussions and model simulations of the fluid behavior. We are grateful for excellent technical assistance by L. Hatahet and for continuous support of this work by E. Bamberg.

Supporting Information Available: Flow at different pressures, fluid acceleration, tube materials, and concentration rise time using different ions and concentrations. This material is available free of charge via the Internet at http://pubs.acs.org.

LA800428H

Methods 46 (2008) 97–103

Contents lists available at ScienceDirect

Methods

journal homepage: www.elsevier.com/locate/ymeth

SSM-based electrophysiology

Patrick Schulz, Juan J. Garcia-Celma, Klaus Fendler *

Department of Biophysical Chemistry, Max Planck Institute of Biophysics, Max von Laue Str. 3, D-60438 Frankfurt/Main, Germany

ARTICLE INFO

Article history:
Accepted 2 July 2008
Available online 31 July 2008

Keywords:
Solid supported membrane
Lipid membrane
Vesicle
Proteoliposome
Assay technique
Transport protein
Solution exchange
Capacitive coupling
Drug discovery

ABSTRACT

An assay technique for the electrical characterization of electrogenic transport proteins on solid supported membranes is presented. Membrane vesicles, proteoliposomes or membrane fragments containing the transporter are adsorbed to the solid supported membrane and are activated by providing a substrate or a ligand via a rapid solution exchange. This technique opens up new possibilities where conventional electrophysiology fails like transporters or ion channels from bacteria and from intracellular compartments. Its rugged design and potential for automation make it suitable for drug screening.

1. Introduction

Electrophysiology has evolved in the past from the simple detection of neural activity of excitable tissues to a powerful instrument for the investigation of transport processes on the molecular level. This was possible by the continuous improvement of the technology and the introduction of revolutionary concepts like the patch clamp technique. All these methods of "standard" electrophysiology have in common, that their principle tool is the electrolyte filled micro-pipette electrode. In this review, we introduce a technique that detects charge translocation via a solid supported membrane electrode, which for a number of applications offers an advantage over the standard electrophysiological approach.

Electrophysiological measurements based on solid supported membranes (SSM)[1] have been used for the functional characterization of ion pumps and transporters. In this technique, proteoliposomes, membrane vesicles, or membrane fragments are adsorbed to an SSM and are activated using a rapid substrate concentration jump. Then charge translocation is measured via capacitive coupling of the supporting membrane. This method has the advantage of providing an aqueous environment on both sides of the membrane for the incorporated transport proteins.[2] In addition, adsorption of proteoliposomes or membrane fragments allows a large number of transporters to be immobilized on the electrode in a simple spontaneous process. In contrast, direct incorporation of the proteins into the planar membrane is not very effective and requires complicated reconstitution procedures (compare e.g. [1]).

SSM-based electrophysiology is extremely useful in cases where conventional electrophysiology cannot be applied. Apart from a few rare exceptions bacterial transporters cannot be investigated using voltage clamp or patch clamp methods because of the small size of bacteria and because they are difficult to express in mammalian cells or oocytes. On the other hand, SSM-based electrophysiology was very successful in this field [2–6]. But also physiologically relevant mammalian transporters could be investigated [7,8]. In this case SSM-based electrophysiology is attractive for transporters from intracellular membranes and for screening applications in drug discovery because of its robustness and its potential for automation [9,10]. Furthermore, SSM-based electrophysiology can be employed for the investigation of ion channels [11].

Using standard electrophysiology, also time resolved characterization of transporters is challenging. Since the turnover of trans-

* Corresponding author. Fax: +49 069 6303 2222.
E-mail address: Klaus.Fendler@mpibp-frankfurt.mpg.de (K. Fendler).

[1] *Abbreviations used:* SSM, solid supported membrane; NA, non-activating solution; A, activating solution; R, resting solution; nAChR, nicotinic acetylcholine receptor; IC_{50}, half maximal inhibitory concentration; EC_{50}, half maximal effective concentration; EDTA, ethylenediaminetetraacetic acid; EGTA, ethylene glycol-bis(2-aminoethylether)-*N*,*N*,*N*′,*N*′-tetraacetic acid; NMG, *N*-methyl D-glucamine; CHO cells, Chinese hamster ovary cells.

[2] The exact adsorption geometry of the proteoliposomes, membrane vesicles and membrane fragments is still unknown. Especially in the case of adsorbed membrane fragments it is not immediately obvious that a sufficient aqueous space exists between the fragments and the SSM. However, the kinetic data obtained so far with different transporters and different preparations gave no indication for an obstruction of substrate uptake or release at the SSM-oriented face of the adsorbed membranes.

1046-2023/$ - see front matter © 2008 Elsevier Inc. All rights reserved.
doi:10.1016/j.ymeth.2008.07.002

porters is low (<100 s^{-1} in most cases) ~10^4–10^5 transporters are required to generate a measurable signal. This can only be obtained in a 'giant patch' or a 'whole cell' configuration which have an inherently low time resolution in a solution exchange experiment. The complication can be overcome using photolytic substrate release from protected ("caged") substrates (see e.g. [12–14]). However, only a limited number of substrates are available in caged form. Here the rapid solution exchange at the SSM offers the unique opportunity to perform electrophysiological studies with a high time resolution using arbitrary substrates. Recently, it has been demonstrated that transporter currents can be measured with a time resolution of <4.5 ms [15].

2. Description of method

2.1. The instrument for SSM-based electrophysiology

2.1.1. SSM cuvette

The cuvette is made from Plexiglas (Fig. 1). After mounting of the sensor chip with the gold electrode, the cuvette base plate and the cuvette body are screwed together. Inlet and outlet bores have a diameter of 1 mm. The cuvette volume is cylindrical and 0.75 mm deep with an internal volume of 17 µl (net volume with O-ring mounted). When mounted, the circular active area of the electrode (diameter 1 mm) which is covered by the SSM is centered under the inlet bore. In the outlet pathway the reference electrode assembly is placed. The reference electrode is a Ag/AgCl electrode which is separated from the main fluid pathway by an acrylamide salt bridge saturated with 100 mM KCl. The gold electrode is connected to the current amplifier (Stanford Research, amplification 10^9 V/A), the reference electrode to the function generator or to ground (Fig. 2). For details of the set-up see also [3,7].

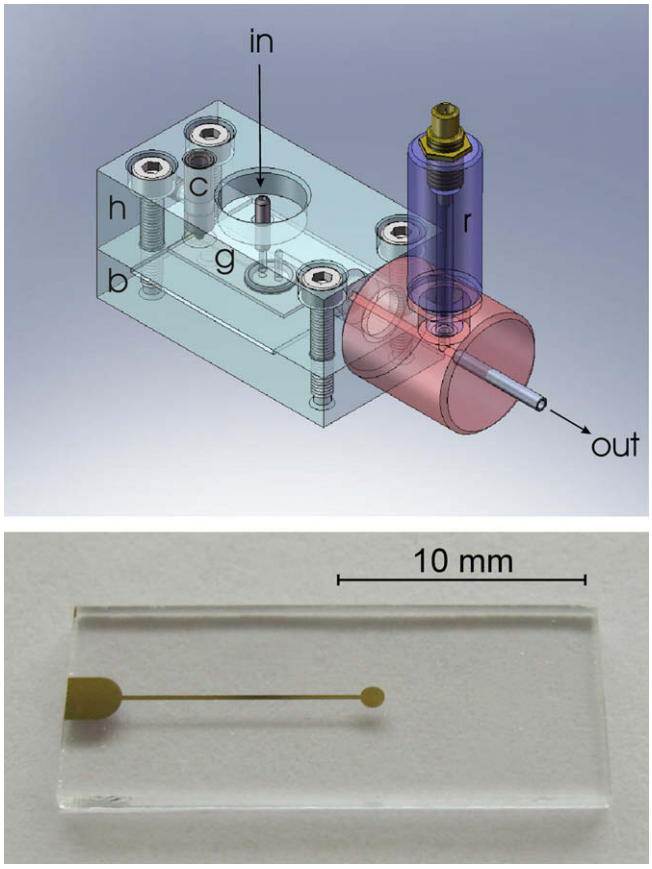

Fig. 1. Cuvette (upper panel) and sensor chip with gold electrode (lower panel). Cuvette head (h) and base (b) are made out of Plexiglas. Inlet (in) and outlet (out) bores have a diameter of 1 mm. The reference electrode assembly (*r*) is placed in the outlet pathway. The cuvette volume is cylindrical and 0.75 mm deep with an internal volume of 17 µl (net volume with O-ring mounted). The SSM is formed on a gold coated glass slide, the sensor chip (g), and has a diameter of 1 mm. It is connected to the contact pad via a 0.2 mm wide contact strip. Contact to the amplifier is made through a spring contact pin (c). When mounted the SSM is centered under the inlet bore.

2.1.2. SSM set-up and flow protocol

The cuvette and the entire fluid pathway including solution containers and valves are mounted in a faraday cage (Figs. 2 and 3). The solution containers (A, NA, R in Figs. 2 and 3) are standard 100 ml polyethylene bottles which are pressurized with compressed nitrogen gas. Pressures of 0.2–1.0 bar were used in the experiments. The valves are switched using home made valve drivers which are controlled via computer. Solution flow is controlled via the valves V_1 (NR225T011), V_2 (NR360T331) and V_3 (NR225T031, all valves from NResearch, West Caldwell, USA). For fast switching the valves are driven with a voltage of 17 V, which is slightly larger than the specified value (12 V). Also the current is recorded by computer. For both purposes an AD/DIO card PCI 6023E (National Instruments, Austin, TX, USA) and SURFE^{2}R software (IonGate Biosciences, Frankfurt/Main, Germany) is employed.

Two different solution exchange protocols are generally employed for the experiments: a single and a double solution exchange protocol. In the single solution exchange protocol (Fig. 2A) two different solutions are sequentially conducted through the cuvette: the non-activating solution (NA) followed by the activating solution (A) containing the substrate of the transporter immobilized on the SSM. This produces a substrate concentration jump at the SSM initiating transport and concomitant charge displacement. Finally the activating solution is again replaced by non-activating solution, so that before and in between experiments, the SSM is incubated with non-activating solution. Note that V_2 is a mechanically coupled 3 × 3-way valve. This design ensures that during the entire experiment both, activating and non-activating solutions are in motion. Electrical signals are observed at the concentration jumps taking place at the beginning (on-signal) and at the end of phase A (off-signal) (Fig. 4). Usually, only the on-signal (exchange from non-activating to activating solution) is used for analysis.

The double solution exchange experiment (Fig. 2B) requires an additional resting solution, which is conducted through the cuvette after the NA/A/NA solution exchange. Thus, in between experiments the SSM is incubated in resting solution allowing the establishment and/or maintenance of ion gradients. For example, for a ligand gated ion channel, the resting solution is free of permeant ions while the non-activating and the activating solutions contain the permeant ions. In addition, the activating solution contains the ligand. Therefore, in the first concentration jump, resting versus non-activating solution, a concentration gradient of the permeant ion is established. Subsequently, upon non-activating versus activating solution exchange, transport is activated by the ligand concentration jump. Note that in this solution exchange protocol the SSM is incubated before and in between experiments with resting solution to remove the permeant ion from the internal volume of the proteoliposomes/membrane vesicles.

2.1.3. Commercial instruments

In the meantime commercial instruments for SSM-base electrophysiology are available which are adapted to the requirements of industrial drug screening. Initial developments focused on a single-channel, semi-automated analysis system (SURFE^{2}R One, IonGate Biosciences, Frankfurt, Germany) with a closed flow cell comparable to the laboratory set-up outlined above. A critical evaluation of

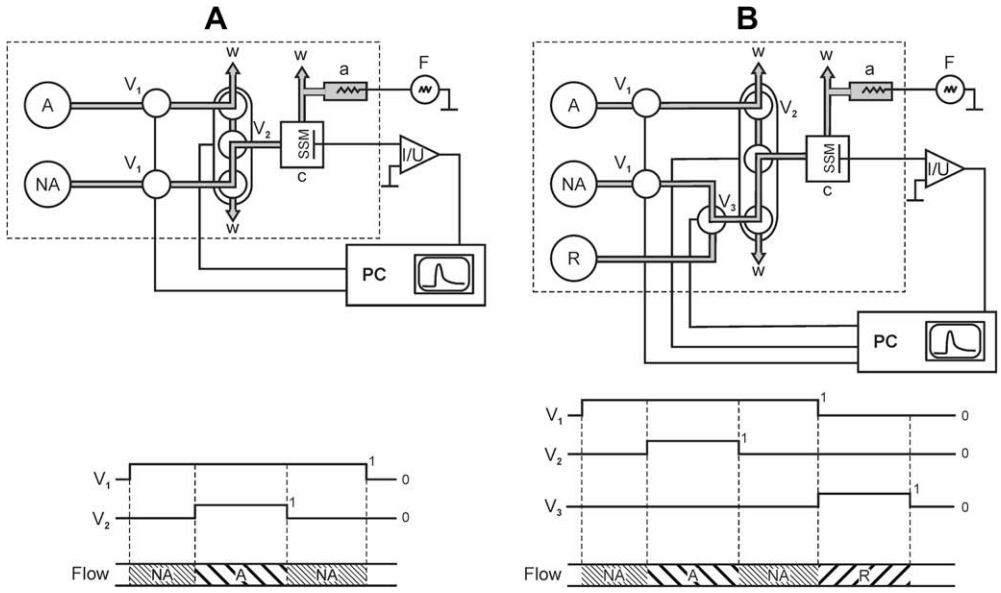

Fig. 2. Flow configuration valve timing and flow protocol for the single solution exchange (A) and the double solution exchange (B) configuration. The entire fluid pathway is mounted in a Faraday cage (dashed line). The current is measured with reference to an Ag/AgCl electrode (a) and amplified by a current/voltage converter (*I*/*U*). A function generator (*F*) is used to measure the electrical properties of the SSM. Valves are controlled and current is recorded by computer (PC). After passing through the cuvette, the solutions are directed to a waste container (w). The two pressurized containers with non-activating (NA) and activating (A) solutions are connected to the cuvette (c) via 2-way isolation valves V_1 and a 3×3-way isolation valve V_2. Opening of valves V_1 initiates flow of NA. Subsequently, when V_2 is switched on A is directed to the cuvette. For double solution exchange an additional container for the resting solution (R) is added. Resting solution is directed through the cuvette after each experiment via valve V_3.

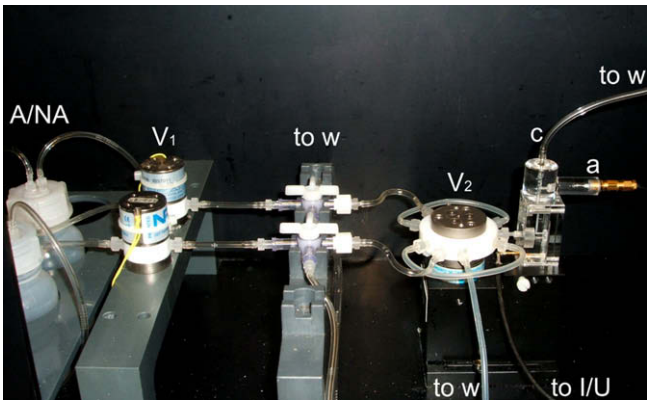

Fig. 3. Faraday cage containing valves and cuvette assembly in the single exchange configuration. Labelling of the components as in Fig. 2.

the application of this instrument for drug screening can be found in Ref. [10]. The demand for a higher throughput and lower reagent consumption triggered the development of a product family of fully automated SURFE^{2}R Workstations. Unlike the semi-automated system, the Workstations operate in an open configuration with 96-sensor plates in a standard microtiter plate format (Fig. 5). A movable fluidic unit, the IonJet, collects solutions for each measurement and injects them on the sensor surface in individual wells of a 96-well plate, thus generating a rapid solution exchange. The SURFE^{2}R Workstation 500 performs 400–600 measurements per day. Further parallelization of the technology has been achieved recently (eight parallel channels, SURFE^{2}R Workstation 5000) and provides a significantly higher throughput.

2.2. Materials

2.2.1. Lipid solution for formation of the SSM

375 μl of a stock solution of diphytanoyl-phosphatidylcholine (20 mg/ml in chloroform) together with 25 μl of octadecylamine (5 mg/ml in chloroform) is added to a small vial and the solvent is removed by a gentle stream of nitrogen gas. Then 500 μl of *n*-decane are added yielding a lipid solution of 15 mg/ml and 1:60 (w/w) octadecylamine.

2.2.2. Sensor chips

The sensor chips are prepared by a photolithographic lift-off process on a 4 inch 1 mm thick borofloat glass substrate (Fraunhofer Institut für Schicht und Oberflächentechnik, Braunschweig, Germany). The 100 nm thick gold structure on a 10 nm adhesive layer consists of a 1 mm diameter circular active area which is connected to a contact pad via a thin contact strip (Fig. 1). After cutting, the glass chips (9×22 mm) carrying the electrode are incubated for 6 h in an ethanolic solution of 1 mM octadecanethiol. For long time storage the sensor chips are kept in nitrogen atmosphere and shielded from light.

2.2.3. Protein preparations

A number of different electrogenic proteins have been tested on the SSM. These proteins come in many different preparations: purified and reconstituted into proteoliposomes, in membrane vesicles from native tissue, in enriched membrane fragments from native tissue, recombinantly expressed in bacteria and mammalian cell lines. Table 1 summarizes the various preparations and proteins. A short compendium of the most common preparations is given below.

2.2.4. Membrane fragments and membrane vesicles

Recombinantly expressed protein can be studied in bacteria and mammalian cell lines. Protein expressing bacterial strains are grown to an appropriate OD_{600} (e.g. 1.0), collected by centrifugation and lysed by three passages through a French press in a DNA-ase and protease-inhibitor containing buffer (see e.g. [16]). After ultracentrifugation the resulting pellet contains the membrane fraction with the target protein, which can be directly adsorbed to the SSM. Membranes are frozen and stored at −80 °C. Mammalian cells are mostly grown adherently, collected by trypsinization

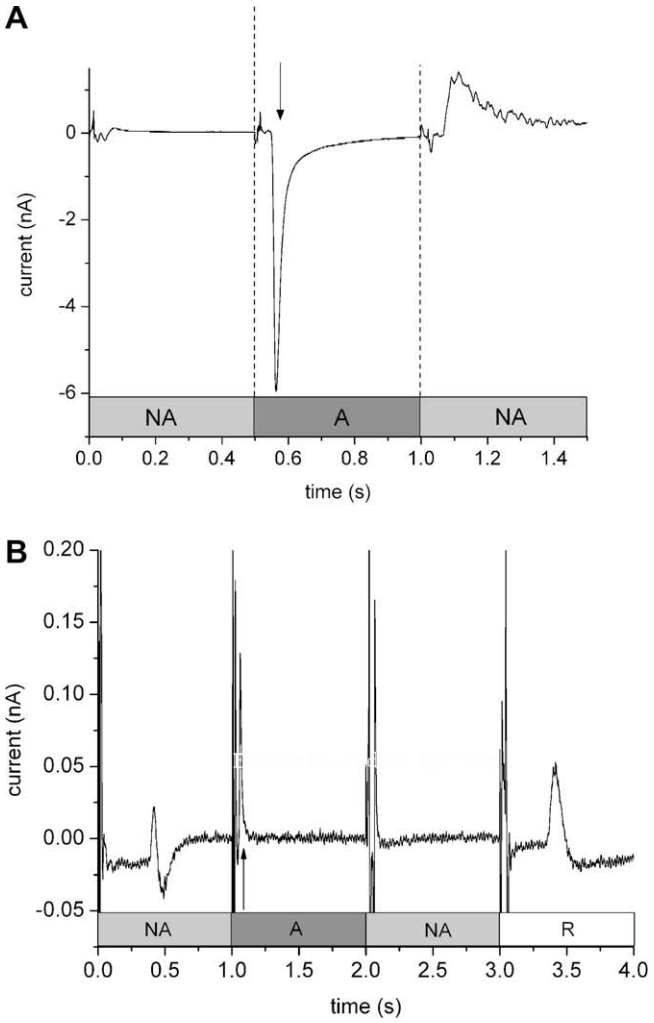

Fig. 4. Solution exchange protocols and transient currents during rapid solution exchange on a SSM using the two flow configurations shown in Fig. 2. (A) NhaA Na^+/H^+-exchanger from *Helicobacter pylori* reconstituted into proteoliposomes. The negative transient current indicated by the arrow corresponds to the exchange activity of NhaA initiated by a 100 mM Na^+ concentration jump. Buffer composition: 100 mM KPi pH 8.5 plus 300 mM KCl in the non-activating (NA) and 200 mM KCl + 100 mM NaCl in the activating (A) solution. (B) Ligand gated cation channel, nAChR, in membrane vesicles. The positive transient current indicated by the arrow corresponds to the carbamylcholine induced Na^+ influx into the membrane vesicles. Basic buffer in all solutions: 30 mM Tris(HCl), pH 7.5, 3 mM EDTA, 1 mM EGTA. In addition, the different solutions contained: 100 mM NaCl in the non-activating solution (NA), 100 mM NaCl, and 100 μM carbamylcholine in the activating solution (A) and 100 mM NMGCl in the resting solution (R). Before the experiment the membrane vesicles were filled with 100 mM NMGCl.

and centrifugation and subsequently disrupted in a Parr Bomb (Parr Instruments Deutschland GmbH, Frankfurt/Main, Germany). The membrane fraction is collected by ultracentrifugation and the plasma membranes are isolated by density gradient centrifugation (sucrose-gradient: 9–45%, 3 h/100,000*g*). For long term storage, membranes can be flash frozen in resting buffer with 10% glycerol and stored at −80 °C for months. These membranes contain membrane fragments and/or membrane vesicles with in general unknown orientation (see Section 2.4.4).

2.2.5. Purified and reconstituted proteins

His-tagged proteins are purified from membrane vesicles by Ni^{2+}–NTA affinity chromatography as described elsewhere [3,5,6,17]. The reconstitution process is performed in three parts: liposomes are formed by extrusion from different lipids (we use routinely total or polar *Escherichia coli* lipid extract) with a final concentration of 10 mg/mL of lipid in the reconstitution buffer. Detergent is added in order to destabilize or dissolve the liposomes. Solubilized protein is added in a defined mass ratio to the lipid content and incubated for at least 15 min. Removal of the detergent is accomplished by the addition of polystyrene beads (Bio-Beads, Bio-Rad, München, Germany). The amounts and intervals of addition of the bio-beads are adjusted for every different protein. Typically, incubation overnight and exchange of the bio-beads afterwards is required to achieve a complete removal of the detergent (for reconstitution procedures see e.g. [5,6,16,17]).

2.3. Measurement procedure

2.3.1. Mounting of the sensor chip

Before use, the stored sensor chips are regenerated by incubation for 1 h in a 1 mM octadecanethiol solution in ethanol. The lipid monolayer is deposited using a painting technique where a small amount (2 μl) of the lipid solution is applied to the electrode for the formation of the SSM. Then the sensor chip is mounted into the cuvette. The monolayer forms spontaneously when the electrode is rinsed with buffer in the cuvette. The planar membrane has an area of ~0.8 mm^2.

The experiments were carried out at room temperature (22 °C). After the formation of the SSM its capacitance and conductance were determined until they became constant after a waiting time of ~90 min. Typical values were 300–500 nF/cm^2 for the capacitance and 50–100 nS/cm^2 for the conductance.

2.3.2. Addition of the protein sample

A proteoliposome suspension suitable for the SSM measurement has a typical lipid concentration of ~10 mg/ml and a lipid to protein ratio of ~5–10 (w/w). Membranes from native tissue or from bacterial or mammalian cells were prepared at a total protein concentration of ~2–8 mg/ml. Care was taken that the buffer osmolarity in the preparations was comparable to that of the measurement buffers. The samples were stored in liquid nitrogen or in a freezer at −80 °C. Before use, the proteoliposomes were thawed and briefly sonicated in a bath (three sonication cycles of 10 s with 20 s cooling intervals on ice in between). The natural membranes were diluted after thawing to a final protein concentration of 1–2 mg/ml and sonicated using a tip sonicator (UP50H, 50 W, 30 kHz, 1 mm sonotrode diameter, intensity 20%, cycle 0.5, Dr. Hielscher, Teltow, Germany). Then, 30 μl of the suspension was applied to the SSM using a standard pipette via the exit bore of the cuvette with the reference electrode assembly removed. The membranes were allowed to adsorb to the SSM for 1 h. Finally, the SSM was rinsed with non-activating buffer and was ready for the measurement.

2.3.3. Signal recording

Signals are recorded using a specific solution exchange protocol as discussed above. The solution flow rate is controlled by adjusting the pressure on the solution containers. Typically the flow rate was 0.5–2 ml/s. The solution exchange protocols for a representative single and double exchange experiment and the resulting transient currents are shown in Fig. 4. In Fig. 4A a transient current generated by the NhaA Na^+/H^+-exchanger from *Helicobacter pylori* is shown. Transport is initiated by addition of 100 mM Na^+ in the activating solution (A). This protein transports 2 H^+ for 1 Na^+. Therefore, upon Na^+ addition a negative transient current is observed (indicated by an arrow at $t \sim 0.5$ s) corresponding to the transport of positive charge out of the liposomes. When Na^+ is removed ($t = 1.0$ s) a current in the opposite direction is observed representing the inverse process. Only the current upon addition of the substrate (Na^+) is used for the analysis, because the closing

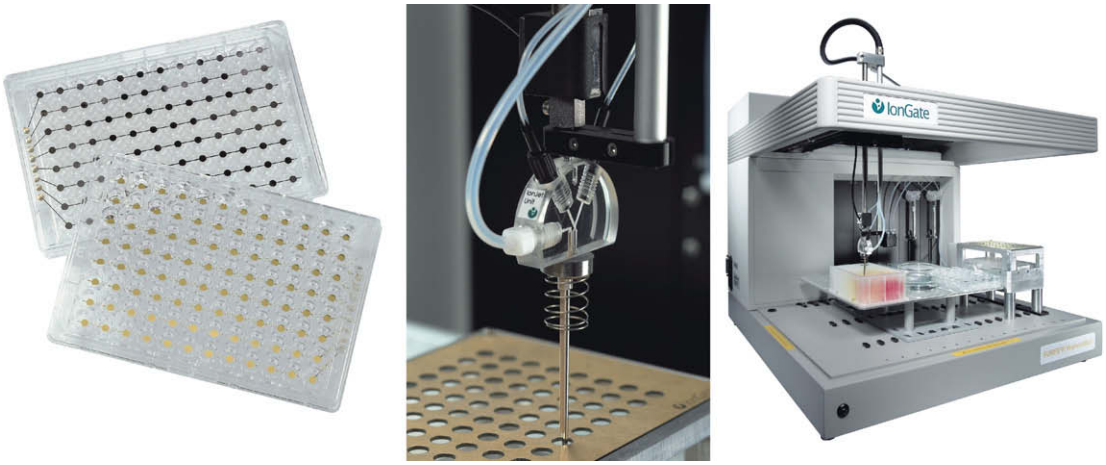

Fig. 5. SSM sensors for the SURFE^{2}R Workstation 500 are arranged in 12 columns and 8 rows to match the standard microtiter plate format (96 wells). The IonJet unit is mounted to an arm moving in *X*, *Y*, and *Z* axes, and it is connected to two syringe pumps. This allows generation of a rapid solution exchange on the electrodes of the individual wells of the 96-well sensor plate. The SURFE^{2}R Workstation 500. A plate holder on the work surface houses an eight channel current-to-voltage converter and holds the sensor plate. Together with the movable arm, the IonJet unit carries out all liquid handling steps necessary for the measurements.

Table 1
Protein preparations measured on the SSM

Protein	Reference	Preparation	Orientation
NaK-ATPase pig	[7]	Enriched membrane fragments from kidney	Inside-out
Ca-ATPase rabbit	[29]	Sarcoplasmatic reticulum vesicles	Rightside-out
Nicotinic acetylcholin receptor *Torpedo californica*	[11]	Enriched membrane vesicles from electric organ	Rightside-out
MelB melibiose permease *Escherichia coli*	[17]	Proteoliposomes	Inside-out
PutP Na/proline carrier *Escherichia coli*	[3]	Proteoliposomes	Inside-out
NhaA Na/H-exchanger *Escherichia coli*	[5]	Proteoliposomes	Rightside-out
		Membrane vesicles	Inside-out
Glt aspartate transporter[a] *Pyrococcus horicoshii*	[6]	Proteoliposomes	Unknown
mEAAC1 glutamate transporter mouse		Heterologous expression CHO cells	Predominantly rightside-out
YdgR peptide transporter *Escherichia coli*	[30]	Proteoliposomes	Rightside-out
hNCX1 Ca/H exchanger *Homo sapiens*	[10]	Heterologous expression CHO cells	Unknown

[a] This putative glutamate transporter [6] has been later identified as an aspartate transporter with low glutamate affinity [31].

behavior of the valves is not well defined and because the proteoliposome is charged when removal of the substrate occurs.

A double exchange experiment is shown in Fig. 4B. Typically, double exchange experiments are applied when ion gradients are required and transport is initiated by addition of a second substrate or a ligand. The example shown in the figure is the nicotinic acetylcholine receptor (nAChR) from *Torpedo marmorata* electric organ. Here first a Na^+ gradient is established and then transport is initiated by addition of the ligand carbamylcholine. The Na^+ gradient is established when the Na^+ free resting solution (R), which is in contact with the SSM before the experiment, is replaced by the Na^+ containing non-activating solution (NA). The solution exchange produces the biphasic artifact at $t \sim 0.5$ s. Then the ligand carbamylcholine is added and channel opening allows the inflow of cations into the membrane vesicles creating a transient current (indicated by the arrow). This transient current shows an EC_{50} for carbamylcholine of 13 μM and is inhibited by the acetylcholine receptor specific antagonist α-bungarotoxin with an IC_{50} of ~1 nM [11].

2.3.4. Buffer preparation and solution exchange artifacts

Because of the strong interaction of the solutes with the SSM, electrical artifacts are generated when solutions of different composition are exchanged. It is, therefore, of utmost importance to keep non-activating and activating solutions as similar as possible. Small differences in ionic concentration, pH and temperature may generate transient currents easily of the magnitude of protein induced signals. However, using a few simple guidelines, these artifacts may be minimized. (1) Prepare the basic buffer for the activating solution and non-activating solution in one batch and adjust pH. Afterwards the buffer is divided into two volumes and the activating compound is added. (2) Use an inert compensation for the activating compound in the non-activating solution to keep both solutions as similar as possible. For instance, if transport by the Na^+/H^+ exchanger NhaA is initiated with 100 mM NaCl in the activating solution, use 100 mM KCl in the non-activating solution as a compensation. (3) High background salt reduces artifacts. Taking the same example, NhaA, 200 mM of inert KCl in both solutions will reduce a possible Na^+ artifact. Also 10–30 mM $MgCl_2$ in the background can be helpful (For examples of buffer composition see e.g. legend of Fig. 4). Test always for artifacts. Before the protein is added, the bare SSM can be used to test the solution exchange protocols you are going to use. This gives you an impression of the magnitude and polarity of the expected artifacts and of the quality of the prepared solutions. (4) Use preferentially activating compounds which are well water soluble. Lipophilic and amphiphilic compounds may generate large artifacts if used in high concentrations.

2.4. Signal analysis and interpretation

2.4.1. The compound membrane and capacitive coupling

The adsorbed membrane fragments, membrane vesicles or proteoliposomes and the underlying planar membrane form a compound membrane. This system and the respective current detection principle (called capacitive coupling) merits some special consideration.

The electrical behavior of the compound membrane can be described and analyzed by an equivalent circuit (Fig. 6) [18,19]. Note that the equivalent circuit and consequently the electrical behavior of the system is essentially the same whether membrane fragments or membrane vesicles or liposomes are used (see Fig. 6). The transporter incorporated in the adsorbed membrane is represented by a current source in the equivalent circuit. It is clear from the equivalent circuit, that the charge displacement in the transport protein is transmitted to the measuring circuit via the capacitance of the planar membrane. The equivalent circuit is characterized by the so called system time constant which is determined by the components of the circuit:

$$\tau_0 = \frac{C_m + C_p}{G_m + G_p}$$

In general, the conductance of the SSM G_m can be neglected and G_p represents the leak conductance of the liposome or the adsorbed membrane fragment. Values for τ_0 determined on black lipid membranes and on SSMs are approximately 100–300 ms [7,18,20].

A qualitative understanding of the electrical signals measured by capacitive coupling may be obtained from Fig. 6C showing the pump current $I_p(t)$ generated by the transporter and the current $I(t)$ measured on the SSM. The two limiting cases are displayed in the figure.

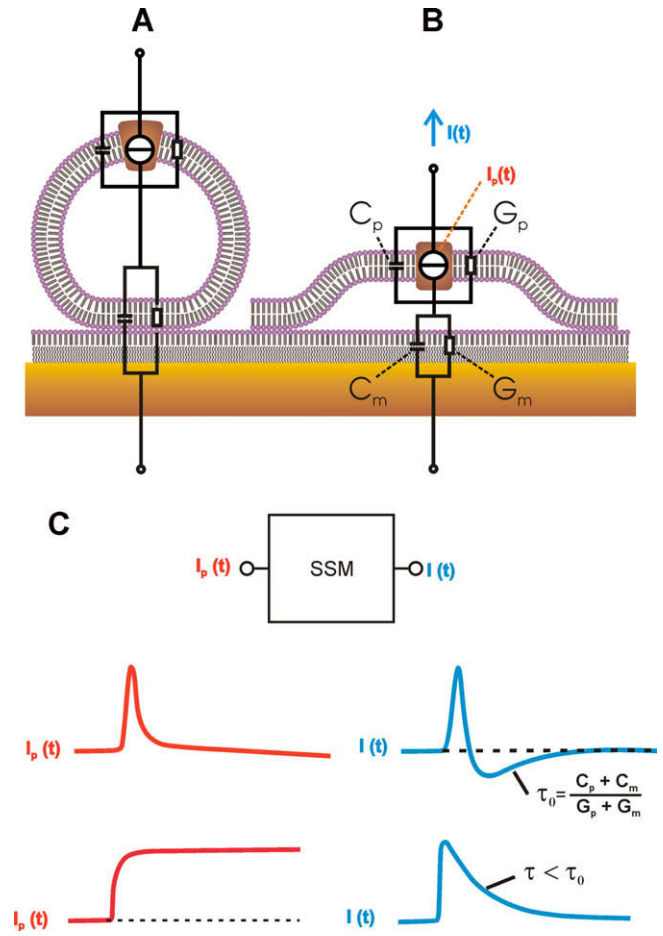

Fig. 6. Putative adsorption geometry of membrane vesicles/proteoliposomes (A) and membrane fragments (B) on the SSM. The SSM consists of the gold layer, the octadecane monolayer and the lipid monolayer on top. The equivalent circuit describing the electrical properties of the compound membrane is included. G_p and G_m are the conductancies of the membrane fragment and of the SSM, C_p and C_m are the respective capacitances. (C) Transmission of the pump current of the transporter through the capacitively coupled system of the compound membrane. $I_p(t)$ is the pump current, $I(t)$ is the current measured on the SSM.

(1) The pump current is a transient current with a time constant much smaller than the system time constant. In this case an additional negative component of time constant τ_0 appears in the measured current but the time constant of $I_p(t)$ is preserved and the measured amplitude is approximately proportional to that of $I_p(t)$ [19]. (2) The pump current is a stationary current. In this case the measured current is a transient decaying with a time constant τ which is smaller than τ_0 and depends on the stationary current [18]. Here the amplitude of $I(t)$ is proportional to the stationary current I_p. Both cases were indeed experimentally observed: for example a rapid charge displacement generated by the NaK-ATPase [7] and stationary turnover of the NhaA Na^+/H^+-exchanger from *E. coli* [5]. But also the mixed case was found for the melibiose permease, MelB, from *E. coli* [21], where a rapid electrogenic conformational transition is followed by stationary transport.

In conclusion, rapid pre-steady-state charge displacements as well as stationary pump currents may be reliably monitored using the capacitively coupled system of the SSM if the limitations and specific properties of the equivalent circuit are kept in mind. A complete reconstruction of the pump current may be obtained by numerical processing the measured current on the basis of circuit analysis [19,20,22].

2.4.2. Charging of the vesicles

In general, the peak value of the measured transient current is used to quantify the transport activity of the investigated protein. Ideally, this current should be measured under short circuit conditions. This is not necessarily the case in the capacitively coupled system because the transport activity of the protein leads to charging of the membrane. However, the peak current is an initial current amplitude recorded just when the substrate reaches the binding site and transport starts. At this point the membrane has not yet build up a significant voltage to affect the kinetic properties of the enzyme. Experimental support for this conclusion comes from a comparison of proteoliposomes with a lipid to protein ratio of 500 and 10. Even at extremely high pump densities the kinetic properties of the transporter were found to be unaltered [5]. Therefore, the peak current recorded on the SSM is a reliable measure for the short circuit kinetic properties of the transport protein.

2.4.3. Time resolution

The time resolution of the SSM system is limited by the solution exchange at the surface of the SSM. Because of unstirred layers a fast solution exchange is difficult. To measure the rise time of the substrate concentration advantage is taken of the strong interaction of ions with the lipid headgroups of the SSM [23]. The displaced charge can be used as a relative measure of the time dependence of the local ion concentration at the surface of the SSM [23]. Here we have determined the concentration risetime for the configuration shown in Fig. 2A by performing a 100 mM NaCl/$NaClO_4$ solution exchange at a flow rate of 1.6 ml/s (Fig. 7). The generated transient current is numerically integrated and the displaced charge is fitted using the empirical function shown in the figure. In this configuration, the concentration rise time is 16 ms. Using a modified flow configuration and a higher flow rate rise times as low as 2 ms may be obtained [15].

2.4.4. Orientation

An important parameter for the interpretation of the measured transport activities is the orientation of the protein in the adsorbed membrane vesicles, membrane fragments or proteoliposomes. In proteoliposomes the protein may be incorporated at random. But also native membranes may be randomly adsorbed to the surface of the SSM. If both populations of transporters are then analyzed on the SSM, the kinetic properties determined in the experiments represent an average of the characteristics of both transport direc-

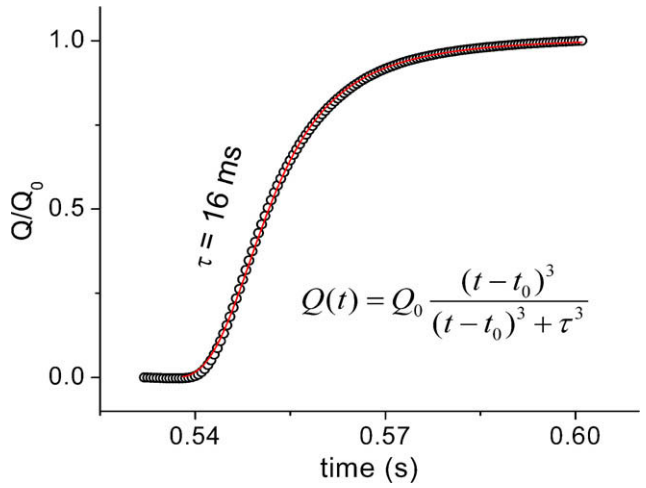

Fig. 7. Normalized integrated current = translocated charge obtained by a NaCl/$NaClO_4$ concentration jump at a flow rate of 1.6 ml/s. The charge is fitted using the equation given in the figure and the concentration rise time τ is determined.

tions. An oriented adsorption or a side selective activation of the proteins is, therefore, desired.

Oriented incorporation of proteins in proteoliposomes can be achieved with special reconstitution procedures because some proteins seem to have a natural tendency for unidirectional incorporation. Interestingly, rightside-out [5] as well as inside-out orientation [17,24] in proteoliposomes has been found depending on the protein and/or the reconstitution technique [25]. But also natural membranes can be prepared to yield preferentially inside-out or rightside-out vesicles [26]. For some transport proteins side selective activation is possible. For example cytochrome oxidase is reduced by electron donors only from its extracellular side [27] and NaK-ATPase binds ATP only at its intracellular side [28]. Therefore, even if randomly incorporated in proteoliposomes or randomly adsorbed to the SSM, only one population of enzymes is active in these preparations and can be selectively analyzed.

3. Concluding remarks

SSM-based electrophysiology has been proven to be a valuable complement to the electrophysiological toolbox. In contrast to conventional electrophysiology, the SSM technique avoids complications involved with the interaction of the transport protein with intracellular components or, in the case of purified preparations, other membrane proteins. Its particular value becomes apparent when membrane proteins from bacteria and intracellular compartments, like the sarcoplasmic reticulum or vesicles from parietal cells, have to be studied. Because of their small size, these structures are in general not accessible for standard electrophysiology, like the two electrode voltage clamp or patch clamp techniques.

The compound membrane is a well suited substrate for the investigated transport protein providing an aqueous space for the protein on both sides of the membrane. A further advantage of adsorbing membrane fragments or proteoliposomes to a planar membrane is the much simpler and more effective procedure compared to direct incorporation of the protein, leading to a superior signal to noise ratio and time resolution of the electrical measurement.

SSM-based electrophysiology has been employed for a direct measurement of charge movements of a variety of electrogenic transporters. Using the high time resolution of the technique rate constants of transport steps can be determined and electrogenic partial reactions can be identified. Besides its use in basic research, the rugged SSM sensor combined with robotized instrumentation contains potential for industrial applications. This is expected to become a promising platform technology for drug screening and development [9,10].

Acknowledgments

We thank Lina Hatahet for excellent technical assistance and the mechanical workshop of the MPI für Biophysik for the construction of the cuvette and the faraday cage. Jürgen Reichert and Robin Krause are acknowledged for contributing to Figs. 1 and 6 and Carola Hunte for providing the *Helicobacter pylori* NhaA protein sample.

Appendix A. Supplementary data

Supplementary data associated with this article can be found, in the online version, at doi:10.1016/j.ymeth.2008.07.002.

References

[1] A. Eisenrauch, E. Bamberg, FEBS Lett. 268 (1990) 152–156.
[2] C. Burzik, G. Kaim, P. Dimroth, E. Bamberg, K. Fendler, Biophys. J. 85 (2003) 2044–2054.
[3] A. Zhou, A. Wozniak, K. Meyer-Lipp, M. Nietschke, H. Jung, K. Fendler, J. Membr. Biol. 343 (2004) 931–942.
[4] K. Meyer-Lipp, C. Ganea, T. Pourcher, G. Leblanc, K. Fendler, Biochemistry 43 (2004) 12606–12613.
[5] D. Zuber, R. Krause, M. Venturi, E. Padan, E. Bamberg, K. Fendler, Biochim. Biophys. Acta 1709 (2005) 240–250.
[6] S. Raunser, M. Appel, C. Ganea, U. Geldmacher-Kaufer, K. Fendler, W. Kuhlbrandt, Biochemistry 45 (2006) 12796–12805.
[7] J. Pintschovius, K. Fendler, Biophys. J. 76 (1999) 814–826.
[8] F. Tadini-Buoninsegni, G. Bartolommei, M.R. Moncelli, R. Guidelli, G. Inesi, J. Biol. Chem. 281 (2006) 37720–37727.
[9] B. Kelety, K. Diekert, J. Tobien, N. Watzke, W. Dörner, P. Obrdlik, K. Fendler, Assay Drug Develop. Technol. 4 (2006) 575–582.
[10] S. Geibel, N. Flores-Herr, T. Licher, H. Vollert, J. Biomol. Screening 11 (2006) 262–268.
[11] B. Dueck, L. Hatahet, A. Mourot, K. Fendler, Biosensors and Bioelectronics, unpublished.
[12] A. Bicho, C. Grewer, Biophys. J. 89 (2005) 211–231.
[13] T. Friedrich, E. Bamberg, G. Nagel, Biophys. J. 71 (1996) 2486–2500.
[14] N. Watzke, E. Bamberg, C. Grewer, J. Gen. Physiol. 117 (2001) 547–562.
[15] J.J. Garcia-Celma, B. Dueck, M. Stein, M. Schlueter, K. Meyer-Lipp, G. Leblanc, K. Fendler, Langmuir 24 (2008) 8119–8126.
[16] M. Venturi, E. Padan, in: C. Hunte, G. Von Jagov, H. Schägger (Eds.), Membrane Protein Purification and Crystallization a Practical Guide, Academic Press, San Diegopp, 2003, pp. 179–190.
[17] H. Jung, S. Tebbe, R. Schmid, K. Jung, Biochemistry 37 (1998) 11083–11088.
[18] E. Bamberg, H.J. Apell, N.A. Dencher, W. Sperling, H. Stieve, P. Lauger, Biophys. Struct. Mechanism 5 (1979) 277–292.
[19] K. Fendler, S. Jaruschewski, A. Hobbs, W. Albers, J.P. Froehlich, J. General Physiol. 102 (1993) 631–666.
[20] T. Gropp, F. Cornelius, K. Fendler, Biochimica et Biophysica Acta-Biomembranes 1368 (1998) 184–200.
[21] C. Ganea, T. Pourcher, G. Leblanc, K. Fendler, Biochemistry 40 (2001) 13744–13752.
[22] R. Borlinghaus, H.J. Apell, P. Lauger, J. Membr. Biol. 97 (1987) 161–178.
[23] J.J. Garcia-Celma, L. Hatahet, W. Kunz, K. Fendler, Langmuir 23 (2007) 10074–10080.
[24] K. Meyer-Lipp, N. Sery, C. Ganea, C. Basquin, K. Fendler, G. Leblanc, J. Biol. Chem. 281 (2006) 25882–25892.
[25] J.-L. Rigaud, B. Pitard, D. Levy, Biochim. Biophys. Acta 1231 (1995) 223–246.
[26] B.P. Rosen, Methods Enzymol. 125 (1986) 328–336.
[27] M. Ruitenberg, A. Kannt, E. Bamberg, B. Ludwig, H. Michel, K. Fendler, Proc. Nat. Acad. Sci. USA 97 (2000) 4632–4636.
[28] K. Fendler, E. Grell, M. Haubs, E. Bamberg, EMBO J. 4 (1985) 3079–3085.
[29] G. Bartolommei, F.T. Buoninsegni, M.R. Moncelli, Bioelectrochemistry 63 (2004) 157–160.
[30] D. Weitz, D. Harder, F. Casagrande, D. Fotiadis, P. Obrdlik, B. Kelety, H. Daniel, J. Biol. Chem. 282 (2007) 2832–2839.
[31] O. Boudker, R.M. Ryan, D. Yernool, K. Shimamoto, E. Gouaux, Nature 445 (2007) 387–393.

Electrophysiological characterization of LacY

Juan J. Garcia-Celma[a], Irina N. Smirnova[b], H. Ronald Kaback[b,1], and Klaus Fendler[a,1]

[a]Department of Biophysical Chemistry, Max Planck Institute of Biophysics, D-60438 Frankfurt am Main, Germany; and [b]Departments of Physiology and Microbiology, Immunology, and Molecular Genetics, Molecular Biology Institute, University of California, Los Angeles, CA 90095-7327

Contributed by H. Ronald Kaback, March 12, 2009 (sent for review January 8, 2009)

Electrogenic events due to the activity of wild-type lactose permease from *Escherichia coli* (LacY) were investigated with proteoliposomes containing purified LacY adsorbed on a solid-supported membrane electrode. Downhill sugar/H^+ symport into the proteoliposomes generates transient currents. Studies at different lipid-to-protein ratios and at different pH values, as well as inactivation by *N*-ethylmaleimide, show that the currents are due specifically to the activity of LacY. From analysis of the currents under different conditions and comparison with biochemical data, it is suggested that the predominant electrogenic event in downhill sugar/H^+ symport is H^+ release. In contrast, LacY mutants Glu-325→Ala and Cys-154→Gly, which bind ligand normally, but are severely defective with respect to lactose/H^+ symport, exhibit only a small electrogenic event on addition of LacY-specific substrates, representing 6% of the total charge displacement of the wild-type. This activity is due either to substrate binding per se or to a conformational transition after substrate binding, and is not due to sugar/H^+ symport. We propose that turnover of LacY involves at least 2 electrogenic reactions: (*i*) a minor electrogenic step that occurs on sugar binding and is due to a conformational transition in LacY; and (*ii*) a major electrogenic step probably due to cytoplasmic release of H^+ during downhill sugar/H^+ symport, which is the limiting step for this mode of transport.

bioenergetics | membrane proteins | permease | solid-supported membrane | transport

Secondary active transporters in the bacterial plasma membrane are of fundamental importance for the cell. To name only a few functions, they catalyze uptake of nutrients, export of toxic compounds, translocation of macromolecules, regulation of cell turgor, and creation of electrochemical ion gradients important for the function of other membrane proteins. Bacterial homologues of mammalian transporters have also become important, because they can be conveniently obtained, purified readily in large amounts, and used for crystallization and structure determination. One of the best-characterized systems is the lactose permease from *Escherichia coli* (LacY), structures of which have been solved recently at atomic resolution (1–3). Because of the wealth of biochemical and biophysical data available for LacY (4–8), it represents an ideal model system for the investigation of the basic principles and molecular details of secondary active transport.

Among the many methods for functional characterization, electrophysiology is arguably the most universal, because it does not require labeled substrate. Also, it is an extremely sensitive, highly time-resolved technique that allows direct measurement of charge movement. Although it has been known for many years that lactose/H^+ symport catalyzed by LacY is an electrogenic reaction (9–11), despite numerous efforts, LacY has so far resisted all attempts at electrophysiological analysis. Although the *lacY* gene is expressed well in frog oocytes and other eukaryotic cells, LacY remains in the *cis*-Golgi and the perinuclear membrane, and does not target to the plasma membrane to any extent whatsoever. In this report, we present the successful electrophysiological study of LacY by using purified, reconstituted proteoliposomes with solid-supported membrane (SSM) based electrophysiology (12).

Results

Downhill Sugar/H^+ Symport Generates Transient Currents. Proteoliposomes containing reconstituted LacY were immobilized on an SSM-coated gold electrode (the sensor), and charge displacement induced by downhill sugar/H^+ symport into the proteoliposomes was detected by capacitive coupling (13). Transport was initiated at 1.5 s by a sugar concentration jump using rapid solution exchange (Fig. 1). Approximately 40 ms later, sugar reaches the surface of the SSM, and a transient current starts abruptly. The time course of the signals is characterized by 2 distinct phases: a rapid rise to a maximum followed by a much slower decay toward the baseline. Because the decay is not exponential, it was quantified by the decay time from peak to half-maximal current, $\tau_{1/2}$, which is ≈50 ms for all LacY substrates tested.

Because the amount of proteoliposomes adsorbed to an individual sensor exhibits some variability, only current amplitudes obtained from the same sensor are compared directly. As shown, the maximal value of the peak current observed after a 50 mM concentration jump of lactose is 950 pA, and the peak currents generated after 50 mM concentration jumps of lactulose and melibiose are ≈65% and ≈50%, respectively, of that recorded with lactose. However, addition of 50 mM sucrose (Fig. 1), a sugar that is not a substrate of LacY, has no effect.

Sugar binding and transport catalyzed by LacY are inactivated by alkylation of Cys-148 primarily (14–16). Consistently, no electrical transient is observed after treatment with *N*-ethylmaleimide (NEM; Fig. S1).

Varying Lipid-to-Protein Ratio (LPR). Electrogenic transport by a reconstituted protein leads to transient currents in the capacitively coupled system (13, 17). With wild-type LacY, downhill sugar/H^+ symport into the proteoliposomes generates an inside-positive potential, which acts to decelerate the downhill symport reaction catalyzed by LacY, leading to transient currents. However, any conformational transition that displaces charged amino acyl side chains or reorients electrical dipoles also represents an electrogenic transition that may contribute to the transient nature of the currents. Indeed, it has been shown with the melibiose permease from *E. coli* (MelB) that melibiose binding triggers an electrogenic conformational transition that is a major component of the transient currents observed (18, 19). To discriminate between downhill sugar/H^+ symport and electrogenic conformational transition, experiments were performed with proteoliposomes reconstituted at different LPR (wt/wt). As shown by freeze–fracture electron microscopy (Fig. S2 *A* and *B*), at LPRs of 10 or 5, liposomes with LacY particle densities of ≈1,000 and ≈4,500 particles per μm^2, respectively, are observed.

Author contributions: J.J.G.-C. and K.F. designed research; J.J.G.-C. performed research; J.J.G.-C., I.N.S., H.R.K., and K.F. analyzed data; and J.J.G.-C., I.N.S., H.R.K., and K.F. wrote the paper.

The authors declare no conflict of interest.

Freely available online through the PNAS open access option.

[1]To whom correspondence may be addressed. E-mail: rkaback@mednet.ucla.edu or klaus.fendler@mpibp-frankfurt.mpg.de.

This article contains supporting information online at www.pnas.org/cgi/content/full/0902471106/DCSupplemental.

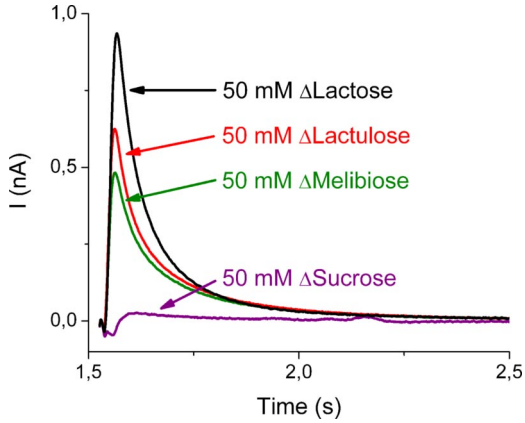

Fig. 1. Transient currents obtained with wild-type LacY proteoliposomes after a 50 mM sugar concentration jump at $t = 1.5$ s. The traces in black, red, and green correspond to concentration jumps of lactose (50 mM; ΔLactose), lactulose (50 mM; ΔLactulose), melibiose (50 mM; ΔMelibiose), and sucrose (50 mM; ΔSucrose), respectively. The nonactivating solution (50 mM glucose) and all activating solutions were prepared in 100 mM potassium phosphate at pH 7.6 plus 1 mM DTT. All traces shown were recorded from 1 sensor.

An electrogenic conformational transition is expected to yield identical time constants for decay of the transients at different particle densities. In contrast, charging of the liposomal membrane by downhill sugar/H^+ symport should lead to decreasing decay time (lower $\tau_{1/2}$) at increasing protein density (i.e., lower LPR). As shown in Fig. 2, increased LacY particle density clearly leads to significantly faster decay. Thus, the transient currents observed for wild-type LacY represent mainly charging of the liposome membrane due to downhill sugar/H^+ symport activity.

Effect of pH. The shape and magnitude of the transients generated by downhill lactose/H^+ symport strongly depends on pH (Fig. 3). An overall increase in pH from 6.6 to 8.5 causes a 5-fold increase in the magnitude of the peak current (Fig. 3; Table 1). The decay time also depends on pH, because $\tau_{1/2}$ decreases from ≈103 to 46 to 27 ms, respectively, at pH 6.6, 7.6, and 8.5 (Fig. 3; Table 1).

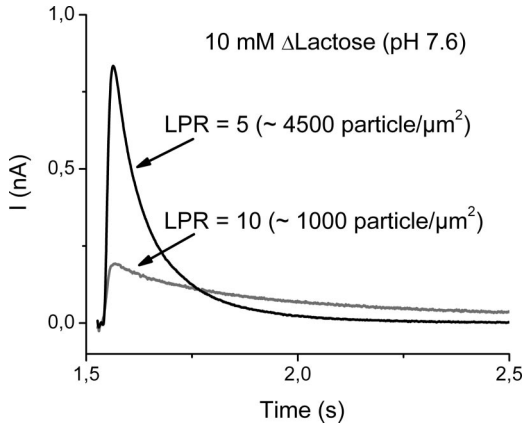

Fig. 2. Transient currents obtained at 2 different LPR (10 and 5). The solution exchange protocol and the nonactivating solution were as described in Fig. 1, but the activating solution contained 40 mM glucose plus 10 mM lactose. Therefore, the difference between the test and nonactivating solutions represents a 10 mM lactose concentration jump (10 mM ΔLactose). Wild-type LacY proteoliposomes reconstituted at a LPR of 10 (≈1,000 particles per μm^2; Fig. S2*A*) or at a LPR of 5 (≈4,500 particles per μm^2; Fig. S2*B*) were activated with a 10 mM lactose concentration jump. The decay phase of the transient currents is decreased almost 5-fold from a $\tau_{1/2} = 53 \pm 2$ ms at an LPR of 5 (black trace) to a $\tau_{1/2} = 260 \pm 2$ ms at an LPR of 10 (gray trace).

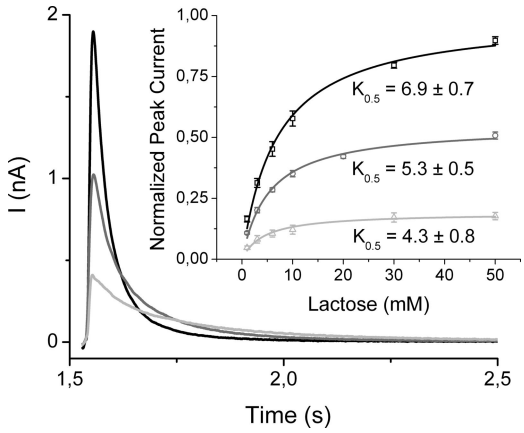

Fig. 3. Effect of pH on the transient currents generated after 50 mM lactose concentration jumps at different pH values. The traces were successively recorded on the same sensor after equilibration was reached and are, therefore, directly comparable. To equilibrate the pH across the proteoliposome membrane after changing the pH of the solutions, the immobilized proteoliposomes are incubated for ≈20 min at the new pH. Subsequent lactose concentration jumps produced constant currents indicating that the pH value had indeed equilibrated. The nonactivating solution contained 50 mM glucose and the activating solutions 50 mM lactose. Both solutions were prepared in 100 mM potassium phosphate buffer at pH 8.5 (black trace), 7.6 (gray trace), or 6.6 (light gray trace) plus 1 mM DTT. (*Inset*) Dependence of peak currents on lactose concentration at 3 pH values. The nonactivating solution contained 50 mM glucose, the activating solutions a given concentration of x mM lactose plus 50 − x mM glucose to maintain a constant sugar concentration. The solutions were prepared in 100 mM potassium phosphate buffer at a given pH value plus 1 mM DTT, and the pH was equilibrated across the proteoliposome membrane. The peak currents recorded at pH 8.5 for each lactose concentration jump were fitted with a hyperbolic function, and all data obtained with that sensor (every lactose concentration at the 3 pH values) were expressed as fraction of maximum value at pH 8.5 (I_{peak}^{max}). This normalization procedure yields datasets that can be directly compared between sensors. For a statistical analysis, the complete dataset was recorded on 3 different sensors, and the averaged values and errors (SE) are shown. From the hyperbolic fits, apparent $K_{0.5}$ values with SE were obtained at every pH (Table 1).

This trend is anticipated, because higher electrogenic activity of the transporter leads to faster charging of the liposome membrane and a concomitant faster current decay (i.e., lower $\tau_{1/2}$) (17). Therefore, the effect of pH on the amplitude and time dependence of the transient currents is consistent with the proposed assignment of the peak currents to the symport activity of LacY.

Proteoliposomes adsorbed to an SSM surface are stable for hours without loss of activity, allowing investigation of the effect of pH on the kinetics of the transient currents induced at different lactose concentrations (Fig. 3 *Inset*; Table 1). An increase in pH from 6.6 to 8.5 generates a 5-fold increase in the saturating peak current (Fig. 3; Table 1). Indeed, rates of efflux (i.e., downhill lactose/H^+ symport in the opposite direction)

Table 1. Kinetic parameters of the transient currents measured for wild-type LacY

pH	Efflux, %	Peak current, %	$\tau_{1/2}$, ms	$K_{0.5}$, mM
8.5	100	100	27 ± 0.6	6.9 ± 0.7
7.6	35	55	46 ± 2	5.3 ± 0.5
6.6	6	19	103 ± 7	4.3 ± 0.8

For comparison the effect of pH on the initial rates of [^{14}C]lactose efflux is given (22). The peak currents and the time constants ($\tau_{1/2}$) refer to the transient currents after 50 mM lactose concentration jumps. Conditions are as described in Fig. 3.

from right-side-out membrane vesicles (20), or proteoliposomes reconstituted with purified LacY (21, 22), exhibit a similar dependence on pH (Table 1). The half saturating concentration increases only slightly with the pH (Fig. 3 *Inset*; Table 1). At pH 7.6, a $K_{0.5}$ of 5.3 ± 0.5 mM is obtained, which is close to that of 3.1 ± 0.7 mM determined for downhill lactose/H^+ influx in proteoliposomes reconstituted with purified LacY (23).

Transient Currents in Mutants. To dissect the overall electrogenic response, mutants of LacY that bind ligand but do little or no lactose/H^+ symport were used. Mutant E325A is specifically defective in all steps involving H^+ release from LacY but catalyzes exchange and counterflow at least as well as wild-type (24, 25). E325A LacY was reconstituted into proteoliposomes at an LPR of 5 and a particle density comparable with that of the wild-type preparation (≈3,500 particles per μm^2; Fig. S3*A*). Concentration jumps of 50 mM lactose, lactulose, or melibiose produce transient currents with virtually identical kinetics and negligible differences in magnitude (Fig. 4*A*), which are abolished after treatment with NEM (Fig. S4*A*). However, the transient currents are ≈5-times smaller than those observed for lactose with wild-type LacY (Table 2), and exhibit mono-exponential decays ($\tau \approx 10$ ms) followed by a shallow negative phase ($\tau \approx 300$ ms). Notably, the nonexponential decay of the wild-type is characterized by $\tau_{1/2}$, whereas here the time constant τ is used. The negative component represents discharge of the liposome membrane after rapid charge translocation. This phenomenon is common for the capacitively coupled system (13), and indicates absence of significant steady-state charge transport across the liposome membrane (i.e., downhill sugar/H^+ symport activity).

Mutant C154G binds sugar as well as wild-type and exhibits extremely low, but significant, transport activities (26–29). Proteoliposomes were prepared at an LPR of 5 and a particle density of ≈3,500 particles per μm^2 (Fig. S3*B*). Concentration jumps with 50 mM lactose, lactulose, or melibiose generate transient currents of comparable magnitude as E325A LacY (compare Fig. 4 *A* and *B*), which are also abolished by NEM treatment (Fig. S4*B*). In contrast to E325A, the magnitude and kinetics of the peak currents recorded with C154G LacY depend on the sugar used (Fig. 4*B*). Concentration jumps of 50 mM lactose or lactulose trigger transient currents that decay mono-exponentially, with time constants of ≈20 ms. Interestingly, a 50 mM melibiose concentration jump generates the largest peak current with a significantly faster exponential decay ($\tau \approx 10$ ms) followed by a small negative phase.

From the transient currents measured, the kinetics of the true transport currents generated by the mutants can be reconstructed by using an iterative least-squares deconvolution algorithm (Fig. S5 *A* and *B*). This operation requires a transfer function for the specific measurements determined as described (30). The transfer function is the derivative of the substrate concentration rise at the surface of the SSM, and corresponds to the time resolution of the measurement (15 ms) (13, 30). However, significantly faster processes ($k < 200\ s^{-1}$; see Fig. S5) can be resolved with a least-square deconvolution algorithm (30). With this deconvolution procedure, the time constants for the underlying charge displacement are determined. For E325A LacY, regardless of the sugar used, the transient currents are indistinguishable from the transfer function, indicating that charge translocation is too fast to be resolved by the measurements. In this case, we can only estimate a lower limit for the rate constant (k) of the process as $>200\ s^{-1}$ from the iterative least-squares algorithm (Fig. S5*A*). For C154G LacY, the rate constants for 50 mM concentration jumps of lactose or lactulose are 53 ± 5 s^{-1} or 72 ± 5 s^{-1}, respectively, but the k for a 50 mM concentration jump of melibiose is too rapid for accurate measurement ($k > 200\ s^{-1}$).

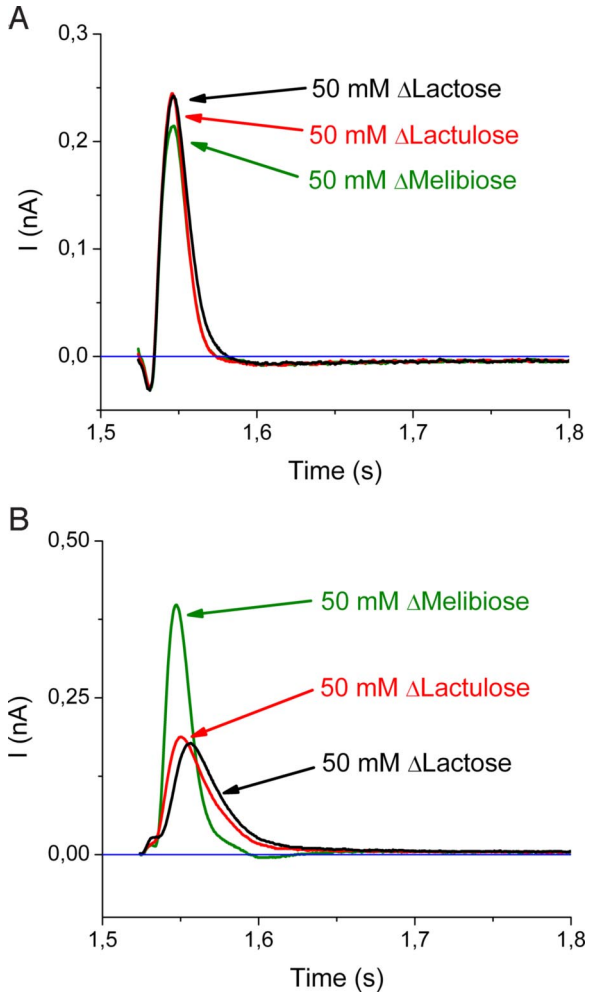

Fig. 4. Transient currents obtained with LacY mutants. The solution exchange protocol and composition of the solutions was the same as described for Fig. 1. The baseline is represented in blue. (*A*) E325A LacY was reconstituted into liposomes, and activated with 50 mM concentration jumps of lactose (50 mM; ΔLactose), lactulose (50 mM; ΔLactulose), or melibiose (50 mM; ΔMelibiose) at pH 7.6. All traces exhibit virtually identical kinetics and only small differences in magnitude with an exponential decay toward the baseline ($\tau \approx 10$ ms) followed by a negative phase ($\tau \approx 300$ ms). (*B*) Transient currents obtained with C154G LacY proteoliposomes after 50 mM sugar concentration jumps at pH 7.6. The transient currents corresponding to 50 mM ΔLactose or 50 mM ΔLactulose decay mono-exponentially toward the baseline, with time constants of ≈20 ms, whereas the transients observed with 50 mM ΔMelibiose exhibit the largest peak current and a significantly faster exponential decay ($\tau \approx 10$ ms) followed by a small negative phase.

Discussion

Wild-Type LacY. Reconstitution of LacY using the procedure described previously (21, 31, 32) results in proteoliposomes with ≈85% of the LacY molecules in the right-side-out orientation (i.e., with the periplasmic side facing the exterior of the proteoliposomes) (33). Therefore, application of a substrate concentration jump corresponds to substrate transport in the physiological direction. All transported sugars trigger positive transient currents, in agreement with the displacement of positive charge (H^+) into the proteoliposomes, as a result of downhill sugar/H^+ symport. Of all sugars tested, lactose generates the largest transient current, consistent with it being the most efficiently transported substrate. The currents depend on pH and substrate concentration, and are blocked by alkylation with NEM. Also, good correlation is observed between kinetic parameters deter-

Table 2. Characteristics of LacY wild-type and mutant preparations

Characteristic	Wild-type LacY	C154G LacY	E325A LacY
Particles per μm^2	≈4,500	≈3,500	≈3,500
Peak current, pA	960 ± 190	102 ± 67	211 ± 50
Q, pC	96 ± 19	5 ± 2	4.4 ± 0.4

The number of particles per μm^2 was estimated from freeze–fracture images (Fig. S2 and Fig. S3). The peak currents refer to the transients after 50 mM lactose concentration jumps at pH 7.6. Conditions are as described in Figs. 1 and 4. The total translocated charge (*Q*) is obtained from numerical integration of the currents. Charge translocation per turnover of the wild-type was estimated by using the current of 960 pA and an estimated turnover rate of 10 s^{-1}.

mined in our electrophysiological measurements and the values previously obtained from downhill sugar/H^+ symport in proteoliposomes (23). All these observations strongly support the contention that the transient currents reflect specifically the electrogenic activity of LacY.

Because the decay time constant of the currents strongly depends on the number of transporters incorporated into the proteoliposomes, and decreases at high transport activity, it is concluded that this phase reflects charging of the liposomes as a result of downhill lactose/H^+ symport. A comparable dependence of the decay time constant on the electrogenic transport activity of bacteriorhodopsin was described for purple membrane adsorbed to a planar lipid bilayer (17). Likewise, increasing the amount of reconstituted Na^+/H^+ exchanger in proteoliposomes adsorbed to the SSM resulted in a faster decay of the transient currents (34). In both cases the measured peak currents have been attributed to the continuous transport activity of the corresponding transporter, and the same applies to LacY.

It is interesting to compare the LacY currents with those observed with MelB, at similar time resolutions. With MelB, biphasic current patterns are observed decaying with time constants of $\tau_1 \approx 17$ ms and $\tau_2 \approx 380$ ms (18). The fast phase τ_1 is due to an electrogenic conformational transition triggered by melibiose binding, whereas the slow phase τ_2 is related to downhill sugar/Na^+ symport activity of MelB. With LacY, a fast initial current phase is not observed. This deficiency is especially apparent in the current recorded at low transporter density, which decays slowly with a $\tau_{1/2} = 260 \pm 2$ ms (Fig. 2). Such behavior can only be explained if the initial electrogenic reactions are slow or if charge translocation occurs late in the LacY reaction cycle. As discussed below, sugar binding occurs with a rate constant of >50 s^{-1}, ruling out a slow initial step. Although this argument is strictly valid for the mutants only, the fact that the mutants are fully capable of sugar binding indicates that the same rate constants apply also to the wild-type. Together, the data indicate that the major electrogenic step in wild-type LacY occurs late in the reaction cycle.

LacY Mutants. The transient currents of the mutants E325A and C154G differ drastically from the response of the wild-type. They are 5–10 times smaller (Table 2) and considerably faster than the transients observed with wild-type LacY. Smaller transient currents could be interpreted as residual downhill sugar/H^+ symport with reduced turnover in E325A and C154G. However, this residual symport would lead not only to smaller current amplitude, but also to slower decay (17). A good example for this behavior is the transient currents observed with wild-type LacY at pH 6.6, which are ≈5 times smaller, and decay 5 times slower than at pH 8.5 (Table 1; Fig. 3). In contrast, the transient currents observed with both mutants at pH 7.5 decay even faster than the transients observed with the wild-type at maximal activity (pH 8.5). This observation indicates that the currents observed with E325A and C154G LacY are not generated by sugar/H^+ symport, but rather represent sugar binding induced electrogenic conformational transitions.

A comparison between mutants and wild-type (Table 2) must take into account the amount of reconstituted protein in the membrane of the adsorbed proteoliposomes on the sensor. Freeze fracture electron microscopy shows a comparable transporter density for both mutants and the wild-type. The integrated charge of C154G and E325A LacY of ≈5 pC (Table 2) represents the charge translocated in a single turnover by all transporters on the SSM electrode. By comparison, the translocated charge per turnover of wild-type LacY is much larger; ≈96 pC (Table 2). By taking into account the somewhat different particle density of wild-type and mutant proteoliposomes, it is concluded that substrate binding to the mutants induces a charge displacement corresponding to the transport of the equivalent of only ≈6% of an elementary charge across the membrane.

Although smaller, these transient currents can be used to estimate binding rate constants for the different sugars and mutants. They range between 50 and >200 s^{-1}, and depend on the nature of substrate and mutant. Recent stopped-flow experiments reveal that the binding of *p*-nitrophenyl α,D-galactopyranoside (α-NPG) to C154G/V331C LacY in detergent micelles is a 2-step process: a binding step followed by a slower conformational change with a rate constant of 238 s^{-1} detected with fluorescent-labeled protein (35). Clearly, sugar binding triggers a conformational change with a rate constant similar to that observed in the electrophysiological experiments, which may be responsible for the charge translocation observed. Unfortunately, a direct comparison of rate constants is not possible because of the strong interaction of α-NPG with the membrane that generates large electrical artifacts.

Electrogenic Steps in the LacY Reaction Cycle. Combining the results obtained with wild-type LacY and the mutants, there is clear evidence for a major electrogenic step late in the reaction cycle, and a rapid electrogenic reaction during or immediately after sugar binding with relatively low electrogenicity (6% of an elementary charge). It seems unlikely that the latter is a unique property of the E325A and C154G mutants. Most probably, this electrogenic event also takes place in the wild-type, but is completely masked by the 20-fold greater charge transport activity of the wild-type, and is only observed under conditions where sugar/H^+ symport is blocked, as in the mutant proteins.

Based on previous observations on the kinetics of LacY (20, 22, 36, 37), and on these electrophysiological findings, we propose that the main electrogenic step corresponds to deprotonation of wild-type LacY in the inward-facing conformation. In this context, it is notable that: (*i*) structural, biochemical, and biophysical data strongly support the contention that wild-type and C154G LacY are predominantly in an inward-facing conformation (1, 2, 5–8); (*ii*) the rate of efflux from proteoliposomes reconstituted with purified LacY is strongly influenced by the voltage across the membrane, whereas exchange is completely voltage independent (21); thus, the main electrogenic step is related to protonation/deprotonation of LacY in either the inward- or outward-facing conformations or the return of the empty carrier; and (*iii*) the shape of the transient currents indicates that the main electrogenic step in wild-type LacY occurs late in the reaction cycle (see above). Considering these points, it is likely that the inward-facing deprotonated transporter is the initial state, and that deprotonation corresponds to the main electrogenic step of the transport cycle. Following this argument, the main electrogenic step would take place at the end of the transport cycle, in agreement with the conclusions obtained from the analysis of the transient currents. Because downhill lactose/H^+ symport is specifically inhibited 3- to 4-fold

in deuterium oxide, deprotonation is probably not only the main electrogenic step, but is also rate limiting (22).

With C154G LacY, all transport reactions, including equilibrium lactose exchange, are almost abolished (16, 38), indicating that the substrate translocation step is blocked. In the absence of substrate, this mutant is in an inward-facing conformation, and paralyzed in an open conformation on the periplasmic side, but able to close on the cytoplasmic side on lactose binding (6–8, 39). E325A LacY exhibits no active transport whatsoever; however, in contrast to C154G LacY, mutant E325A catalyzes exchange and counterflow at least as well as wild-type LacY, indicating that this mutant is permanently protonated (i.e., H^+ dissociation is blocked in E325A LacY but binding is normal) (24, 25, 28). In both mutants, a rapid but weakly electrogenic reaction with similar magnitude and kinetic properties is seen, which agrees with our notion that periplasmic H^+ binding is not responsible for the charge translocation observed, and that the rapid initial charge displacement of minor electrogenicity is associated with sugar binding. Possibly, the rapid conformational transition after sugar binding (35) leads to rearrangement of charged residues within LacY (3, 40), which may account for this phenomenon.

Materials and Methods

Construction of Mutants and LacY Purification. Construction of mutants and purification of the His-tagged proteins were carried out as described (7). Purified proteins (10–15 mg/mL) in 50 mM NaP_i/0.02% *n*-dodecyl-beta-D-maltoside (pH 7.5) were frozen in liquid nitrogen and stored at −80 °C until use.

Reconstitution of Proteoliposomes. Reconstitution of purified wild-type or the E325A and C154G mutants was carried out with *E. coli* phospholipids (Avanti Polar Lipids) by using dodecyl maltoside/octyl glucoside dilution, followed by 1 cycle of freeze–thaw/sonication (41, 42). Purified wild-type LacY and liposomes were mixed at an LPR of 10 or 5 (wt/wt), as indicated. Mutant E325A or C154G was reconstituted at an LPR of 5. Before use, the samples were thawed on ice and gently sonicated for 2–5 s. Reconstitution was verified in all cases by freeze–fracture electron microscopy.

SSM Measurements. SSM measurements were performed as described previously (18, 30, 43). Briefly, 40 μL of proteoliposomes at a protein concentration of 1 mg/mL was allowed to adsorb for 1 h to an octadecanethiol/phosphatidylcholine hybrid bilayer on a gold surface (the sensor). The solution exchange protocol consisted in 3 phases of duration 1.5, 2, and 1.5 s, respectively. The nonactivating solution flows through the cuvette during the first and third phases (from $t = 0$ to 1.5 s, and from $t = 3.5$ to 5 s), whereas the activating solution flows during the second phase (from $t = 1.5$ to $t = 3.5$ s). A valveless diverted fluidic geometry was chosen to apply the different solutions (30) at a flow rate of 0.46 mL/s. The nonactivating solution always contained 50 mM glucose, and the activating solution contained a given sugar at a concentration of 50 mM, unless stated otherwise (Fig. 3). All solutions were buffered in 100 mM potassium phosphate buffer at a given pH value plus 1 mM DTT. Currents were recorded throughout the entire time, and amplified with a current amplifier set to a gain of 10^9-10^{10} V/A and low pass filtering set to 300–1,000 Hz.

ACKNOWLEDGMENTS. We thank Lina Hatahet and Andre Bazzone for excellent assistance in the laboratory, Ernst Bamberg for helpful discussions and support, and Winfred Haase for the excellent freeze–fracture micrographs of the reconstituted liposomes. This work was funded by Deutsch Forschungsgemeinshaft SFB 807 (to K.F.); National Institutes of Health Grants DK051131, DK069463, GM073210, and GM074929; and National Science Foundation Grant 0450970 (to H.R.K.).

1. Abramson J, et al. (2003) Structure and mechanism of the lactose permease of Escherichia coli. *Science* 301:610–615.
2. Guan L, Mirza O, Verner G, Iwata S, Kaback HR (2007) Structural determination of wild-type lactose permease. *Proc Natl Acad Sci USA* 104:15294–15298.
3. Mirza O, Guan L, Verner G, Iwata S, Kaback HR (2006) Structural evidence for induced fit and a mechanism for sugar/H^+ symport in LacY. *EMBO J* 25:1177–1183.
4. Guan L, Kaback HR (2006) Lessons from lactose permease. *Annu Rev Biophys Biomol Struct* 35:67–91.
5. Kaback HR, et al. (2007) Site-directed alkylation and the alternating access model for LacY. *Proc Natl Acad Sci USA* 104:491–494.
6. Majumdar DS, et al. (2007) Single-molecule FRET reveals sugar-induced conformational dynamics in LacY. *Proc Natl Acad Sci USA* 104:12640–12645.
7. Smirnova I, et al. (2007) Sugar binding induces an outward facing conformation of LacY. *Proc Natl Acad Sci USA* 104:16504–16509.
8. Zhou Y, Guan L, Freites JA, Kaback HR (2008) Opening and closing of the periplasmic gate in lactose permease. *Proc Natl Acad Sci USA* 105:3774–3778.
9. West IC (1970) Lactose transport coupled to proton movements in Escherichia coli. *Biochem Biophys Res Commun* 41:655–661.
10. West IC, Mitchell P (1972) Proton movements coupled to transport of beta-galactosides into Escherichia coli. *Biochem J* 127:P56.
11. Patel L, Garcia ML, Kaback HR (1982) Direct measurement of lactose/proton symport in Escherichia coli membrane vesicles: Further evidence for the involvement of histidine residue(s). *Biochemistry* 21:5805–5810.
12. Seifert K, Fendler K, Bamberg E (1993) Charge transport by ion translocating membrane proteins on solid supported membranes. *Biophys J* 64:384–391.
13. Schulz P, Garcia-Celma JJ, Fendler K (2008) SSM-based electrophysiology. *Methods* 46:97–103.
14. Trumble WR, Viitanen PV, Sarkar HK, Poonian MS, Kaback HR (1984) Site-directed mutagenesis of cys148 in the lac carrier protein of Escherichia coli. *Biochem Biophys Res Commun* 119:860–867.
15. Bieseler B, Prinz H, Beyreuther K (1985) Topological studies of lactose permease of Escherichia coli by protein sequence analysis. *Ann N Y Acad Sci* 456:309–325.
16. van Iwaarden PR, Driessen AJ, Lolkema JS, Kaback HR, Konings WN (1993) Exchange, efflux, and substrate binding by cysteine mutants of the lactose permease of Escherichia coli. *Biochemistry* 32:5419–5424.
17. Bamberg E, et al. (1979) Photocurrents generated by bacteriorhodopsin on planar bilayer membranes. *Biophys Struct Mech* 5:277–292.
18. Ganea C, Pourcher T, Leblanc G, Fendler K (2001) Evidence for intraprotein charge transfer during the transport activity of the melibiose permease from Escherichia coli. *Biochemistry* 40:13744–13752.
19. Meyer-Lipp K, Ganea C, Pourcher T, Leblanc G, Fendler K (2004) Sugar binding induced charge translocation in the melibiose permease from Escherichia coli. *Biochemistry* 43:12606–12613.
20. Kaczorowski GJ, Kaback HR (1979) Mechanism of lactose translocation in membrane vesicles from Escherichia coli. 1. Effect of pH on efflux, exchange, and counterflow. *Biochemistry* 18:3691–3697.
21. Garcia ML, Viitanen P, Foster DL, Kaback HR (1983) Mechanism of lactose translocation in proteoliposomes reconstituted with lac carrier protein purified from Escherichia coli. 1. Effect of pH and imposed membrane potential on efflux, exchange, and counterflow. *Biochemistry* 22:2524–2531.
22. Viitanen P, Garcia ML, Foster DL, Kaczorowski GJ, Kaback HR (1983) Mechanism of lactose translocation in proteoliposomes reconstituted with lac carrier protein purified from Escherichia coli. 2. Deuterium solvent isotope effects. *Biochemistry* 22:2531–2536.
23. Viitanen P, Garcia ML, Kaback HR (1984) Purified reconstituted lac carrier protein from Escherichia coli is fully functional. *Proc Natl Acad Sci USA* 81:1629–1633.
24. Carrasco N, Antes LM, Poonian MS, Kaback HR (1986) lac permease of Escherichia coli: Histidine-322 and glutamic acid-325 may be components of a charge-relay system. *Biochemistry* 25:4486–4488.
25. Carrasco N, et al. (1989) Characterization of site-directed mutants in the lac permease of Escherichia coli. 2. Glutamate-325 replacements. *Biochemistry* 28:2533–2539.
26. Menick DR, Sarkar HK, Poonian MS, Kaback HR (1985) cys154 Is important for lac permease activity in Escherichia coli. *Biochem Biophys Res Commun* 132:162–170.
27. Menick DR, Lee JA, Brooker RJ, Wilson TH, Kaback HR (1987) Role of cysteine residues in the lac permease of Escherichia coli. *Biochemistry* 26:1132–1136.
28. Sahin-Toth M, Kaback HR (2001) Arg-302 facilitates deprotonation of Glu-325 in the transport mechanism of the lactose permease from Escherichia coli. *Proc Natl Acad Sci USA* 98:6068–6073.
29. Smirnova IN, Kaback HR (2003) A mutation in the lactose permease of Escherichia coli that decreases conformational flexibility and increases protein stability. *Biochemistry* 42:3025–3031.
30. Garcia-Celma JJ, et al. (2008) Rapid activation of the melibiose permease MelB immobilized on a solid-supported membrane. *Langmuir* 24:8119–8126.
31. Foster DL, Garcia ML, Newman MJ, Patel L, Kaback HR (1982) Lactose-proton symport by purified lac carrier protein. *Biochemistry* 21:5634–5638.
32. Newman MJ, Foster DL, Wilson TH, Kaback HR (1981) Purification and reconstitution of functional lactose carrier from Escherichia coli. *J Biol Chem* 256:11804–11808.
33. Herzlinger D, Viitanen P, Carrasco N, Kaback HR (1984) Monoclonal antibodies against the lac carrier protein from Escherichia coli. 2. Binding studies with membrane vesicles and proteoliposomes reconstituted with purified lac carrier protein. *Biochemistry* 23:3688–3693.
34. Zuber D, et al. (2005) Kinetics of charge translocation in the passive downhill uptake mode of the Na^+/H^+ antiporter NhaA of Escherichia coli. *Biochim Biophys Acta* 1709:240–250.
35. Smirnova IN, Kasho VN, Kaback HR (2006) Direct sugar binding to LacY measured by resonance energy transfer. *Biochemistry* 45:15279–15287.
36. Kaczorowski GJ, Robertson DE, Kaback HR (1979) Mechanism of lactose translocation in membrane vesicles from *Escherichia coli*. 2. Effect of imposed delta psi, delta pH, and delta mu H^+. *Biochemistry* 18:3697–3704.
37. Robertson DE, Kaczorowski GJ, Garcia ML, Kaback HR (1980) Active transport in membrane vesicles from *Escherichia coli*: The electrochemical proton gradient alters the distribution of the *lac* carrier between two different kinetic states. *Biochemistry* 19:5692–5702.

38. van Iwaarden PR, Driessen AJ, Menick DR, Kaback HR, Konings WN (1991) Characterization of purified, reconstituted site-directed cysteine mutants of the lactose permease of Escherichia coli. *J Biol Chem* 266:15688–15692.
39. Nie Y, Sabetfard FE, Kaback HR (2008) The Cys154→Gly mutation in LacY causes constitutive opening of the hydrophilic periplasmic pathway. *J Mol Biol* 379:695–703.
40. Weinglass A, Whitelegge JP, Faull KF, Kaback HR (2004) Monitoring conformational rearrangements in the substrate-binding site of a membrane transport protein by mass spectrometry. *J Biol Chem* 279:41858–41865.
41. Viitanen P, Newman MJ, Foster DL, Wilson TH, Kaback HR (1986) Purification, reconstitution, and characterization of the lac permease of Escherichia coli. *Methods Enzymol* 125:429–452.
42. Costello MJ, et al. (1987) Purified lac permease and cytochrome o oxidase are functional as monomers. *J Biol Chem* 262:17072–17082.
43. Pintschovius J, Fendler K (1999) Charge translocation by the Na^+/K^+-ATPase investigated on solid supported membranes: Rapid solution exchange with a new technique. *Biophys J* 76:814–826.